DNA Hybridization: Fundamental Studies and Applications in Directed Assembly

by

Manish G. Bajaj

B. Chem. Engg. (2000)
University of Mumbai, Department of Chemical Technology, Mumbai

M. S. in Chemical Engineering Practice (2002)
Massachusetts Institute of Technology, Cambridge

Submitted to the Department of Chemical Engineering
in partial fulfillment of the requirements for the degree of

Doctor of Philosophy in Chemical Engineering

at the

MASSACHUSETTS INSTITUTE OF TECHNOLOGY
April, 2005
[June 2005]
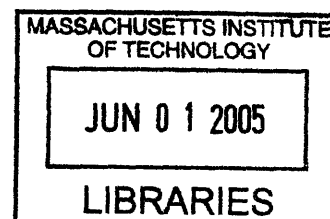
Signature of Author...
Manish G. Bajaj
Department of Chemical Engineering
April 11, 2005
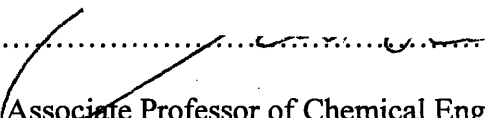
Certified by...
Paul E. Laibinis
Associate Professor of Chemical Engineering, Rice University
Thesis Advisor
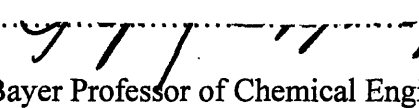
Certified by...
Gregory Stephanopoulos
Bayer Professor of Chemical Engineering& Biotechnology
Thesis Co-Advisor

Accepted by...
Daniel Blankschtein
Professor of Chemical Engineering
Chairman, Committee for Graduate Students

DNA Hybridization: Fundamental Studies and Applications in Directed Assembly

by

Manish G. Bajaj

Submitted to the Department of Chemical Engineering on April 11, 2005
in partial fulfillment of the requirements for the degree of
Doctor of Philosophy of Chemical Engineering

Abstract

Programmed self-assembly using non-covalent DNA-DNA interactions is a promising technique for the creation of next-generation functional devices for electronic, optical, and magnetic applications. This thesis develops the ability to tailor surfaces for the DNA-driven assembly of molecular, nano-, and micron-sized objects. Specifically, DNA hybridization was employed to direct the regiospecific assembly of DNA molecules onto substrates and in the targeted assembly of supraparticulate structures from nanoparticles and microparticles that express DNA molecules on their surfaces. These studies provide fundamental information needed for deploying a programmable process for the 'bottom-up' assembly of smaller species into large aggregates.

DNA-based assembly spans areas of molecular biology and nanotechnology. In the former area, DNA microarrays have become a standard tool for gene expression analysis. In spite of the large number of studies that employ DNA microarrays, fundamental aspects of DNA hybridization on these platforms have been largely unexplored. In this thesis, the effects of immobilized probe density on DNA hybridization were examined by employing a mixed silane chemistry to systematically control the density of immobilized probe DNA strands (0.2×10^{13} probes/cm^2 to 5.2×10^{13} probes/cm^2) on glass surfaces. The surface density of the immobilized species was found to significantly affect the hybridization yields; the equilibrium dsDNA amounts being highest on surfaces with ss-DNA probe densities corresponding to average inter-strand distances of 18 Å. The strong effects of surface probe density on hybridization performance indicate that it can be a useful parameter for improving the signal-to-noise ratios for assays performed on microarrays.

A target in nanotechnology is the generation of larger functional units from smaller nanoscale objects. Using a mixed silane chemistry, the DNA-directed assembly of gold nanoparticles was investigated on surfaces with different probe densities. Gold nanoparticles could be assembled at a dense coverage of ~28% corresponding to a density of ~1070 particles/μm^2. As with DNA-DNA hybridization, particle coverage was reduced at high probe densities due to strong steric and electrostatic hindrances. Non-specific adsorption—crucial for the creation of defect-free assembled devices—was three orders of magnitude lower than the specific adsorption of nanoparticles demonstrating the effectiveness of the surface chemistry in blocking extraneous particle-substrate interactions. The effect of probe density on the

thermodynamics of nanoparticle adsorption was found to be fundamentally different than that on the thermodynamics of molecular DNA adsorption due to the multivalent nature of nanoparticle attachment.

Asymmetric building blocks can substantially broaden the creation of novel self-assembled devices because of their morphological and/or chemical asymmetry. In this thesis, DNA-based recognition was employed to achieve orthogonal self-assembly on asymmetric microspheres. Dual-functional microspheres with two different DNA sequences were made by a shadow deposition of gold onto silica microspheres in conjunction with DNA immobilization procedures using thiol and silane chemistries. The prepared microspheres were used as templates for the selective orthogonal assembly of fluorophore-tagged target oligonucleotides and for the regiospecific assembly of nanoparticles of two different sizes. The selective attachment of nanoparticles and DNA molecules onto different specified regions of the building block was achieved solely by the sequence complementarity of the various components. Extending the shadow deposition technique a step further, tri-functional particles were formed by the shadow deposition of gold and aluminum. After functionalizing the silica and gold surfaces with two different DNA sequences and passivating the aluminum surface with stearic acid, an orthogonal assembly of DNA molecules was successfully performed within specified regions on these tri-functional particles. The flexibility for specifying the regio-selective attachment of DNA molecules and nanoparticles onto these building block objects will be important for the modular creation of a variety of novel self-assembled devices.

In order to expand the assembly to other asymmetric structures and to understand the effect of shape on DNA-mediated attachment, microrods were selectively assembled via DNA-DNA interactions on complementary surfaces. Because of the weak nature of the DNA-DNA interactions, a large contact area between the building block and substrate—as made possible by the microrod geometry—was essential in ensuring robust assembly. Further, dual-functional microrods were prepared by a shadow deposition of gold and could be assembled on flat surfaces in an orientation-specific manner highlighting another advantage of DNA-directed assembly beyond regiospecificity. In essence, employing DNA as the linker molecule and a robust chemistry for DNA attachment, asymmetric multi-functional particles were assembled into novel configurations, which would be difficult to realize using symmetrical building blocks. This programmable self-assembly approach exploits the multiplicity and specificity of DNA-DNA interactions and provides a powerful strategy for the generation of novel 1-D, 2-D, and 3-D functional devices.

Thesis Advisors:

Paul E. Laibinis, Associate Professor of Chemical & Biomolecular Engineering, Rice University
Gregory Stephanopoulos, Bayer Professor of Chemical Engineering & Biotechnology, MIT

To my family and friends

Acknowledgements

My thesis advisor, Prof. Paul Laibinis, for all his mentoring and guidance throughout the course of my PhD research. It was a great experience working with him. He was always available for discussions on scientific matters and was instrumental in my personal and professional development.

Members of the Laibinis lab: Ivan Lee, Jiehyun Seong, Tseh-Hwan Yong, Shinae Jun, and Hyun-Goo Choi for their inputs during the various brainstorming sessions to find solutions to vexing research problems. They made my time in 66-425 enjoyable and memorable. Ivan Lee was a great mentor for me without whose help I wouldn't have been able to accomplish as much as I did in the early years of my PhD research.

Prof. Gregory Stephanopoulos for accepting me as his co-advised student and for all his support and help. Members of the Stephanopoulos lab for helping me in my research progress by their constructive feedback and for listening to my research queries and offering valuable advice.

My office mates - Bharath, Sara, Nina, and Jeremy – for their good humor and friendship during the final years of my PhD. My other friends at MIT without whose help and camaraderie MIT wouldn't have been such a lovely place for me.

Table of Contents

List of Figures

11

List of Tables

Chapter 1.   Introduction – DNA Surface Hybridization

1.1 Introduction

The vast amount of genomic information made available by the Human Genome Project has spurred the development of solid-state DNA based assays. These assays are based on the principle of selective hybridization between two DNA strands according to the Watson-Crick base pairing of adenine with thymine (A-T) and cytosine with guanine (C-G). This selective binding process can be used to identify DNA strands with different sequences and assemble them to specific locations. These assays have been used to measure the mRNA or gene expression levels in cells,[1] to determine the polymorphisms in various alleles,[2] to detect pathogens in water,[3,4] to elucidate biochemical pathways,[5] and to perform transcript profiling of tumors[6,7]. Over the last decade or so, there has been an explosion in the use of DNA-based assays for obtaining genetic information. Advances in gene expression monitoring and the establishment of their correlations to disease phenotypes have the potential to expand clinical abilities in prognosis, diagnosis, and treatment of diseases.[8] The genome-wide expression profiles made possible by the annotation of the Human Genome and the availability of whole-genome based DNA assays will play a vital role in developing a more holistic view of biology.[9]

The application of DNA assays to combinatorial studies was brought about by the development of the DNA microarrays. Southern and coworkers[10] were the first to form arrays of nucleic acids, in their case oligonucleotides, on a surface for the purpose of large-scale genetic studies. Since then, DNA microarrays have been improved to yield systems capable of high-throughput analysis of genetic material.[11]

1.1.1 DNA microarrays

DNA microarrays consist of a solid substrate such as a microscopic glass slide, a silicon wafer, or a polypropylene sheet, that is patterned with thousands of different DNA sequences (probes) in an array format at defined locations on its surface. In a typical use of a DNA microarray, messenger RNA (mRNA) is extracted from pathological and normal samples. The mRNA is then converted to cDNA (complementary DNA) using the enzyme reverse transcriptase (RT) and amplified using the polymerase chain reaction (PCR). The cDNA strands are tagged either by incorporating fluorophore-tagged nucleotides into their sequences during the reverse transcription/amplification process or by chemically coupling fluorophores to the modified nucleotides added during the reverse transcription/amplification process. These fluorophore-tagged cDNA samples are then brought in contact with the DNA microarray. After the requisite time for hybridization and the necessary washing steps, the microarray is scanned for fluorescence by laser excitation of the fluorophores. Image analysis and statistical tools are used to convert the fluorescence signal intensities into gene expression levels. The differences in the expression levels of different genes between the normal and pathological samples are used to correlate their link to the disease phenotype. DNA microarrays provide the platform for performing these nucleic acid analyses on a combinatorial scale. The important issues in constructing microarrays are the design of the probe sequences and their appropriate immobilization. For the DNA assays to be useful, each of the following steps—immobilization, hybridization, and detection—has to be properly designed and optimized. Surface issues play a key role in the first two steps involving immobilization and hybridization.

1.1.2 Immobilizing probe DNA molecules on the substrate

Immobilization can be achieved either by synthesizing oligonucleotides in a combinatorial fashion on the array surface or by individually spotting pre-synthesized oligonucleotides or cDNAs (complementary DNAs) sequentially onto the array surface. This process requires the substrate and/or the oligonucleotides to be suitably functionalized so that selective coupling can occur. Ultra high densities of probes (as high as 1,000,000 different probes on a 1 cm x 1 cm slide[12]) can be achieved by employing sophisticated robotic and fluidic delivery equipment or photolithographic tools along with photo-labile reagents. After probe immobilization, the microarrays are ready to be used for hybridization with target DNA. The sensitivity and selectivity of hybridization depends on the characteristics of the probe surface, the composition of the hybridizing medium, and the hybridization conditions.

1.1.3 Surface hybridization of probe and target DNA molecules

The hybridizing solution that is put in contact with a DNA microarray usually contains genomic fragments (for polymorphism studies) or a mixture of cDNAs (for gene expression studies) that have been amplified by PCR (polymerase chain reaction) and include labels useful for detection. The solution also contains salt to stabilize the negatively charged phosphodiester backbone of the DNA strands and other additives like surfactants to enhance hybridization and to reduce non-specific adsorption. The substrate should be derivatized such that it does not promote the non-specific DNA binding to its probe sites. For example, a positively charged substrate would readily adsorb polyanionic target in the absence of immobilized DNA probes. After hybridization has occurred, the substrate is washed with a buffer solution to remove any non-specifically adsorbed DNA molecules. Hybridization efficiencies typically vary from 1 to 100%

depending on the surface packing density of the immobilized probes, and the length of the target DNA, the hybridization conditions (time, temperature, salt concentration) employed.

The detection of hybridization event and quantification of its extent has been performed using labeling or non-labeling techniques. For analysis of high-density microarrays, constraints on the detection scheme require that it should have a spatial resolution of a few microns and should be able to distinguish changes even at the pico gram level.

1.1.4 Detection

The most popular method for detecting hybridization events is the introduction of either a fluorescent, chemiluminescent, or radioactive tag in the target DNA molecules. After hybridization, the chips are scanned for the presence of the signals from the tags using either an optical or a radioactivity scanner. The location and intensity of the acquired signals give information about the identity of and the approximate quantity of the target DNA. Various label-free techniques have been used for DNA detection and these methods take advantage of the change in the charge, mass, or refractive index at particular surface sites in order to detect a hybridization signal. These methods include electrochemical detection,[13] quartz crystal microbalance,[14] and surface plasmon resonance[15] (SPR) and allow monitoring the hybridization process in real-time. For example, Krull et al.[16] have immobilized oligonucleotides on fused silica optical fibers, and used these fibers as a medium to transfer the fluorescence of the hybridized targets by a total internal reflection process in order to generate denaturation profiles for the hybrid duplexes.

1.2 Array formats used currently

Currently available DNA microarrays or "DNA chips" can be broadly classified into two categories depending on whether their probe DNA molecules are synthesized on- or off-chip:

i) On-chip oligonucleotide synthesis:

On-chip synthesis of probes is accomplished by solid-state phosphoramidite chemistry where the bases are added stepwise to prepare the attached oligonucleotides with lengths of 15-70 bases. The solid substrates in this case are often derivatized with molecules that expose hydroxyl groups as reaction sites. Arrays of thousands of probes can be created by either ink-jet techniques[17] or by the Affymetrix's photolithographic technique[18] using photo-labile deprotecting groups on the phosphoramidites. The stepwise coupling yield for the photo-deprotection technique is ~95%[19], whereas it is 98-99% for the conventional phosphoramidite chemistry. For comparison, the photo-deprotection technique would have a 35% yield for a 20-mer while the conventional chemistry will form a 65-mer at greater than 35% yields.

ii) Spotting of cDNAs / oligonucleotides:

Another method for preparing microarrays is to spot pre-synthesized oligonucleotides or cDNAs directly onto a functionalized surface. Patrick Brown of Stanford developed one of the most commonly used protocols for spotting[20,21]. Here, cDNAs are first produced by reverse transcription from mRNAs, followed by amplification by PCR and purification, and then robotically spotted in nanoliter quantities onto a glass slide coated with polylysine or amino-terminated organic moieties. The system is subsequently illuminated with UV light to effect crosslinking between the thymine residues on the cDNAs and the positively charged amine groups on the functionalized surface. As each DNA strand is attached via various sites along its backbone, the length and the sequences available for subsequent hybridization can vary with the

hybridization conditions. Other immobilization chemistries for this format involve derivatizing the oligonucleotide at one end with a selective linking agent so that it can attach directly to a surface functionality surface or another agent that has been immobilized on the surface.

1.2.1 Problems with currently available formats

Although the currently available formats are becoming widely used in the research community, nonetheless, they are plagued with shortcomings that are being increasingly realized to hamper their reliability. For example, poor control over immobilization densities, lack of reproducibility, on-chip heterogeneity, lack of flexibility, high background adsorption levels, and lack of reusability are some of the problems that need attention and improvement. Some of the most important are discussed below in detail.

Lack of reproducibility - The results obtained by using commercially available systems lack reproducibility from one batch to other because of the variability caused by the present surface derivatization chemistries and immobilization techniques. The lack of control over the orientation and density of the reactive sites that are the agent for immobilization compounds the problem of reproducibility. Previously, most of the experiments conducted were based on single measurements because of the prohibitive cost for repeating microarray studies. As the microarrays have gotten cheaper, multiple experiments for the same measurements have been made possible and have revealed the extent of chip-to-chip deviation for these measurements. These deviations raise questions about the fidelity of the data and the validity of the conclusions drawn from them.

Lack of reusability - The assay systems are irreversibly changed once they pass through one cycle of hybridization, denaturation and washing. Thus reduced signals are obtained if the chips are used again for the next round of hybridization. The surface chemistry employed is not

robust enough to sustain the washing and denaturation treatments. The lack of reusability has made these systems too expensive for frequent use and beyond the reach of smaller labs.

Low signal-to-noise ratios - Low signal-to-noise ratios result from lower density of hybridization sites and /or large amount of non-specific hybridization. Most of the chemistries employed do not have enough reactive probes on the surface to guarantee large signals after hybridization. Others have too much of non-specific adsorption which is not removed even after stringent washing conditions.

Most of these problems stem directly from the surface derivatization and immobilization chemistry used for making these chips. A targeted design of the surface derivatization and immobilization techniques could help to improve the performance of these systems and improve the reliability of the data obtained from these assays.

1.3 Techniques for DNA immobilization

DNA immobilization on solid surfaces can be achieved by a variety of methods. An ideal immobilization scheme should enable the immobilized nucleic acids to mimic their solution phase behavior. Also such a scheme should ensure the operational effectiveness of these systems including issues of specificity, reproducibility, and reusability. The factors that must be taken into consideration while designing a DNA immobilization scheme are: type of immobilization (covalent, non-covalent etc.), point of attachment, linker length, and linker characteristics.

Non-covalent immobilization schemes such as immobilization on nitrocellulose filters[22] and association on lipid bilayer[23] generally result in poorly defined strand orientations, low packing densities, low mobilities, and regions of the nucleic acid sequence being unavailable for hybridization due to the immobilization. Gel entrapment of DNA[24] leads to excessive diffusional

limitations for the target DNA and thus the kinetics of hybridization are slow. Also in these cases, the DNA molecules are susceptible to removal from the surface under high salt or high temperature conditions. Covalent attachment provides far more stable situation for the experimental conditions employed for hybridization.

Regarding the site for attachment, end immobilization through either the 3' or 5' end seems to be the best option as they allow almost all the bases to be available for hybridization. Covalent immobilization either through the backbone or the bases increases the chances of non-specific adsorption because of poor accessibility of the entire sequence for hybridization. It has been found that DNA could become totally inaccessible for hybridization when only 3% of its bases are involved in the covalent linkage.[25]

The hybridization rates on the surface are much slower than those in solution. By having a long enough linker to distance the molecule from any interactions with the surface, it is possible to have a sequence mimic its solution phase behavior even while being immobilized. Various research groups have suggested different required linker lengths between the support and the DNA for their examined experimental conditions. Kawasaki et al.[26] report that a linker at least 28 Å in length when fully extended between the support and the DNA is required to approach solution phase hybridization rates. Southern et al.[27] suggest an optimal length of at least 40 atoms for best hybridization yields. In contrast, Beattie and coworkers[28] have found that such linker arms were not necessary for achieving the efficient hybridization of long PCR products (> 500 bases).

1.3.1 End-immobilization chemistries

Over the years, many alternative immobilization chemistries have been proposed because of inherent problems with the commercially available systems. A number of these have been

commercialized. The general approach is to end-immobilize the DNA/oligonucleotide through its 3' or 5' end. A few systems have also been constructed to address issues of density control and non-specific adsorption. In most of these studies, the substrates used are glass, silicon, fused silica optical fibers, and polypropylene.

Reactive groups can be added to the 3' or 5' end of the DNA/oligonucleotides when phosphoramidite synthesis or PCR is employed for generation of the DNA sequences. These end-functionalized DNA/oligonucleotides can then be attached to functionalized surfaces directly or through a crosslinker. DNA has been end -functionalized with amino[24], carboxylic[29], phosphate[30], silyl[31], acrylic[31], and thiol[32] groups. Amino terminal oligonucleotides have been bound to isothiocyanate-activated[33] glass, to aldehyde-activated[34] glass and to glass modified with epoxide[35] without the use of a crosslinker. Thiol-terminated[36] and disulfide-terminated oligonucleotides have been bound to aminosilane derivatized glass using a heterobifunctional crosslinker. Disulfide-modified[37] and acrylic-modified oligonucleotides have been immobilized onto thiol-functionalized surfaces directly. Amino-modified oligonucleotides have been attached to amine-terminated surfaces using glutaraldehyde[38] as a crosslinker. Alternatively, because of its intrinsic stability the highly specific biotin-avidin[39] interaction has also been used for DNA immobilization. However, since avidin is a protein, there is a large possibility for non-specific adsorption. Also, the surface densities with this system have been an order of magnitude lower than for other systems. In an interesting departure from other methods, Kumar et al.[31] have utilized an immobilization chemistry wherein they attach silanized DNA to unmodified glass. They have demonstrated different procedures to covalently conjugate an active silyl moiety onto the oligonucleotides or cDNAs in solution thereby forming a new class of modified nucleic acids, namely silanized nucleic acids.

The specificity of the immobilization chemistry must compete with the inherent reactivity contained in DNA. Specifically, the nucleic acids contain many reactive functionalities: the negatively charged phosphates, the exocyclic amines on the bases, the enolizeable carbonyl groups on the bases, and cleavable glycosidic bonds. In most of the immobilization schemes described above, the crosslinkers employed for specific attachments can react with the other reactive sites on the nucleic acids and cause unwanted side reactions. Further, competing side reactions with water due to the large amount of water molecules (55 M) relative to probe oligonucleotides (μm or less) presents an important challenge as it can reduce the amount of surface-active groups such as activated ester or isocyanate groups that provide sites for oligonucleotide immobilization only when in an active, non-hydrolyzed form. Zammatteo et al.[40] while comparing different strategies for covalently attaching DNA to glass surfaces found that the best immobilization and hybridization results occurred for fixing aminated DNA to an aldehyde-modified glass. Lindroos et al.[34], on the other hand, found that disulfide-modified oligonucleotides immobilized onto thiol-terminated glass work better than the aldehyde-amine immobilization chemistry as regards background fluorescence and signal-to-noise ratios. The literature is filled with competing claims revealing that a flexible, reliable procedure for DNA immobilization is not yet available.

Methods for controlling probe density are also beset with problems. For example, most of the chemistries that use glass and silicon as substrates employ short chain silanes such as the glycidoxy propyl triethoxysilane (GOPS) (an epoxy silane that yields -OH terminations), mercaptopropyl trimethoxysilane (MPS) (-SH terminated), aminopropyltriethoxy silane (APTES) (-NH$_2$ terminated) to generate reactive surface sites for DNA attachment. A problem is that these silanes have a tendency to form multilayers of poorly controlled structures and these

films can be hydrolytically removed from surfaces. Also, crosslinking reactions between adjacent immobilized molecules can reduce the number of reactive sites available for the immobilization of the oligonucleotide/DNA thereby causing difficulties in controlling the density of reactive sites. As such, only a few research groups have tried to address the issue of controlling the surface density of the immobilized probes and have been successful in tackling it (see Chapter 3).

1.4 DNA surface hybridization

The process of surface hybridization can be schematically pictured to begin with the diffusion of the target DNA molecules from the solution phase to the probe layer (Figure 1-1). The diffusion coefficient of DNA in solution is in the range of 10^{-6}-10^{-8} cm^2/s. In a second step, the diffusion of the DNA in the probe layer is affected by hindrance due to steric and electrostatic repulsions offered by the immobilized probe strands. The higher the packing density of the immobilized DNA strands, the slower is the diffusion in this layer. Hindered diffusion in the immobilized layer can cause the target DNA to collide with the surface where it can be non-specifically adsorbed or with the several immobilized probe strands. Collisions with a probe strand at the correct base site could lead to nucleation of hybridization. The nucleation process can be severely impeded by secondary structures found in long target DNA molecules. Once nucleated at the correct spot, the duplex would form by zippering complementary bases together at a rapid rate. The resulting duplex formation between the target DNA and the probe DNA is an equilibrium process since thermal energy can later lead to dissociation of the non-covalently H-bonded DNA duplexes.
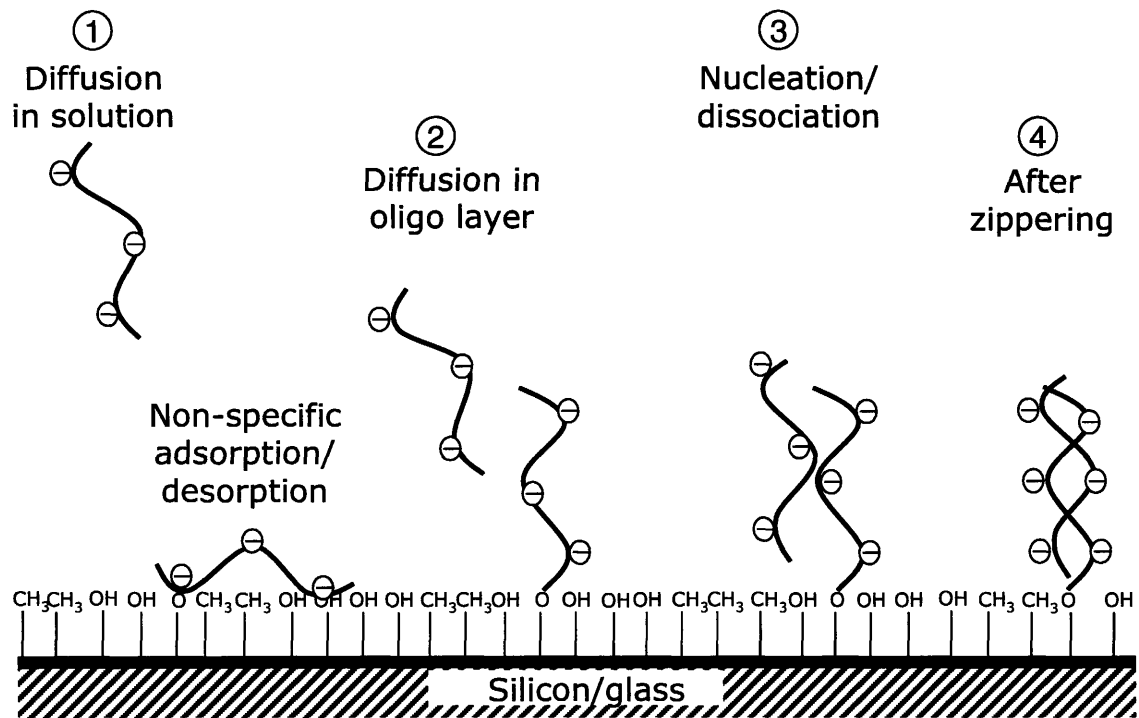
Figure 1-1 Steps involved in the surface hybridization process. 1) The target strands have to undergo diffusion in the bulk solution, followed by 2) diffusion in the probe layer. Next, 3) the target molecules collide with the immobilized probes leading to a nucleation event followed by 4) a quick zippering step to form the DNA duplex. Competing processes include non-specific adsorption and duplex dissociation.

26

1.4.1 Factors affecting DNA surface hybridization

Hybridization on surfaces is influenced by factors such as surface chemistry and surface probe density as well as those factors that influence hybridization in solution: pH, salt concentration, temperature, solvent properties, GC content, and DNA length. Higher GC content increases the stability of DNA duplexes since a GC base pair produces three hydrogen bonds resulting in greater stability than does a AT base pair that produces just two hydrogen bonds. The addition of salt stabilizes DNA by screening the charges between two polyanionic oligonucleotide strands. Further, higher salt concentration helps in improving the kinetics of the process, but at the same time reduces the stringency of discriminating between mismatch sequences. Higher temperatures help to provide better discrimination between mismatches by denaturing the less stable mismatched duplexes. On the downside, higher temperatures may also cause the dissociation rate to increase and thus decrease equilibrium-hybridized duplex amounts. Surfactants like SDS (sodium dodecyl sulphonate) help in improving the signal-to-noise ratios from hybridization experiments by reducing non-specific adsorption events. However, the addition of too much surfactant can inhibit the hybridization process by interacting with the charged polyanionic backbones.

The length of the complementary DNA sequences plays an important role in setting the stability of the DNA duplex. Longer the length of the oligonucleotide the higher is the melting point of the duplex as a result of a greater enthalpic driving force for duplex formation. In contrast, the greater restrictions to the degrees of freedom for these longer oligonucleotide upon hybridization leads to larger entropic losses. Thus, a balance of these two factors defines the overall equilibrium hybridization levels. Beyond these factors, longer DNA molecules have

larger diffusional limitations in accessing the probe oligonucleotides and mismatch discrimination also gets more difficult with longer oligonucleotide sequences.

At surfaces, probe density is one of the important parameters affecting the process of DNA-DNA hybridization. Generally, it is desired that the number of surface-bound DNA probes be substantially higher than the number of targets in solution in order to achieve large hybridization signals even for low target concentrations. However, higher surface probe densities can increase the diffusional limitations on the incoming target DNA molecules by providing steric as well as electrostatic repulsion to the target molecules. The interplay of these opposing effects leads to an optimal surface probe density where the availability of the probes, the hybridization equilibrium and kinetics are within acceptable limits. Any study on the effects of probe density on the thermodynamics and kinetics of hybridization requires a system where it is possible to systematically vary the surface density of the reactive groups and thus vary the amount of immobilized oligonucleotides in a controlled and measurable manner.

1.5 Chemistries for controlling probe densities

The packing density of the probes determines the surface charge and steric crowding at the hybridization sites. It has important implications in the thermodynamics and kinetics of hybridization and also in those of denaturation when used for certain SNP analysis. The few successful attempts at achieving this control are discussed below.

Tarlov et al.[32,41] have used a system wherein they deposit thiol-modified oligonucleotides from a micromolar solution onto gold surfaces and then immerse the substrate in a millimolar solution of 6-mercapto-1-hexanol to achieve a range of densities for the immobilized oligonucleotides. In this system, the thiol-Au bond responsible for oligonucleotide attachment is heat sensitive. A limitation to this chemistry is that the amount of immobilized oligonucleotides

would be reduced after going through one complete cycle of hybridization, washing, and denaturation thereby making these systems useful generally for single investigations.

Smith et al.[42] have used mixtures of t-butyloxycarbonyl (t-BOC)-protected 10-aminodec-1-ene and dodecene to derivatize the surface of hydrogen-terminated silicon (001) with controlled densities of amine groups. They used UV light to remove the t-BOC protecting groups. Although this substrate has a highly defined crystalline structure and presents a homogeneous surface, it oxidizes under ambient conditions. To protect the substrate from possible side reactions, experiments must be performed under controlled atmospheres in order to control the density of reactive groups. This system allows density control but is handicapped somewhat by its lack of operational flexibility.

Other groups such as Krull et al.[43] have tried to modulate the surface probe density by changing the delivery times of linker molecules to substrates within an oligonucleotide synthesizer. In another approach, Gou et al[33] have tried to change surface densities by spotting different concentrations of oligonucleotide solution to a substrate. A comprehensive comparison of various immobilization chemistries with regards to packing density, density control, and hybridization time is provided in Table 1.[43,44]

1.5.1 Our approach

The surface immobilization chemistry developed in our laboratory by a previous graduate student (Ivan Lee) meets most of the above requirements. Specifically, the immobilization process utilizes the concept of mixed monolayers[45] where two silane compounds with different end groups—one with a protected reactive (hydroxyl) end group and the other with an inert (methyl) end group—are mixed in desired proportions to obtain controlled densities of reactive groups on surface.[46] Figure 1-2 shows an illustration of the self-assembly of two silanes onto a

surface yielding film of mixed composition. Experimentally, the surface composition is related to the silane composition in solution. Once covalently attached, the end groups of the silanes are base deprotected to expose the reactive hydroxyl functional groups. These functionalized surfaces are then used for synthesis of oligonucleotides on the surface. The inert end groups ensure that the non-specific adsorption of DNA is small. Our approach is compatible with soft lithography techniques such as micro-contact printing thereby allowing surfaces with regions of high reactive group density and other regions with inert groups to be obtained. These patterned surfaces provide a substrate for array construction as spots are defined by differences in their reactivity and hydrophilicity. In this process, the silane compounds form covalent bonds with the surface and are more stable to heat treatments than are systems constructed using thiol-Au bonds. Our chemistry provides a fairly good control over surface composition as needed to achieve a wide range of probe densities. The resulting system is reliable, flexible, reproducible, and generates probe surfaces that yield hybridization results with high signal-to-noise ratios. The thermodynamic and kinetic study of DNA-DNA surface hybridization can be accomplished in a more systematic manner with access to such an immobilization chemistry.

After
SELF-ASSEMBLY

After
DEPROTECTION

Trichloroacetyl
protecting group

OH

CH$_3$

(CH$_2$)$_n$

SiCl$_3$
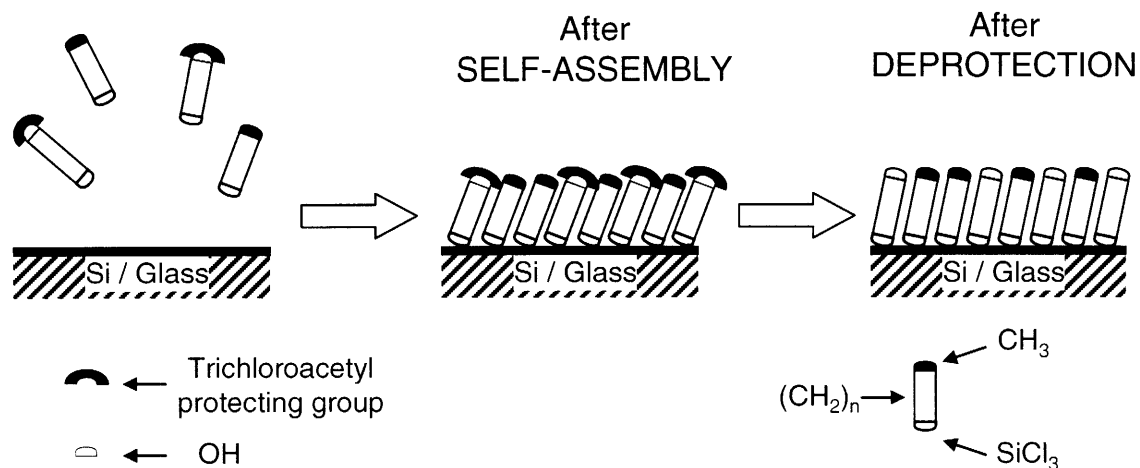
Figure 1-2. Schematic illustration of formation of mixed self-assembled monolayers. Two silanes—one with a protected-hydroxyl group and other with an inert methyl group—are first brought in contact with the glass or Si/SiO$_2$ surface. The two silanes assemble on the surface based on their solution composition. After the assembly, the protecting trichloroacetate groups are removed using a basic solution to expose the hydroxyl groups.

1.6 Previous Work

Although the use of microarrays is increasing rapidly, there has been little in-depth theoretical or experimental research on the factors that influence DNA-DNA surface hybridization. For example, in diagnostic applications, a system with fast kinetics is desired so that a measurable signal can be obtained within a reasonable time. In gene-expression studies, reliable quantitative data is desired even if experiments require longer hybridization times. Thus, there is a need to better understand factors that influence both the kinetics and thermodynamics of surface hybridization in order to provide improvements for this process. Such a study necessitates the availability of a well-defined system with controllable immobilization chemistry and also effective detection techniques to characterize the system at various points during its operation. Georgiadis et al.[47] have explored the effects of probe density for the hybridization of 25-mer DNA strands to surfaces. They observed decreasing hybridization efficiencies with increases in probe density. Also, they observe two different kinetic profiles for hybridization onto surfaces with probe densities below and above a particular threshold value. Krull et al.[48] immobilized 20-mers onto fused silica optical fibers and used a total internal reflection fluorescence instrument to monitor the hybridization in real time. They observed that the standard enthalpic changes for the hybridization process on surface were 2-3 fold lower than the values obtained in a bulk solution. They also observed a decrease in the surface T_M values with increases in probe density.

On the theoretical side, only a few research groups have tried to describe the surface hybridization process via fundamental equations. Chan et al.[49] have tried to model the system based on a Brownian dynamics model. However, they failed to take any ionic effects into consideration. Also, they have modeled only a system with a low probe density. The current

trend in experiments is to have systems at higher surface densities so that the number of probes is greater than the number of targets, but low enough to avoid detrimental electrostatic effects on surface hybridization reactions. Wong et al.[50] have tried to model the hybridization phenomenon using molecular dynamics. But due to the enormity of atoms even in a single 10-mer oligonucleotide and the number of degrees of freedom in its 3-D structure, not to mention the electrostatic effects due to the phosphate backbone, they have been able to simulate the system only for few nanoseconds despite using a very powerful computing facility. As the phenomenon of hybridization takes place on a time scale of a few microseconds it is difficult to characterize the validity of these hybridization results based on simulations of only a few nanoseconds. Thus, for molecular dynamics simulations to gain more insight into such systems, they would require tremendous increase in computing power. As such these approaches do not appear useful at this time. Less detailed models like Brownian dynamics or simpler diffusion-limited reaction models would be easier to implement. In another approach, Pettitt et al.[51-55] have modeled the target DNA molecules as ion-penetrable charged spheres and the probe surface as a charged plate. They employed the linearized Poisson-Boltzmann theory of the electric double-layer interaction in order to model the electrostatic interactions. Their estimations suggest the presence of strong electrostatic forces even at high salt concentrations and predict a 'Coulomb blockage' of the target hybridization at high surface probe densities.

The current state of research in this field suggests that more effort is required into understanding the fundamentals of hybridization both at the kinetic and thermodynamic level so as to achieve better control over the behavior of these systems. Based on the previous work, the main motivation for this part of this thesis was to systematically explore the effects of surface density on the DNA surface hybridization process. I was particularly interested in understanding

the trade-offs involved with low and high probe densities. Additionally I wanted to use our immobilization chemistry to also explore nanoparticle adsorption on surfaces via DNA-DNA hybridization, a promising technique for ultra-sensitive detection of DNA fragments and a potential assembling strategy for materials synthesis.

1.7 References & Footnotes

(1) Duggan, D. J.; Bittner, M.; Chen, Y. D.; Meltzer, P.; Trent, J. M. *Nat Genet* **1999**, *21*, 10-14.

(2) Kwok, P.-Y. *Annual Reviews in Genomics and Human genetics* **2001**, *2*, 235-258.

(3) Wang, J. L. *Progress in Biochemistry and Biophysics* **2001**, *28*, 125-128.

(4) Cheng, J. F., P. Surrey, S. Kricka, L. J. Wilding, P. *Mol. Diagn.* **1996**, *1*, 183-200.

(5) Ideker, T.; Thorsson, V.; Ranish, J. A.; Christmas, R.; Buhler, J.; Eng, J. K.; Bumgarner, R.; Goodlett, D. R.; Aebersold, R.; Hood, L. *Science* **2001**, *292*, 929-934.

(6) Dhanasekaran, S. M.; Barrette, T. R.; Ghosh, D.; Shah, R.; Varambally, S.; Kurachi, K.; Pienta, K. J.; Rubin, M. A.; Chinnaiyan, A. M. *Nature* **2001**, *412*, 822-826.

(7) Welsh, J. B.; Zarrinkar, P. P.; Sapinoso, L. M.; Kern, S. G.; Behling, C. A.; Monk, B. J.; Lockhart, D. J.; Burger, R. A.; Hampton, G. M. *Proc Natl Acad Sci U S A* **2001**, *98*, 1176-1181.

(8) Sevenet, N.; Cussenot, O. *Clin Exp Med* **2003**, *3*, 1-3.

(9) Shoemaker, D. D.; Linsley, P. S. *Curr Opin Microbiol* **2002**, *5*, 334-337.

(10) Southern, E. M.; Maskos, U.; Elder, J. K. *Genomics* **1992**, *13*, 1008-1017.

(11) Heller, M. J. *Annu Rev Biomed Eng* **2002**, *4*, 129-153.

(12) Lipshutz, R. J.; Fodor, S. P. A.; Gingeras, T. R.; Lockhart, D. J. *Nat Genet* **1999**, *21*, 20-24.

(13) Steel, A. B.; Herne, T. M.; Tarlov, M. J. *Anal Chem* **1998**, *70*, 4670-4677.

(14) Caruso, F.; Rodda, E.; Furlong, D. F.; Niikura, K.; Okahata, Y. *Anal Chem* **1997**, *69*, 2043-2049.

(15) Thiel, A. J.; Frutos, A. G.; Jordan, C. E.; Corn, R. M.; Smith, L. M. *Anal Chem* **1997**, *69*, 4948-4956.

(16) Piunno, P. A. E.; Krull, U. J.; Hudson, R. H. E.; Damha, M. J.; Cohen, H. *Anal Chim Acta* **1994**, *288*, 205-214.

(17) Hughes, T. R.; Mao, M.; Jones, A. R.; Burchard, J.; Marton, M. J.; Shannon, K. W.; Lefkowitz, S. M.; Ziman, M.; Schelter, J. M.; Meyer, M. R.; Kobayashi, S.; Davis, C.; Dai, H. Y.; He, Y. D. D.; Stephaniants, S. B.; Cavet, G.; Walker, W. L.; West, A.; Coffey, E.; Shoemaker, D. D.; Stoughton, R.; Blanchard, A. P.; Friend, S. H.; Linsley, P. S. *Nat Biotechnol* **2001**, *19*, 342-347.

(18) Fodor, S. P. A.; Read, J. L.; Pirrung, M. C.; Stryer, L.; Lu, A. T.; Solas, D. *Science* **1991**, *251*, 767-773.

(19) McGall, G. H.; Barone, A. D.; Diggelmann, M.; Fodor, S. P. A.; Gentalen, E.; Ngo, N. *J Am Chem Soc* **1997**, *119*, 5081-5090.

(20) Shalon, D.; Smith, S. J.; Brown, P. O. *Genome Res* **1996**, *6*, 639-645.

(21) Schena, M. *Bioessays* **1996**, *18*, 427-431.

(22) Southern, E. M. *J Mol Biol* **1975**, *98*, 503-&.

(23) Schouten, S.; Stroeve, P.; Longo, M. L. *Langmuir* **1999**, *15*, 8133-8139.

(24) Proudnikov, D.; Timofeev, E.; Mirzabekov, A. *Anal Biochem* **1998**, *259*, 34-41.

(25) Bunemann, H. *Nucleic Acids Res* **1982**, *10*, 7181-7196.

(26) Zhang, Y.; Coyne, M. Y.; Will, S. G.; Levenson, C. H.; Kawasaki, E. S. *Nucleic Acids Res* **1991**, *19*, 3929-3933.

(27) Shchepinov, M. S.; CaseGreen, S. C.; Southern, E. M. *Nucleic Acids Res* **1997**, *25*, 1155-1161.

(28) Beattie, W. G.; Meng, L.; Turner, S. L.; Varma, R. S.; Dao, D. D.; Beattie, K. L. *Mol Biotechnol* **1995**, *4*, 213-225.

(29) Kumar, A.; Advani, S. *Nucleosides Nucleotides* **1992**, *11*, 999-1002.

(30) Henke, L.; Piunno, P. A. E.; McClure, A. C.; Krull, U. J. *Anal Chim Acta* **1997**, *344*, 201-213.

(31) Kumar, A. L., O. Parodi, D. Liang, Z. *Nucleic Acids Res* **2000**, *28*, e71.

(32) Herne, T. M.; Tarlov, M. J. *J Am Chem Soc* **1997**, *119*, 8916-8920.

(33) Guo, Z.; Guilfoyle, R. A.; Thiel, A. J.; Wang, R. F.; Smith, L. M. *Nucleic Acids Res* **1994**, *22*, 5456-5465.

(34) Lindroos, K., Liljedahl, U. Raitio, M. Syvanen, A.C. *Nucleic Acids Res* **2001**, *29*, e69.

(35) Maskos, U.; Southern, E. M. *Nucleic Acids Res* **1992**, *20*, 1679-1684.

(36) Chrisey, L. A.; Lee, G. U.; Oferrall, C. E. *Nucleic Acids Res* **1996**, *24*, 3031-3039.

(37) Rogers, Y. H.; Jiang-Baucom, P.; Huang, Z. J.; Bogdanov, V.; Anderson, S.; Boyce-Jacino, M. T. *Anal Biochem* **1999**, *266*, 23-30.

(38) Yang, M. S.; McGovern, M. E.; Thompson, M. *Anal Chim Acta* **1997**, *346*, 259-275.

(39) Nikiforov, T. T.; Rendle, R. B.; Goelet, P.; Rogers, Y. H.; Kotewicz, M. L.; Anderson, S.; Trainor, G. L.; Knapp, M. R. *Nucleic Acids Res* **1994**, *22*, 4167-4175.

(40) Zammatteo, N.; Jeanmart, L.; Hamels, S.; Courtois, S.; Louette, P.; Hevesi, L.; Remacle, J. *Anal Biochem* **2000**, *280*, 143-150.

(41) Levicky, R.; Herne, T. M.; Tarlov, M. J.; Satija, S. K. *J Am Chem Soc* **1998**, *120*, 9787-9792.

(42) Strother, T.; Hamers, R. J.; Smith, L. M. *Nucleic Acids Res* **2000**, *28*, 3535-3541.

(43) Henke, L.; Krull, U. J. *Can. J. Anal. Sci. Spectrosc.* **1999**, *44*, 61-70.

(44) Cavic, B. A.; McGovern, M. E.; Nisman, R.; Thompson, M. *Analyst* **2001**, *126*, 485-490.

(45) Prime, K. L.; Whitesides, G. M. *Science* **1991**, *252*, 1164-1167.

(46) Lee, I. H. In *Chemical Engineering*; Massachusetts Institute of Technology: Cambridge, 2001.

(47) Peterson, A. W.; Heaton, R. J.; Georgiadis, R. M. *Nucleic Acids Res* **2001**, *29*, 5163-5168.

(48) Watterson, J. H.; Piunno, P. A. E.; Wust, C. C.; Krull, U. J. *Langmuir* **2000**, *16*, 4984-4992.

(49) Chan, V.; Graves, D. J.; McKenzie, S. E. *Biophys J* **1995**, *69*, 2243-2255.

(50) Wong, K. Y.; Pettitt, B. M. *Theor. Chem. Acc.* **2001**, *106*, 233-235.

(51) Vainrub, A.; Pettitt, B. M. *Chem. Phys. Lett.* **2000**, *323*, 160-166.

(52) Vainrub, A.; Pettitt, B. M. *Biophys J* **2000**, *78*, 404A-404A.

(53) Vainrub, A.; Pettitt, B. M. *Phys. Rev. E* **2002**, *66*.

(54) Vainrub, A.; Pettitt, B. M. *J Am Chem Soc* **2003**, *125*, 7798-7799.

(55) Vainrub, A.; Pettitt, B. M. *Biopolymers* **2003**, *68*, 265-270.

(56) Piunno, P. A. E.; Watterson, J.; Wust, C. C.; Krull, U. J. *Anal Chim Acta* **1999**, *400*, 73-89.

Table 1-1 Comparison of various immobilization chemistries

Group	Immobilization Chemistry	Substrate	Probe / Target, Length	Probe Density Molecule/cm²	Density Control	Hybrid. Time	Hybridization Conditions
Kumar et al.[31]	Silanized DNA	Glass slide	20 nt / 20 nt	2×10^{13}	No	30 min – 12 h	37 °C, 20 nM to 1 µM oligo, 750 mM NaCl, 125 mM Na citrate, 0.1% Tween
McGall et al.[19]	OH-silane + oligo synthesis	Glass slide	20-25 nt / PCR product	-	No	4 h	35-40 °C, 6x SSPE, 0.001% Triton X-100
Shalon et al.[20]	Poly-lysine + PCR product	Glass slide	PCR / PCR products	-	No	14-18 h	65 °C, 0.5 M NaCl, 0.05 M Na citrate, 0.3% SDS
Piunno et al.[56]	Glycidoxy propyl silane + DMT-HEG linker + oligo synthesis	Fused silica	20 nt / 20 nt	9×10^{10} to 4.6×10^{12}	Some	40 min	90 °C, 0.62 µM oligo, 1 M NaCl, 50 mM NaH₂PO₄
Shchepinov et al.[27]	Glycidoxy propyl silane + linker + oligo synthesis	Glass slide	12 nt / 12 nt	6×10^{12}	Some	2 h	30 °C, 3 nM oligo, 0.1 M NaCl
Guo et al.[33]	NH₂ propylsilane + PDC + 5' NH₂-PCR product	Glass slide	157 nt / 182 nt	6×10^{12} to 3×10^{13}	Some	3 h	30 °C, 20-50 nM PCR product, 5x SSPE, 0.5% SDS
Graves et al.[49]	NH₂ propylsilane + PDC + 5' amino oligo/ PCR product	Glass slide	15 nt / 15 nt	1×10^{12} (appx.)	Some	3-6 h	46 °C, 2 µM oligo, 0.9 M NaCl, 0.06 M NaH₂PO₄, 6 mM EDTA, pH 7.4
Chrisey et al.[36]	NH₂ silane + SMPB + 3' SH-oligo	Si/SiO₂, Fused silica	20 nt / 20 nt	1.2×10^{13}	Some	2 h	25°C, 1µM oligo, 10 mM HEPES, 5 mM EDTA buffer
Strother et al.[42]	(NH₂-decene + dodecene) + SSMCC + SH-oligo	Si (001)	16 nt / 16 nt	2.3×10^{12}	Yes	30 min	25 °C, 2 µM oligo, 2x SSPE, 0.2% SDS
Cavic et al.[44]	(SH-silane + Alkane silane) + BMH + 3' SH-oligo	Si/SiO₂	25 nt / 25 nt	2×10^{13}	Yes	1.5 h	25 °C, 20 µM oligo, 10 mM Tris-HCl, 1 mM EDTA, 1.5 M NaCl
Tarlov et al.[32,41]	(5' SH-oligo + mercapto hexanol)	Au-coated silicon	25 nt / 25 nt	5.7×10^{12}	Yes	90 min	24°C, 1µM oligo, 10mM Tris-HCl, 1 mM EDTA, 1 M NaCl
Our system[46]	(OH-silane + alkane silane) + oligo synthesis	Si/SiO₂, Glass slide	12 nt / 12 nt	$\sim 3 \times 10^{13}$ (optim.)	Yes	24 h	4°C, 0.5 µM oligo, 1 M NaCl, 0.1 M Na citrate, 0.1% SDS

PDC- Phenylenediisothiocyanate
HEPES- N-2-hydroxyethylpiperazine-N'-2-ethanesulfonic acid
Tween- Polyoxyethylene sorbitan monolaureate
DMT-HEG- Dimethoxy trityl hexaethylene glycol
SSMCC- Sulfo-succinimidyl 4-(N-maleimidomethyl) cyclohexane-1-carboxylate

SMPB- Succinimidyl 4-[maleimidophenyl] butyrate
EDTA- (Ethylenedinitrilo) tetraacetic acid
SDS- Sodium dodecyl sulphonate
BMH- Bis(maleimido) hexane
nt - nucleotide

Chapter 2.   Introduction – DNA-Directed Assembly

2.1 Self-assembly

Self-assembly—the formation of often complex supramolecular structures by non-covalent interactions—remains a powerful strategy for manipulating chemical systems and their properties. The broad use of surfactants, the generation of micro-domains within block co-polymers, and the folding of polypeptide chains into proteins are examples where local interactions between individual molecules or segments produce such assembled structures. The strength of the specific interactions that drive self-assembly within a system play a key role in defining the effects that temperature and concentration have on the integrity of such structures and their tolerance of other present chemical species. In many cases, self-assembly is guided by the generic preference for one species type (charged, polar, non-polar) for its counterpart (as in the case of charged species[1-5]) or its kin (as for polar and non-polar species[6]), with these interactions being quite general. Indeed, most synthetic self-assembled systems are based on the inclusion of two interactions where a molecular fragment or polymer segment A strongly prefers to interact with A over B and similarly B prefers to interact with B over A. Synthetic systems that expand this local complexity of interactions to include a third or more components are limited by mutual complementarity for specificity or preference. Candidate possibilities for providing this driving force for self-assembly include the use of metal ligation[7-10] along with highly specific biomolecular systems using proteins[11], antibodies[12], DNA or other species.

The richness present in biology provides motifs for self-assembly that are compatible with water and that themselves can operate independently and in the presence of a wide range of other species. Of these, oligonucleotides offer the specific advantage that their intermolecular self-assembly depends directly on primary sequence information, in contrast with that for

polypeptide-based systems that involve secondary and tertiary structures resulting from specific folding events that rely on polar and non-polar interactions. Further, the rules and energetics for their assembly are straightforward and much better understood than are de novo approaches to predicting peptide folding and recognition based on primary sequence. To be useful, a critical element for the consideration, adoption, and broader inclusion of such motifs within synthetically prepared self-assembling systems is their widespread availability and easy tailorability. Advances in molecular biology have led to the development of routine methods for the synthetic preparation of oligonucleotides by automated means. In fact, the on-demand custom synthesis of oligonucleotides by commercial vendors has become a routine part of many genetic investigations and has been a key element underlying the rapid growth in this area. Their availability has led to the design of unnatural self-assembling systems that incorporate oligonucleotide sequences.

The top-down methods of device manufacture are now approaching their physical limits as far as the lateral resolution of functional components is concerned. E-beam lithography and extreme UV lithography (EUVL) may enhance the resolution further, but entirely different ways of manufacturing devices need to be invented to maintain further pace with Moore's law. Researchers are now increasingly looking at novel bottom-up ways to create faster, denser, and more energy efficient devices.[13] One of the key areas—directed assembly—involves the assembly of nano-sized components in a highly parallel fashion into predetermined forms, based on the instructions programmed onto their surfaces. DNA hybridization has features which will be beneficial for use in bottom-up assembly techniques.

2.2 Properties of DNA

Each strand of DNA is a linear oligoanion (polyanion) made up of nucleotides. Each nucloetide consists of a sugar moiety, a negatively charged phosphate linkage, and a base. The diameter of the duplex DNA is around 2 nm and each nucleotide is 0.34 am long. The bases— adenine (A), guanine (G), cyotsine (C), and thymine (T)—are responsible for the highly specific interactions between two anti-parallel DNA strands. The base pairing between A-T and C-G occurs via hydrogen bonding (see Figure 2-1) and can be dissociated by thermal energy and other denaturating agents. At its melting temperature T_m, 50% of the strands are in the dissociated state. The melting temperature of a sequence depends on the GC content, salt concentration, presence of mismatch, and DNA length. The dissociated DNA strands can be annealed back together if the temperature is reduced below T_m. In the duplex form, the DNA strands have high mechanical rigidity owing to the helical structure.

Advances in DNA synthesis now provide routine access to sequences of selectable properties. For example, programmable automated synthesis using phosphoramidite chemistry allows direct chemical synthesis of oligonucleotides where a broad range of non-natural agents (dyes, polymerizable groups, etc.) can be included in the synthesized DNA strands. In addition, small amounts of DNA can be amplified readily by the polymerase chain reaction (PCR) and various naturally existing enzymes (ligases, nucleases, polymerases, etc.) can be used to modify DNA. The aqueous compatibility of DNA allows facile handling and manipulation for self-assembly.
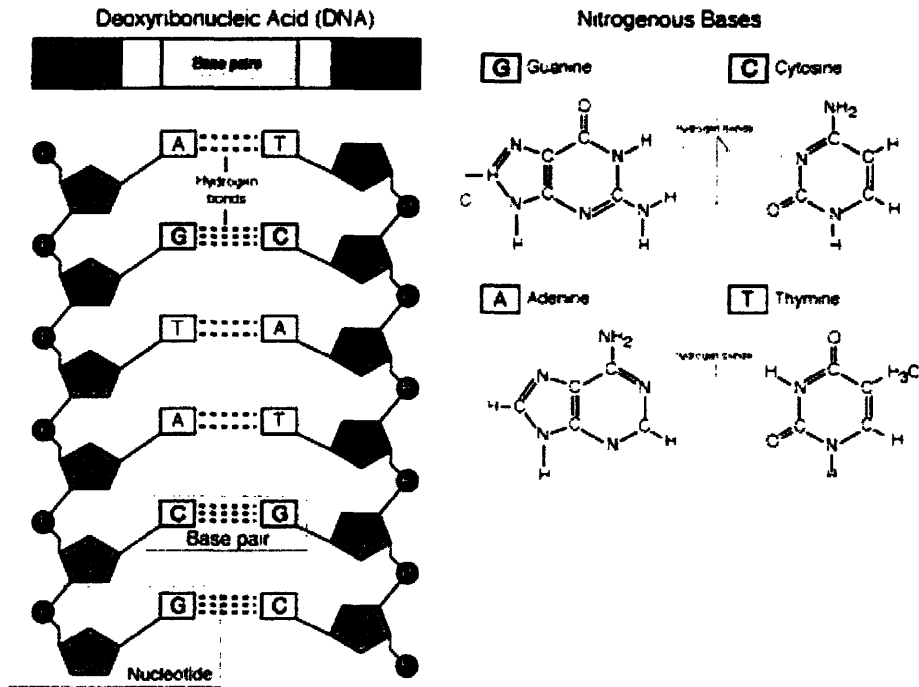
Figure 2-1 Structure of double stranded DNA and the hydrogen binding characteristics of the bases G, C , A, and T.

2.2.1 DNA immobilization

A key requirement for using DNA-directed assembly is the ability to functionalize various agents and surfaces with DNA molecules. Substantial research has been done on immobilizing DNA onto different substrates. As discussed in Chapter 1, an ideal immobilization scheme should not hinder or modify the fundamental properties of the nucleic acids. Immobilizations can be achieved either by synthesizing oligonucleotides (oligos) on ae surface or by spotting pre-synthesized oligonucleotides or cDNAs (complementary DNAs) onto a surface. After suitable derivatization, DNA can be immobilized onto glass,[14] silicon,[15,16] gold,[17] aluminum,[18] indium tin oxide,[19] and other substrates. The immobilization can occur via covalent or non-covalent interactions, and occurs either through the phosphate groups, the bases or the terminating 3' or 5' end. As regards the point of attachment, end-immobilization through either the 3' or 5' end seems to be the best option as the resulting structure allows almost all the bases to freely interact with the medium. Reactive groups for surface immobilization can be added to the 3' or 5' end of a DNA/oligonucleotide during phosphoramidite synthesis or PCR. These end-functionalized DNA/oligonucleotides can then be attached to functionalized surfaces/species directly or through a crosslinker. The DNA attachment to gold is normally accomplished using the thiol-Au linkage.[17] Silanes are commonly used for immobilizing DNA on glass and silicon surfaces. The avidin-biotin interaction has been used for attaching oligonucleotides to a variety of biological species including proteins, enzymes, and antibodies. Surface functionalization chemistries using mixed monolayers can provide substantial control over the density and orientation of the immobilized DNAs. High-density patterned DNA arrays containing up to 1,000,000 different sequences per cm^2 can be generated either by using photolithography[20] and

phosphoramidite synthesis, inkjet printing[21] or by successive attachment of pre-synthesized DNA by robotic devices.[22]

2.3 Advantages of DNA-directed assembly

DNA-DNA sequence complementarity provides a large number of specific interactions that can be used to program components with instructions for their directed assembly. For instance, 20^4 different specific interactions are possible if we limit the overlap length of the assembling DNA molecules to 20 nucleotides. The ease of DNA synthesis and the ability to incorporate novel precursors into the phosphoramidite synthesis gives access to oligonucleotides with novel chemical reactivities. Automated synthesis allows the synthesis of DNA sequences with a variety of lengths (up to 60 bases) which would further increase the range of possible specific recognition motifs. Various enzymes can be used for post-assembly modifications of DNA strands. Keating et al.[23] have demonstrated the enzymatic extension of nanoparticle-bound oligonucleotides. Josephson et al.[24] have used restriction endonucleases to disassemble magnetic nanoparticles bound by complementary DNA strands. The strength of the DNA-DNA interactions can be modulated by the length of the hybridizing DNA strands, the DNA sequence, and environmental conditions such as salt and pH. These factors provide additional tools to regulate the assembly process. As various surface chemistries have been developed to immobilize DNA onto metal, semiconductor, insulator, polymer surfaces, building blocks of various kinds can be functionalized with DNA strands for use in the DNA-directed assembly process.

2.4 DNA-directed assembly of biomolecular fragments

For various diagnostic and biosensor applications, highly specific, functional biological moieties such as enzymes and antibodies need to be immobilized on solid surfaces. To fabricate

spatially-defined active biomolecule arrays, the immobilization strategy should be site-specific and should not affect the activity of the biomolecules. DNA-mediated assembly uses DNA fragments, which are easier to handle than other biomolecules, for lateral patterning. The generation of these biomolecular arrays has been one of the motivations behind the investigations of biomolecule assembly by DNA hybridization.

As discussed in Chapter 1, DNA microarrays have gained immense importance in various biological and medical laboratories for gene expression analysis and SNP analysis.[25] These microarrays involve the self-assembly of DNA fragments from solution onto their complementary sequences on a substrate surface. The identity of the self-assembled DNA fragments is then determined by the location of their attachment. Double-stranded DNA (dsDNA) arrays,[26,27] useful for studying dsDNA-protein interactions, can also be assembled using this technique.

Niemeyer and coworkers (at the University of Bremen) have done pioneering work in extending this DNA-based assembly process to the self-assembly of enzymes, antibodies and other species. Figure 2-2 shows the basic principle used in these DNA-directed assemblies. A streptavidin molecule is chemically attached to the 3' or 5' end of the DNA fragments. These streptavidin-tagged DNA strands can then be attached to biotinylated biomolecules through a streptavidin-biotin linkage. Biotin-streptavidin system was selected because of its high thermal and chemical stability and because mild chemical procedures can be used to biotinylate various biomolecules. These DNA-tagged biomolecules were then assembled to their complementary DNA strands on the surface with the DNA serving as the specific recognition domain. Niemeyer et al.[28] formed DNA-tagged immunoglobins using the streptavidin-biotin linkage and allowed them to hybridize on an array of complementary capture oligonucleotides. The self-assembly

was validated by means of specific immunosorption of target molecules. In another study, biotinylated enzymes such as alkaline phosphatase, b-galactosidase, and horseradish peroxidase were coupled to DNA-streptavidin adapters, and the resulting preconjugates were allowed to hybridize to complementary, surface-bound capture oligonucleotides.[29] Alkaline or thermal denaturation of the DNA double helix can selectively remove the self-assembled biomolecules. This feature makes the self-assembly process reversible and leads to easy reuse and reconfiguration of the sensor chips.

Since one streptavidin molecule can attach to four biotin molecules, multiple biomolecules can be attached to each DNA strand. Niemeyer et al.[30] functionalized streptavidin-modified DNA with two different biomolecules by adding a biologically active compound such as an enzyme, followed by saturation of the remaining sites with a low-molecular weight species that enhance the biological activity of the active compound (cofactors) or that provide additional functionality (fluorophores). These self-assembly principles can also be used to form a linear array of biomolecules along a single strand of a long DNA with the biomolecules tagged with sequences complementary to different regions on the template strand. This linear assembly of biomolecules can be particularly useful in the formation of multi-enzyme complexes. The controlled proximity of the various catalytic enzymes can accelerate the multistep catalytic transformation of a substrate.[31] Various other species, like viruses,[32] microtubules,[33] and block copolymers[34] etc. have also been functionalized and assembled using DNA-DNA interactions.

The specific interaction between the complementary strands of DNA can be used to construct supramolecular structures through modular assembly. Seeman's group (at New York University) has been involved in the construction of various DNA structures such as DNA knots, Holliday junctions, 2-D DNA crystals, DNA quadrilaterals, octahedrons etc. by using branched

DNA molecules as building blocks. Initially, they attempted creating repetitive structures from DNA using three-arm junctions followed by enzymatic ligation of the "sticky ends". This procedure yielded a mixture of linear and cyclic oligomers. They extended this strategy to four-, five-, and six-arm junctions. The inability to generate large repetitive structures highlighted the flexibility of these molecules as a possible impediment to large-scale assembly to form 2-D crystals. An improvement in yields and simplification in the assembly procedure was done by employing a solid-support based methodology to create geometrical objects.[35] Here, one of the edges of the structure is synthesized on a solid support and the remaining edges are later added one after another with necessary enzymatic modification steps. The arm attached to the support is like an "umbilical arm" which helps retain the structure on the surface and eases the separation of reactants and products with reduced cross talk between adjacent structures. The flexibility of the building blocks was reduced by using double-crossover[36] (DX) and triple-crossover[37] (TX) molecules (see Figure 2-3). Double-crossover molecules are analogues of intermediates in meiosis that consist of two side-by-side double-stranded helices linked at two crossover junctions. Using tetravalent DX molecules, the group reported the assembly of two-dimensional crystalline forms as large as 2 x 8 μm with uniform thickness between 1 and 2 nm. They have also performed a cumulative XOR operation on a string of binary bits using one-dimensional algorithmic self-assembly of DNA triple-crossover molecules.[38] LaBean et al.[39] have created nanoribbons and 2-D nanogrids with periodic square cavities using four four-arm DNA junctions. They also guided the assembly of streptavidin onto biotinylated nucleotides located at specific locations on these organized nanostructures (Figure 2-4).
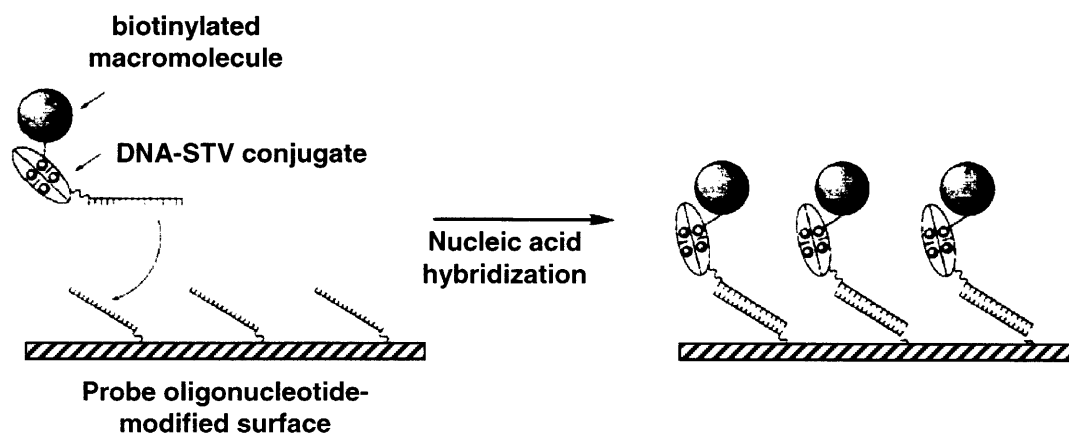
Figure 2-2 Schematic representation of the DNA-directed assembly of biomolecules to probe oligonucleotides immobilized on a surface. The biotinylated biomolecules to be assembled are attached to biotinylated DNA strands via streptavidin molecules. Upon hybridization, the biomolecules are located at specific locations based on the complementarity of their coding DNA strands (Adapted from Niemeyer et al.[29]).
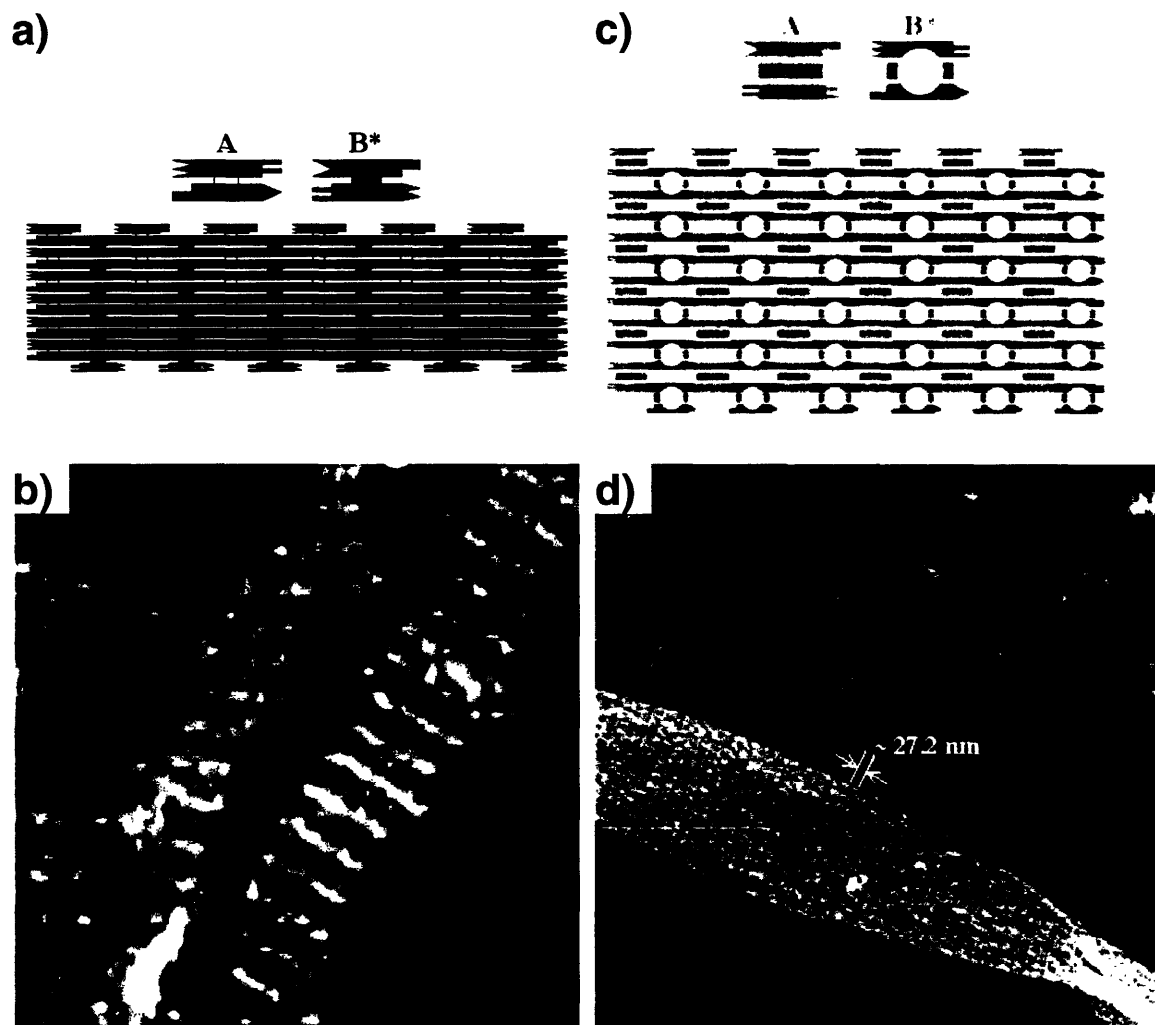
Figure 2-3 Double crossover (DX) and triple crossover (TX) molecules and their assemblies. A and B* are double crossover (DX) and triple crossover (TX) molecules in (a) and (c), respectively. B* has a hairpin structure that projects out of the plane of the helices. On mixing, A and B* form 2-D arrays based on the interactions of the 'sticky ends'. (b) and (d) represent the AFM images of the hydrogen-bonded 2-D arrays (several microns long and hundreds of nanometers wide) formed by mixing the two DX molecules and the two TX molecules respectively. The rows of projecting hairpins appear as stripes when visualized by AFM. (Source: http://seemanlab4.chem.nyu.edu)
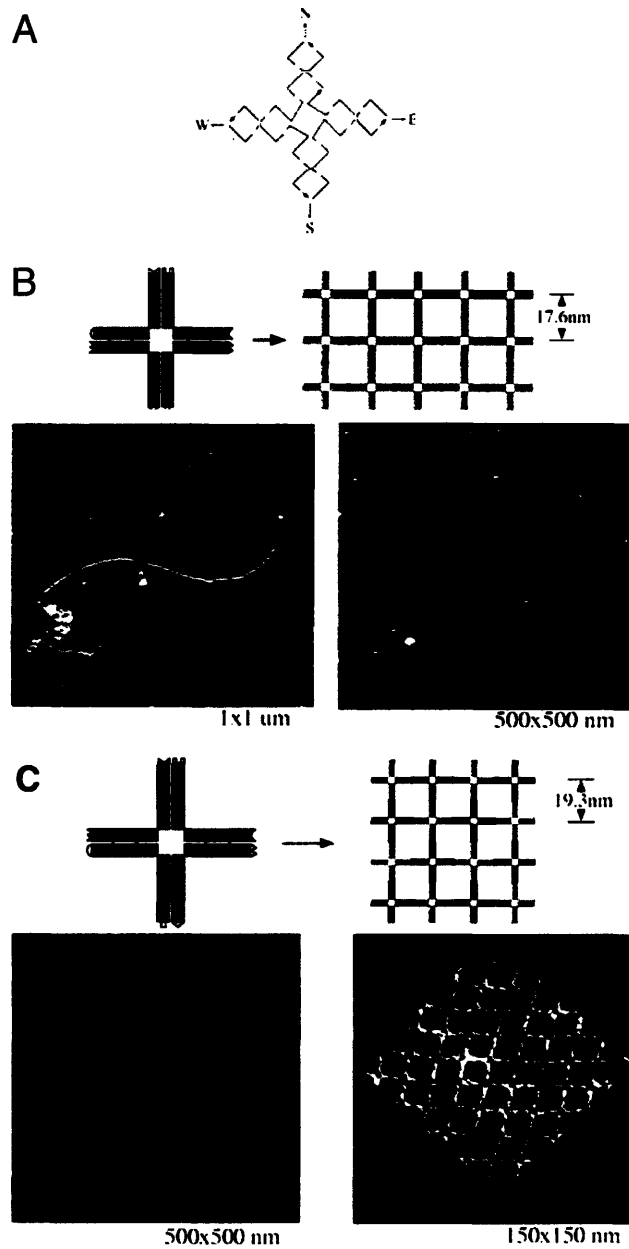
Figure 2-4 Self-assembly of DNA nanoribbons and nanogrids using a 4 x 4 DNA tile. (**A**) The 4 x 4 tile strand structure. The tile contains nine oligonucleotides, shown as simplified backbone traces. (**B**) Self-assembly of nanoribbons with original design. Upper left: Double-helical domains are illustrated as rectangles, and paired rectangles represent four-arm junctions. Upper right: Designed structure of self-assembled lattice. Bottom: AFM images of the nanoribbons. (**C**) Self-assembly of 2D nanogrids with corrugated design. Upper left: The component tile is drawn similar to that in B. Upper right: Corrugated self-assembled structure. Bottom: AFM images of the 2D lattices (nanogrids) formed from the corrugated design. (Adapted from LaBean et al.[39])

2.5 DNA-directed assembly of solid-state systems

In the previous section, various self-assembly schemes of biomolecules using DNA hybridization were discussed. In this section, I will discuss more about the assembly of inorganic and polymeric structures using DNA. Mirkin and coworkers (at Northwestern University) have published a significant amount of work in this area with particular emphasis on the assembly of metal and semiconductor nanoparticles. The assembly of these inorganic materials has been facilitated either by DNA hybridization or by using the polyanionic network of DNA as a template for synthesis and assembly.

Mirkin et al.[40] and Alivisatos et al.[41] were among the first to report the assembly of nanoparticles using DNA hybridization. In their first paper, Mirkin et al.[40] described a method to rationally and reversibly aggregate 13-nm gold nanoparticles. They attached different DNA sequences to two batches of the nanoparticles and used a linking duplex DNA with "sticky ends" to aggregate them. They observed that the color of the gold sol turned from red to purple immediately upon addition of the linking DNA and later turned colorless with the precipitation of the hybridized aggregate (Figure 2-5). They extended this technique to self-assemble nanoparticles of different types[42] and different sizes[43]. With careful choice of the ratio of the two different-sized oligonucleotide-functionalized nanoparticles, they were able to create satellite structures (Figure 2-6). They also observed a much sharper melting curve for the DNA-linked nanoparticle network as compared to that without the nanoparticles. They have also demonstrated the interparticle assembly of quantum dots (CdSe) by DNA hybridization. The assembly of nanoparticles by DNA hybridization can also be performed on planar solid surfaces in a stepwise manner to create multilayers of nanoparticles with controlled interlayer distances and particle periodicities.[44] Niemeyer et al.[45] have created oligofunctional DNA-Au nanoparticle

51

conjugates by functionalizing the nanoparticles simultaneously with multiple thiolated DNA sequences. These multifunctional nanoparticles can be assembled to create controlled multilayer nanoparticle structures. However, the functionalities on these particles are randomly located and thus these particles cannot be used to generate designed nanostructures based on the spatial arrangement of the functionalities. Mirkin et al.[44] have shown that the layer-by-layer assembly of nanoparticles can be used to design DNA-detection schemes with enhanced sensitivity because of the sharper melting profile for even a single layer of DNA-linked nanoparticles on a glass surface. Based on this principle, they have developed a scanometric detection scheme for DNA hybridization on combinatorial arrays.[46] They have shown that the labeling of the oligonucleotides with nanoparticles and subsequent detection with a flatbed scanner has thrice the selectivity to detect single mismatches over conventional fluorescence-based methods. In addition, signal amplification by silver deposition on the gold nanoparticles yielded a 100-fold increase in sensitivity over fluorescence-based systems (Figure 2-7).

In another approach, they have used the nanoparticle-based assembly to recognize multiple proteins in one solution.[47] Each hapten (protein-recognition element) is functionalized with a unique oligonucleotide and is prehybridized to the oligonucleotide attached to a nanoparticle. Once the protein is involved in the nanoparticle network through hapten binding, the specific proteins can be detected either by the thermal denaturation profile of the nanoparticle assembly or by dehybridizing the entire network and detecting the linker oligonucleotides on a DNA microarray. They have recently expanded this approach to create a powerful technique for ultrasensitive detection of proteins (see Figure 2-8).[48] In this method, they functionalized magnetic microparticles with antibodies that bind specifically to a target protein (PSA). Additonally, they prepared Au nanoparticles functionalized with antibodies and a dsDNA probe

that encoded for the particular protein. They captured the target protein by sandwiching it between the antibodies immobilized on the microparticles and nanoparticles. The particles were magnetically separated from the unreacted components. Later, they dehybridized the 'bar-code' dsDNA and detected the strands using scanometric detection. With this technique, they could detect the target protein (PSA) at attomolar concentrations, six orders of magnitude more sensitive than conventional assays. This method shows the applicability of DNA-functionalized probes for ultrasensitive detection of proteins. Most of the work in the field of DNA-mediated nanoparticle assembly has been restricted to gold nanoparticles because of the ease of immobilizing DNA on gold nanoparticles by the Au-thiol linkage and the ease of synthesis of gold nanoparticles of different sizes. The range of work done by the Mirkin lab shows the versatility of the DNA-directed assembly of nanoparticles and its wide-ranging applications. Niemeyer et al.[49] have also explored the assembly of biometallic nanostructures by biotinylating the metal nanoparticles, attaching them streptavidin-tagged oligonucleotides, and finally assembling these particles on complementary portions of a long DNA strand.

There have been various studies to exploit the polyelectrolyte nature of the DNA and use it as a template for synthesis. Braun et al.[50] have used a DNA molecule as a template for the vectorial growth of a 12 μm long, 100 nm wide conductive silver wire (see Figure 2-9). Two gold electrodes separated by a distance of 12-16 μm were functionalized with 12-mer oligonucleotides complementary to the ends of a 16 μm long and fluorescently labeled λ-DNA. Hybridization of the λ-DNA was carried out on the ends of the electrodes followed by the deposition of silver. The templated deposition of silver on the DNA involved the following steps: Ag^+/Na^+ ion exchange followed by reduction with basic hydroquinone and finally further silver development to yield the coarse grain structure. AFM images showed the silver wire

deposited along the DNA backbone with grains of 30-50 nm in diameter. Extensive silver deposition reduced the non-linear I-V characteristics of the wire to give an almost ohmic behavior at voltages greater than 50 V. This approach can be applied for the construction of nanometer-scale circuits using DNA. He et al.[51] have utilized the dsDNA strands as templates for the synthesis of polyaniline conducting nanowires. Coffer and coworkers used the phosphate backbone to assemble Cd^{2+} ions.[52] These ions were reduced using Na_2S to yield CdS nanoparticles along the backbone with an average diameter of 5.6 nm as revealed by high-resolution TEM analysis. Positively charged CdS nanoparticles,[53] polycations,[54] positively charged fullerene molecules,[55] and organic molecules containing cationic side-chains[56] have also been assembled by electrostatic interactions along the negatively-charged phosphate backbone of DNA molecules.
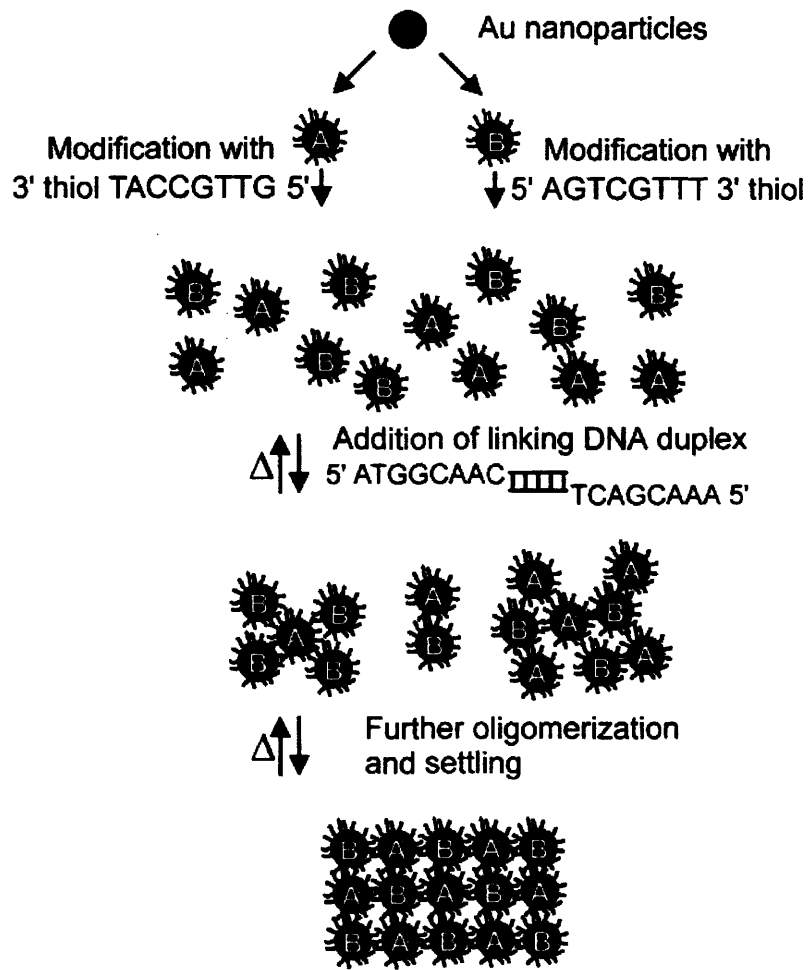
Figure 2-5 Schematic illustration of the DNA-directed assembly of colloidal nanoparticles. Two sets of nanoparticles functionalized with different sequences are prepared. When the solutions of these particles are brought in contact in the presence of a linker DNA molecule complementary to both the DNA strands, the nanoparticles agglomerate and change their color from red to blue. (Adapted from Mirkin et al.[40])
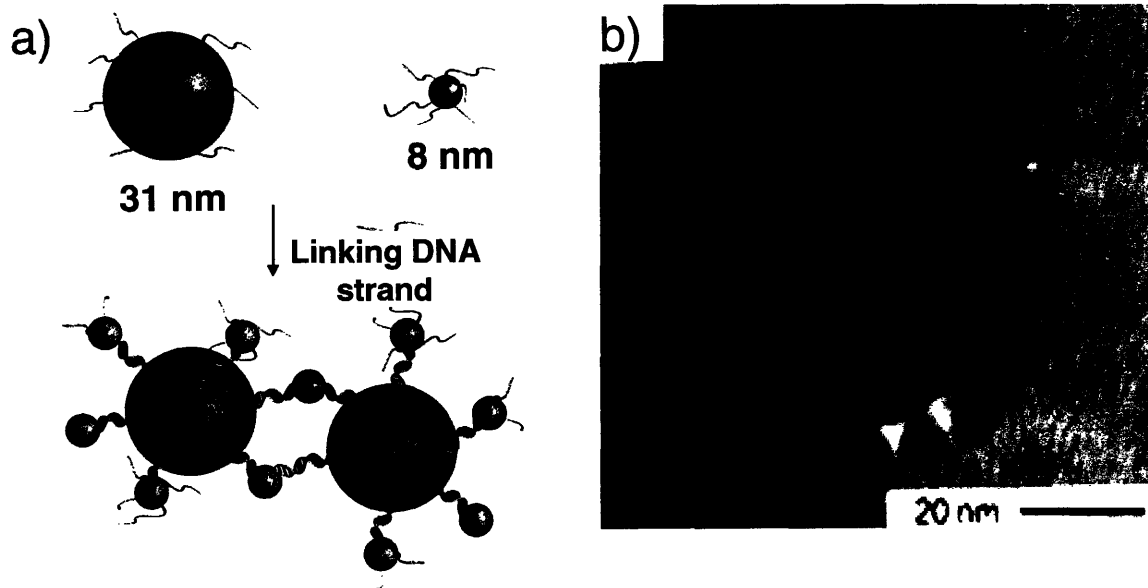
Figure 2-6 Schematic representation of the DNA-directed binary nanoparticle assembly. (a) DNA-functionalized nanoparticles of two different sizes (31 nm and 8 nm) are brought together in the presence of a linker molecule complementary to the DNA on both the particles. (b) TEM image of the satellite structures formed at specific concentration ratios of the two nanoparticle solutions. (Adapted from Mirkin et al.[43])
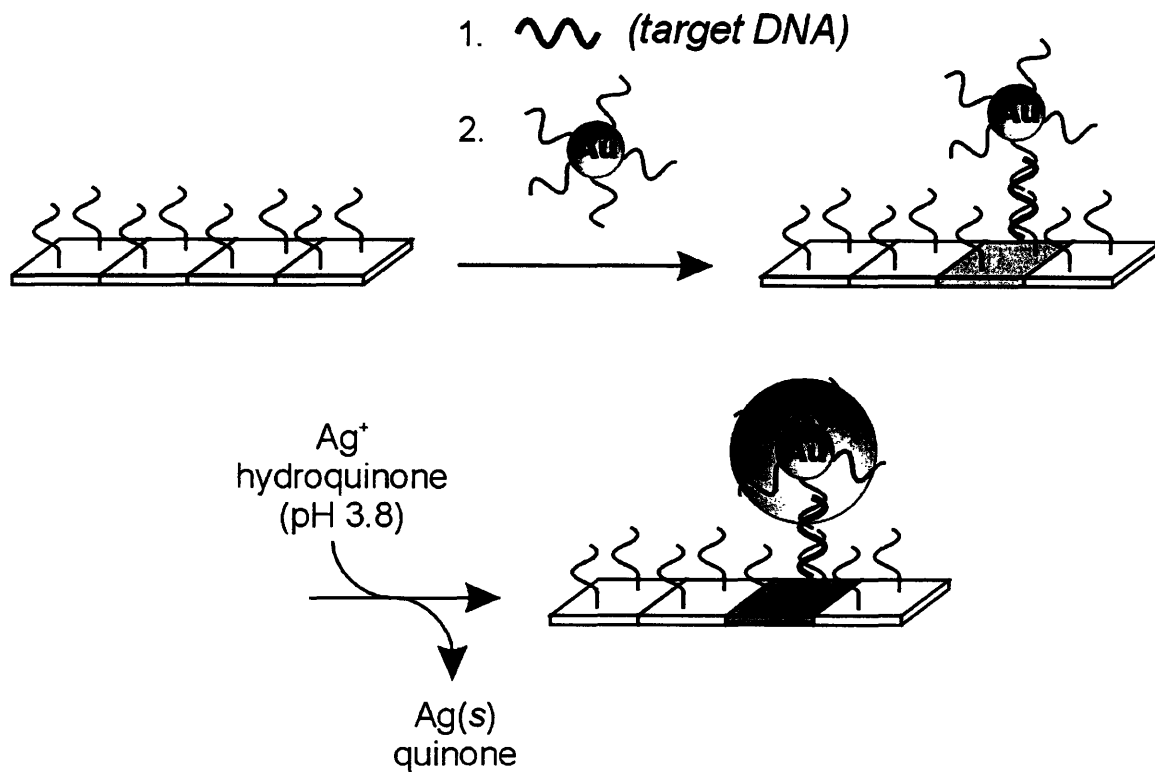
Figure 2-7 Schematic representation of the scanomteric detection of DNA surface hybridization. The target oligonucleotides are sandwiched between the probe molecules immobilized on the surface and the DNA-tagged nanoparticles. Signal amplification is carried out by reducing silver ions by hydroquinone to silver metal. The silver enhancement step leads to a substantial increase in sensitivity. (Adapted from Mirkin et al.[46])
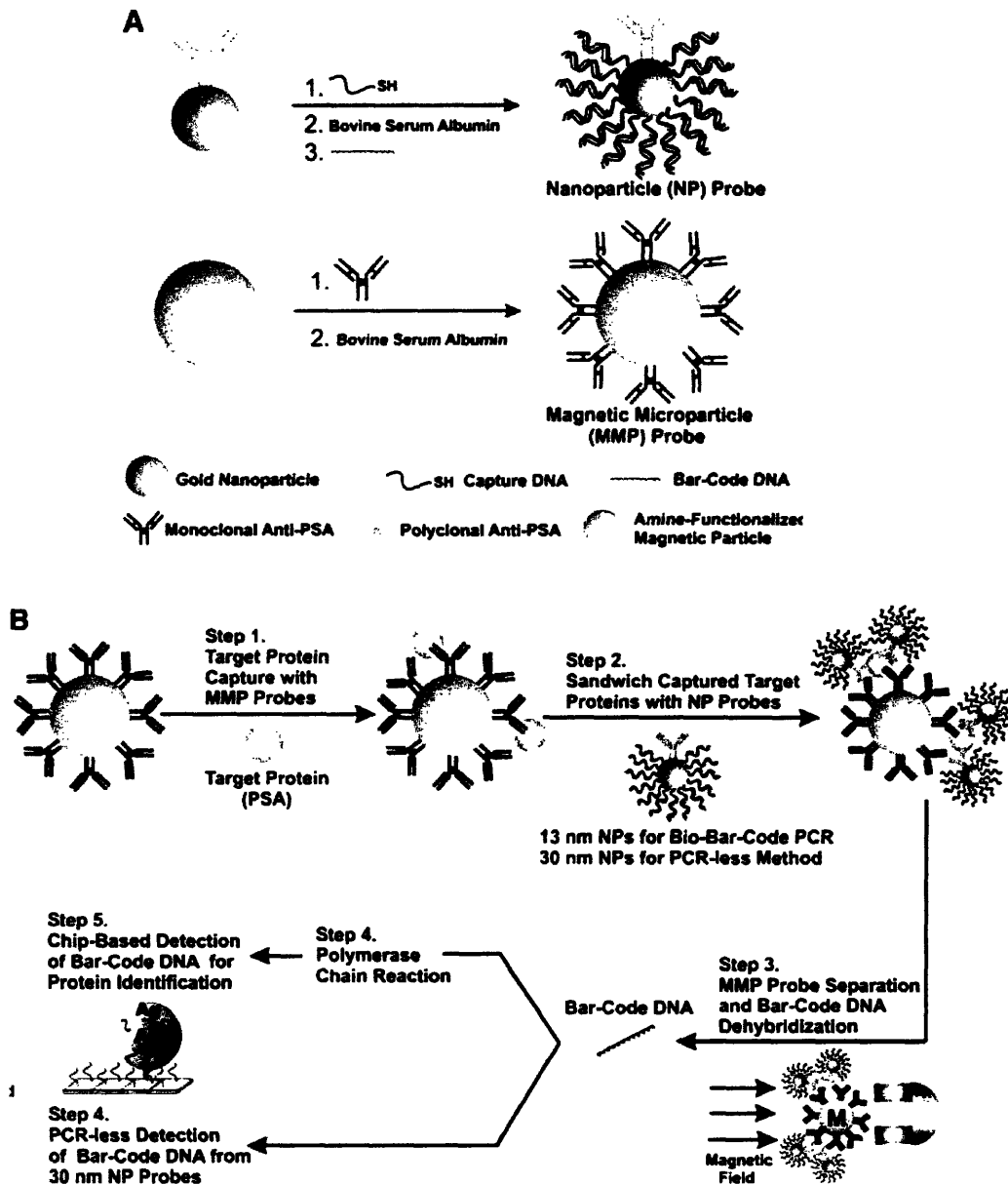
Figure 2-8 Schematic illustration of the ultrasensitive detection of proteins using DNA-tagged nanoparticles. (A) Derivatization of the nanoparticles (NPs) with bio-barcode DNA and antibodies and of the magnetic microparticles (MMPs) with antibodies. (B) Target capture by sandwiching between the MMPs and NPs. Magnetic separation of the particles from the unreacted components followed by the release of the bio-barcode DNA. The barcode DNA is then detected using scanometric detection technique with or without PCR leading to a highly sensitive detection of the proteins. (Adapted from Mirkin et al.[48])
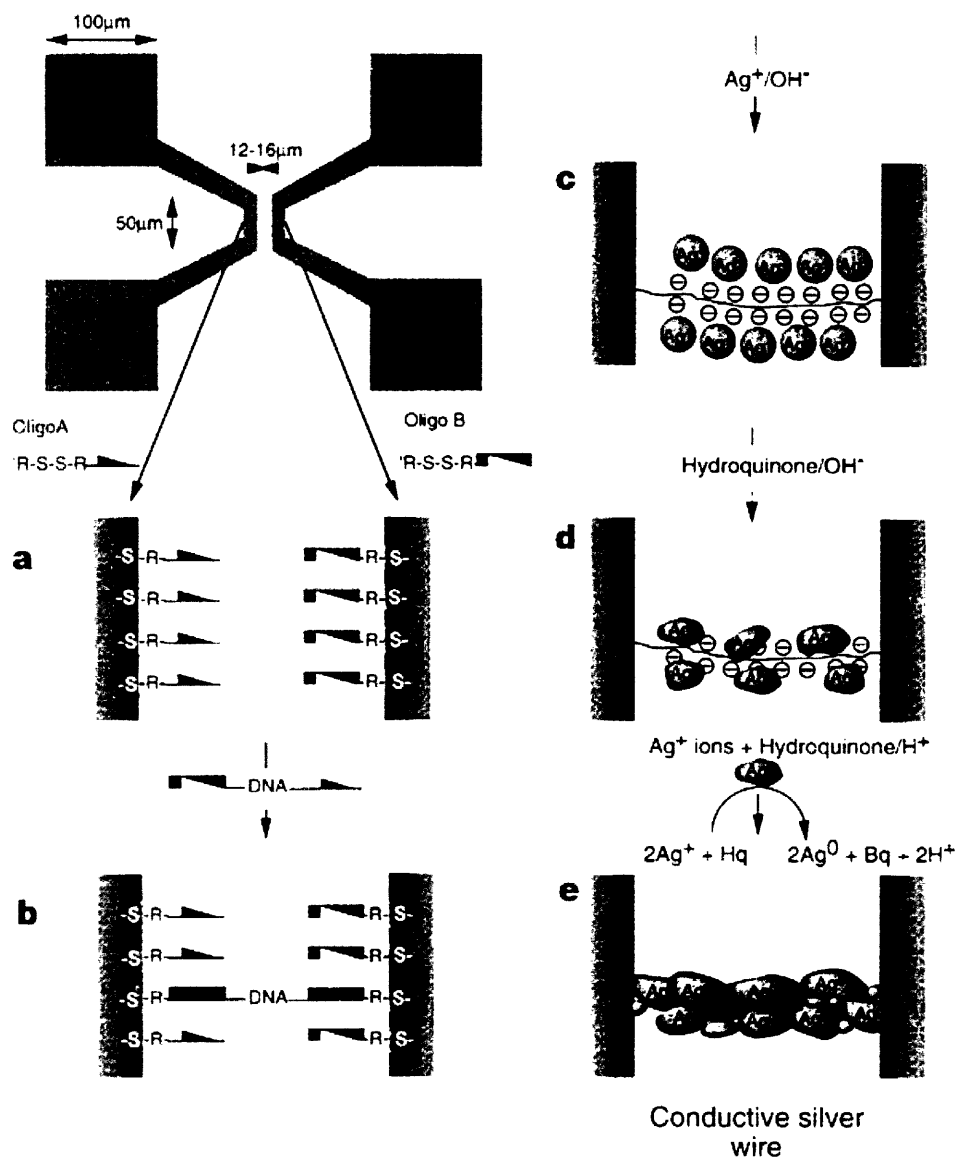
Figure 2-9 Scheme showing the metallization of dsDNA to construct a conductive silver wire connecting two gold electrodes. (a) Oligonucleotides with two different sequences attached to the electrodes. (b) The DNA template (λ-DNA) assembled on the two gold electrodes via its 'sticky ends'. (c) Ag⁺/Na⁺ ion-exchange to load the DNA bridge with silver ions. (d) & (e) Reduction of the silver ions to create a conductive silver wire on the DNA template. (Adapted from Ben-Yoseph et al.[50])

59

2.6 DNA-directed meso-to-micro-scale assembly

DNA hybridization has also been used to direct assembly of meso-scale and micro-scale objects on solid surfaces. Mallouk et al.[57] have reported the DNA-directed assembly of gold nanowires of 0.2 μm in diameter and up to 6 μm in length on complementary surfaces. They have also demonstrated that the gold nanowires can be exclusively functionalized with DNA only at their tips or at desired lengths on the ends using passivating layers to cover the remaining portion of the wires. This site-selective functionalization was validated by performing hybridization with a fluorescently labeled target DNA. This ability to functionalize the gold nanowires at selective portions can help in forming 1-D, 2-D, and 3-D structures and the tip-functionalization procedure can potentially lead to "self-wiring" of the gold nanowires. Natan et al.[58] have synthesized multimetal microrods using sequential electrochemical deposition of metal ions and used them for assembly of DNA molecules. The different regions of the microrods were distinguished by the differences in their optical reflectivities. Bashir et al.[59] have functionalized micron-sized objects created using silicon-on-insulator technology with DNA and assembled them electrophoretically on positively charged regions. They, however, did not use the complementarity of the DNA sequences as a means for assembly. Esener et al.[60] have reported the successful assembly of microbeads functionalized with four different sequences on a surface with a pattern of the four complementary sequences. The process of self assembly can be expedited by directed-electrophoretic transport.[61] The electrophoretic site-selective concentration leads to rapid transport of DNA or DNA-tagged objects and greatly helps the self-assembly process.

2.7 Motivation

The motivation for my thesis work was to explore the assembly of novel building blocks using DNA-DNA interactions. Previous work in this field had been mostly limited to assembling nano-scale structures. The future of directed assembly would follow a modular format wherein nano-scale structures are assembled on micron-scale features which are then assembled and coordinated to create the functional devices. Further research was needed into understanding the various parameters affecting the assembly of micron-scale structures by the rather weak DNA-DNA interactions. Additionally, asymmetric building blocks have the potential to facilitate a higher level of organization and hierarchy into the assembled structures. The asymmetry can be either in composition, shape, or functionality or any combination of these. I wanted to demonstrate the DNA-directed assembly on both the micron and nano scales, adding complexity by means of shape asymmetry as well as by programming multiple functionalities on the building blocks. The higher the number of different specific interactions programmed into an directed-assembly system, the lesser will be the number of steps required for constructing the assembled structure.

In Chapter 3, I discuss the results from my studies on the effects of probe density on the kinetics and thermodynamics of DNA surface hybridization. Chapter 4 discusses the effects of probe density on the DNA-directed assembly of nanoparticles. It also illustrates the difference in the thermodynamics of DNA-directed nanoparticle adsorption vs. molecular DNA adsorption. Chapter 5 explores the effect of shape on the DNA-directed assembly of microparticles and demonstrates the orientation-specific assembly of dual-functional microrods. Chapter 6 describes the shadow deposition method for creating dual- and tri-functional microspheres and their use in the orthogonal assembly of fluorophore-tagged DNA molecules. Chapter 7 extends

this concept of orthogonal assembly of species by DNA interactions to demonstrate the regio-specific assembly of nanoparticles of two different sizes onto the two sides of dual-functional particles.

2.8 References & Footnotes

(1) Wang, H.; Wang, C. C.; Lei, C. X.; Wu, Z. Y.; Shen, G. L.; Yu, R. Q. *Anal. Bioanal. Chem.* **2003**, *377*, 632-638.

(2) Zhu, T.; Fu, X. Y.; Mu, T.; Wang, J.; Liu, Z. F. *Langmuir* **1999**, *15*, 5197-5199.

(3) Bhat, R. R.; Fischer, D. A.; Genzer, J. *Langmuir* **2002**, *18*, 5640-5643.

(4) Bhat, R. R.; Genzer, J.; Chaney, B. N.; Sugg, H. W.; Liebmann-Vinson, A. *Nanotechnology* **2003**, *14*, 1145-1152.

(5) Bhat, R. R.; Tomlinson, M. R.; Genzer, J. *Macromol. Rapid Commun.* **2004**, *25*, 270-274.

(6) Srinivasan, U.; Liepmann, D.; Howe, R. T. *J. Microelectromech. Syst.* **2001**, *10*, 17-24.

(7) Laibinis, P. E.; Hickman, J. J.; Wrighton, M. S.; Whitesides, G. M. *Science* **1989**, *245*, 845-847.

(8) Lehn, J. M. *Science* **1985**, *227*, 849-856.

(9) Lehn, J. M. *Science* **2002**, *295*, 2400-2403.

(10) Sun, F.; Castner, D. G.; Mao, G.; Wang, W.; McKeown, P.; Grainger, D. W. *J. Am. Chem. Soc.* **1996**, *118*, 1856-1866.

(11) Olofsson, L.; Rindzevicius, T.; Pfeiffer, I.; Kall, M.; Hook, F. *Langmuir* **2003**, *19*, 10414-10419.

(12) Tang, D. P.; Yuan, R.; Chai, Y. Q.; Zhong, X.; Liu, Y.; Dai, J. Y.; Zhang, L. Y. *Anal. Biochem.* **2004**, *333*, 345-350.

(13) Service, R. F. *Science* **2001**, *293*, 782-785.

(14) Shchepinov, M. S.; CaseGreen, S. C.; Southern, E. M. *Nucleic Acids Res.* **1997**, *25*, 1155-1161.

(15) Strother, T.; Hamers, R. J.; Smith, L. M. *Nucleic Acids Res.* **2000**, *28*, 3535-3541.

(16) Strother, T.; Cai, W.; Zhao, X. S.; Hamers, R. J.; Smith, L. M. *J. Am. Chem. Soc.* **2000**, *122*, 1205-1209.

(17) Herne, T. M.; Tarlov, M. J. *J. Am. Chem. Soc.* **1997**, *119*, 8916-8920.

(18) Xu, X. H.; Bard, A. J. *J. Am. Chem. Soc.* **1995**, *117*, 2627-2631.

(19) Zeng, J.; Krull, U. J. *Chimica Oggi-Chemistry Today* **2003**, *21*, 48-52.

(20) Fodor, S. P. A.; Read, J. L.; Pirrung, M. C.; Stryer, L.; Lu, A. T.; Solas, D. *Science* **1991**, *251*, 767-773.

(21) Hughes, T. R.; Mao, M.; Jones, A. R.; Burchard, J.; Marton, M. J.; Shannon, K. W.; Lefkowitz, S. M.; Ziman, M.; Schelter, J. M.; Meyer, M. R.; Kobayashi, S.; Davis, C.; Dai, H. Y.; He, Y. D. D.; Stephaniants, S. B.; Cavet, G.; Walker, W. L.; West, A.; Coffey, E.; Shoemaker, D. D.; Stoughton, R.; Blanchard, A. P.; Friend, S. H.; Linsley, P. S. *Nat. Biotechnol.* **2001**, *19*, 342-347.

(22) Shalon, D.; Smith, S. J.; Brown, P. O. *Genome Res.* **1996**, *6*, 639-645.

(23) Pena, S. R. N.; Raina, S.; Goodrich, G. P.; Fedoroff, N. V.; Keating, C. D. *J. Am. Chem. Soc.* **2002**, *124*, 7314-7323.

(24) Perez, J. M.; O'Loughin, T.; Simeone, F. J.; Weissleder, R.; Josephson, L. *J. Am. Chem. Soc.* **2002**, *124*, 2856-2857.

(25) Schena, M. *Bioessays* **1996**, *18*, 427-431.

(26) Lee, I. H. In *Chemical Engineering*; Massachusetts Institute of Technology: Cambridge, 2001.

(27) Bamdad, C. *Biophysical Journal* **1998**, *75*, 1997-2003.

(28) Niemeyer, C. M.; Sano, T.; Smith, C. L.; Cantor, C. R. *Nucleic Acids Res.* **1994**, *22*, 5530-5539.

(29) Niemeyer, C. M.; Boldt, L.; Ceyhan, B.; Blohm, D. *Anal. Biochem.* **1999**, *268*, 54-63.

(30) Niemeyer, C. M.; Ceyhan, B.; Blohm, D. *Bioconjugate Chem.* **1999**, *10*, 708-719.

(31) Niemeyer, C. M. In *Nano-surface chemistry*; M, R., Ed.; Marcel Dekker, Inc.: New York, 2001, pp 391-459.

(32) Strable, E.; Johnson, J. E.; Finn, M. G. *Nano Lett.* **2004**, *4*, 1385-1389.

(33) Muthukrishnan, G.; Roberts, C. A.; Chen, Y. C.; Zahn, J. D.; Hancock, W. O. *Nano Lett.* **2004**, *4*, 2127-2132.

(34) Li, Z.; Zhang, Y.; Fullhart, P.; Mirkin, C. A. *Nano Lett.* **2004**, *4*, 1055-1058.

(35) Zhang, Y. W.; Seeman, N. C. *J. Am. Chem. Soc.* **1992**, *114*, 2656-2663.

(36) Winfree, E.; Liu, F. R.; Wenzler, L. A.; Seeman, N. C. *Nature* **1998**, *394*, 539-544.

(37) LaBean, T. H.; Yan, H.; Kopatsch, J.; Liu, F. R.; Winfree, E.; Reif, J. H.; Seeman, N. C. *J. Am. Chem. Soc.* **2000**, *122*, 1848-1860.

(38) Mao, C. D.; LaBean, T. H.; Reif, J. H.; Seeman, N. C. *Nature* **2000**, *407*, 493-496.

(39) Yan, H.; Park, S. H.; Finkelstein, G.; Reif, J. H.; LaBean, T. H. *Science* **2003**, *301*, 1882-1884.

(40) Mirkin, C. A.; Letsinger, R. L.; Mucic, R. C.; Storhoff, J. J. *Nature* **1996**, *382*, 607-609.

(41) Alivisatos, A. P.; Johnsson, K. P.; Peng, X. G.; Wilson, T. E.; Loweth, C. J.; Bruchez, M. P.; Schultz, P. G. *Nature* **1996**, *382*, 609-611.

(42) Mitchell, G. P.; Mirkin, C. A.; Letsinger, R. L. *J. Am. Chem. Soc.* **1999**, *121*, 8122-8123.

(43) Mucic, R. C.; Storhoff, J. J.; Mirkin, C. A.; Letsinger, R. L. *J. Am. Chem. Soc.* **1998**, *120*, 12674-12675.

(44) Taton, T. A.; Mucic, R. C.; Mirkin, C. A.; Letsinger, R. L. *J. Am. Chem. Soc.* **2000**, *122*, 6305-6306.

(45) Niemeyer, C. M.; Ceyhan, B.; Hazarika, P. *Angew. Chem.-Int. Edit.* **2003**, *42*, 5766-5770.

(46) Taton, T. A.; Mirkin, C. A.; Letsinger, R. L. *Science* **2000**, *289*, 1757-1760.

(47) Nam, J. M.; Park, S. J.; Mirkin, C. A. *J. Am. Chem. Soc.* **2002**, *124*, 3820-3821.

(48) Nam, J. M.; Thaxton, C. S.; Mirkin, C. A. *Science* **2003**, *301*, 1884-1886.

(49) Niemeyer, C. M.; Burger, W.; Peplies, J. *Angew. Chem.-Int. Edit.* **1998**, *37*, 2265-2268.

(50) Braun, E.; Eichen, Y.; Sivan, U.; Ben-Yoseph, G. *Nature* **1998**, *391*, 775-778.

(51) Ma, Y. F.; Zhang, J. M.; Zhang, G. J.; He, H. X. *J. Am. Chem. Soc.* **2004**, *126*, 7097-7101.

(52) Bigham, S. R.; Coffer, J. L. *Colloid Surf. A-Physicochem. Eng. Asp.* **1995**, *95*, 211-219.

(53) Torimoto, T.; Yamashita, M.; Kuwabata, S.; Sakata, T.; Mori, H.; Yoneyama, H. *J. Phys. Chem. B* **1999**, *103*, 8799-8803.

(54) Blessing, T.; Remy, J. S.; Behr, J. P. *J. Am. Chem. Soc.* **1998**, *120*, 8519-8520.

(55) Cassell, A. M.; Scrivens, W. A.; Tour, J. M. *Angew. Chem.-Int. Edit.* **1998**, *37*, 1528-1531.

(56) Gibbs, E. J.; Tinoco, I.; Maestre, M. F.; Ellinas, P. A.; Pasternack, R. F. *Biochem. Biophys. Res. Commun.* **1988**, *157*, 350-358.

(57) Mbindyo, J. K. N.; Reiss, B. D.; Martin, B. R.; Keating, C. D.; Natan, M. J.; Mallouk, T. E. *Adv. Mater.* **2001**, *13*, 249-+.

(58) Nicewarner-Pena, S. R.; Freeman, R. G.; Reiss, B. D.; He, L.; Pena, D. J.; Walton, I. D.; Cromer, R.; Keating, C. D.; Natan, M. J. *Science* **2001**, *294*, 137-141.

(59) Lee, S. W.; McNally, H. A.; Guo, D.; Pingle, M.; Bergstrom, D. E.; Bashir, R. *Langmuir* **2002**, *18*, 3383-3386.

(60) Hartmann, D. M.; Heller, M.; Esener, S. C.; Schwartz, D.; Tu, G. *J. Mater. Res.* **2002**, *17*, 473-478.

(61) Edman, C. F.; Raymond, D. E.; Wu, D. J.; Tu, E. G.; Sosnowski, R. G.; Butler, W. F.; Nerenberg, M.; Heller, M. J. *Nucleic Acids Res.* **1997**, *25*, 4907-4914.

Chapter 3.   Effect of Probe Density on DNA Surface Hybridization

3.1 Introduction

With the completion of the Human Genome Project, there has been a widespread use of DNA microarrays for understanding gene expression profiles and characterizing single base nucleotide polymorphisms. The main operating principle of these solid-state DNA-based assays is the selective hybridization between two complementary DNA molecules: one immobilized on a surface and the other that adsorbs from solution onto this platform. The increasing popularity of these assays has spurred research efforts to gain a better understanding of DNA hybridization on solid surfaces.[1-6] Various methods such as quartz crystal microbalance,[7] chronocoulometry,[8] atomic force microscopy,[9] and surface plasmon resonance[10] have been used to gain insight into the hybridization process. A few efforts have also been directed toward the modeling of these systems.[11-16] The primary motivation has been to improve the performance of the microarrays: namely, to enhance their signal-to-noise ratio, to improve mismatch discrimination, and to reduce slide-to-slide variability. Surface chemistry for DNA attachment is a key determinant of these performance variables. Prudent choice of surface chemistry can ameliorate many problems associated with microarray performance.

DNA hybridization onto microarrays is greatly affected by the conditions at the surface. Local properties such as pH, ion concentration, and dielectric constant can depend on the surface probe density and can be substantially different from the bulk values. DNA attachment chemistries that offer a control over probe density provide an effective means for modulating the surface characteristics of a microarray. Ideally, such an attachment chemistry should be able to modulate the probe densities over a wide range and provide surfaces that reduce non-specific

adsorption. Additionally, the attached species should remain stable on the surface under normal hybridization and dehybridization conditions. Recent modeling studies have shown that oligonucleotide surface probe density can affect hybridization performance due to electrostatic interactions that reduce the thermodynamic stability of the DNA duplex on the surface.[12] In this regard, various attachment chemistries that offer control over probe density have been developed. In one example, Tarlov et al.[17] have used a system wherein they sequentially self-assemble a thiol-modified oligonucleotide and then 6-mercapto-1-hexanol as an inert spacer onto gold surfaces to achieve a range of immobilized probes densities. A limitation to this approach is that the thiol-Au bond responsible for probe attachment is heat labile and can cleave during the washing and denaturation steps. Krull et al.[18] have prepared surfaces with covalently attached oligonucleotides with modulated surface probe densities by placing samples within an oligonucleotide synthesizer and restricting the contact times between samples and the nucleotide reagents used in the stepwise solid-phase synthesis of the oligonucleotide sequence. Guo et al.[19] have instead tried to change the probe densities at a surface by spotting different concentrations of oligonucleotide solution. This last strategy fails to address problems associated with non-specific adsorption.

In this paper, I have combined the use of self-assembled monolayers and solid-phase phosphoramidite synthesis of oligonucleotides for generating end-immobilized strands of DNA on glass surfaces. The main objective of these experiments was to study the effects of probe density on hybridization kinetics. I modulated the site density of immobilized probes on the surface using silane films of tailored composition, using a methyl-terminated C_8 trichlorosilane (C_8 silane) and a hydroxyl-terminated, trichloroacetate (TCA)-protected C_{11} silane (TCA silane). The mixed silane films coat the glass surface to reduce non-specific adsorption as compared to

the bare surface and include terminal hydroxyl groups at controllable surface densities that provide sites for oligonucleotide synthesis. Stepwise phosphoramidite synthesis was used to immobilize 16-mer DNA probes on these surfaces. The hybridization kinetics was followed on six different probe densities using a fluorophore-tagged oligonucleotide at room temperature and 1 M NaCl salt concentration. Using this setup, I have systematically studied the effects of the surface probe density on the hybridization kinetics of a 12-mer target oligo over a broad range of probe densities with some in the regime not yet examined in current literature.

3.2 Experimental Section

Chemicals. Undecylenyl alcohol, trichloroacetyl chloride, pyridine, trichlorosilane, octyl trichlorosilane, octadecyl trichlorosilane, octadecyl thiol, anhydrous THF, anhydrous toluene, isooctane, and chloroplatinic acid were obtained from Aldrich (Milwaukee, WI). Gold pellets were supplied by J&J Materials, Inc. (Neptune City, NJ), and chromium wires were supplied by R. D. Mathis and Company (Long Beach, CA). Hexanes, acetonitrile, methanol, ethanol, acetone, ethyl acetate, sodium chloride, sodium citrate, EDTA, tris-HCl, potassium carbonate, and potassium iodide were obtained from Mallinckrodt (Paris, KE). Phosphoramidites and reagents used for oligonucleotide synthesis, and empty TWIST™ columns were obtained from Glen Research (Sterling, MA). Piperidine (20%) in dimethyl formamide was obtained from Protein Technologies, Inc. (Tucson, AZ). Deionized water (Resistance = 18.2 MΩ) was provided by a MilliQ deionization system (Millipore Corp., Bedford, MA). The target oligo cA 5' –CAC AGG TCG CAT-TAMRA- 3' modified with tetramethyl rhodamine (TAMRA) at the 3' end was obtained from Sigma-Genosys (Woodlands, TX). All materials were used as received.

Synthesis of (1-trichlorosilyl undecyl) trichloroacetate. In the first step of the synthesis,[20] two equiv (10.7 g) of trichloroacetyl chloride were added dropwise to a solution containing 1

equiv (5 g) of undecylenyl alcohol and 2 equiv (4.65 g) of pyridine (proton scavenger) in dry THF (100 mL) under nitrogen. After 24 h, reaction completion was checked by thin layer chromatography using ethyl acetate as the mobile phase. The mixture was combined with 1 equiv (0.5 mL) of water, filtered to remove the pyridinium salt, and extracted with hexane. Hexane was then removed under reduced pressure to yield the ω-undecylenyl trichloroacetate (90% yield). ^{1}H NMR δ 5.8 (t, 1 H), δ 5.0 (d, 2 H), δ 4.4 (t, 2 H), δ 2.0 (t, 2 H), δ 1.7 (t, 2 H), δ 1.3-1.45 (m, 12 H).

In the second step, 1 equiv (2.5 g) of ω-undecylenyl trichloroacetate was combined with 4 equiv (4.3 g) of trichlorosilane and 5 mg of chloroplatinic acid in dry THF (10-20 mL) under nitrogen and magnetically stirred for 24 h. The product solution was concentrated under reduced pressure and vacuum distilled to yield (1-trichlorosilyl undecyl) trichloroacetate (55% yield) as a colorless oil. ^{1}H NMR δ 4.4 (t, 2 H), δ 1.8 (t, 2 H), δ 1.6 (m, 4 H), δ 1.3-1.45 (m, 14 H). Figure 3-1 shows the two-step reaction scheme.

Surface preparation. Regular microscope glass slides were cleaned by immersing in 'piranha' solution (7/3 v/v mixture of concentrated H_2SO_4 and 30% aqueous H_2O_2) for 30 min at 90 °C. (CAUTION: 'Piranha' solution reacts violently with many organic materials and should be handled with care). The slides were rinsed with copious amounts of deionized water and dried in a stream of nitrogen. After cleaning, the slides were coated with octadecyl trichlorosilane using a PDMS stamp[21] to define twenty circular hydrophilic zones each having a diameter of around 2 mm contained within a circular hydrophobic region of diameter 2.5 cm. To achieve the patterning, a coat of 10 mM solution of octadecyl trichlorosilane in hexane was applied to the PDMS stamp with a cotton tip applicator. The coat was dried under a N_2 stream for 30 s to evaporate the solvent. The stamp was then gently applied to the surface of the slide ensuring that

no air bubbles were entrapped between the stamp and the slide. After ~1 min, the stamp was gently removed and the slide was sequentially rinsed with acetone, water, and ethanol, and dried under N_2. The stamp was also rinsed with acetone and ethanol and stored for reuse. The PDMS stamps could be used 4-5 times without affecting the quality of the mm-size stamped features.

Silanization. The silanizing solution was prepared by adding octyl trichlorosilane (C_8 silane) and trichloroacetate (TCA) protected ω-hydroxyundecyl trichlorosilane (TCA silane) in requisite proportions to anhydrous toluene (>99.5%) to yield 1 μL/mL (~mM) solution of the silanes in toluene. The patterned slides were immersed in this solution for 4 h at room temperature to coat the twenty circular zones that were left unfunctionalized by the microcontact printing step with a mixed silane layer exposing methyl and trichloroacetyl groups on the surface. After 4 h, the slides were sequentially rinsed with acetone and ethanol and dried with a N_2 gas stream. To expose the TCA-protected hydroxyl groups prior to DNA synthesis, the TCA groups were removed by immersing the slides in 5 mM K_2CO_3 solution in 1:1 H_2O: methanol for 15 min. The slides were then rinsed with copious amounts of water to remove the salt, followed by ethanol, and finally dried in a stream of N_2. The density of OH groups on the surface could be modulated by changing the proportions of the C_8 and TCA silanes in the silanizing solution.

Oligonucleotide synthesis. A custom-built flow cell was employed to allow the synthesis of oligonucleotides on 2.5 cm x 7.5 cm glass slides using an Applied Biosystems ABI-392/394 automated DNA synthesizer. The flow cell consists of a Teflon base plate having inlet and outlet streams that were connected to the fluidic manifold of the synthesizer; the sealed flow chamber was constructed by sandwiching an o-ring between the glass slide and the base plate. UltraMild® phosphoramidites were used for synthesis in order to avoid exposing the silane films to a strong base such as ammonium hydroxide as needed for removing the base-protecting groups. The

delivery and reaction times of the various reagents were manipulated to optimize the oligonucleotide synthesis on the patterned areas on the glass slide surfaces. To retain the synthesized oligonucleotides on the glass surface, the ammonium hydroxide step used to normally detach the oligonucleotide from the support was disabled. Instead, the slides were washed sequentially with acetonitrile, acetone, and ethanol after synthesis and dried with N_2 gas stream. Following the automated synthesis, the slides were immersed in a 20-wt% piperidine in dimethyl formamide (DMF) solution for 4 h to remove the cyanoethyl protecting groups. The base protecting groups were removed by immersing the slides in a 0.05 M K_2CO_3 solution in anhydrous methanol for 4 h. The above procedure was used to synthesize 5'-ATG CGA CCT GTG TTT T- 3' as the probe oligonucleotide (oligo A) on the glass slides.

Hybridization setup. The hybridization experiments were performed at room temperature (20 °C) in a chamber at >95% relative humidity in order to minimize evaporation of the spotted hybridization solutions on the slide. The hybridizing solution, 0.5 μM oligo cA in a 7x SSC (1 M NaCl, 0.1 M sodium citrate) solution, was spotted at different times to get the kinetic profile of the hybridization process. On a single slide, two spots were used for each time interval. After hybridization, the slides were washed with 1x TE buffer and dried with N_2. The slides were stored in the dark until scanned.

Fluorescence measurements. The slides were scanned after washing on a GenePix® microarray scanner (Axon Instruments, Union City, CA) at λ = 532 nm. Prior to analysis, two 2 μL spots of 0.033 μM Rhodamine solution were placed after hybridization on each slide and allowed to dry. The fluorescence signals from these spots were used to normalize the fluorescence intensities from the hybridization spots. The normalized fluorescence intensities were calibrated versus the fluorophore-tagged target oligonucleotide density by spotting

solutions containing different amounts of the target oligonucleotide, allowing the spots to dry, and then measuring the normalized fluorescence signals. Fluorescence intensities scaled linearly with the target density over the density range examined. The drying was allowed to take place gradually in a fairly humid environment over a period of few hours to avoid multilayer formation that could cause fluorescence quenching.

X-ray photoelectron spectroscopy (XPS) measurements. XPS spectra were obtained with a Surface Science Instruments Model X-100 spectrometer using a monochromatized Al Kα X-ray source (elliptical spot of 1.0 mm x 1.7 mm) and a concentric hemispherical analyzer (pass energy = 50 eV). The detector angle with respect to the surface parallel was 35°. Peak positions were referenced to $Au(4f_{7/2})$ = 84.00 eV and were fit with 80% Gaussian/20% Lorentzian profiles and a Shirley background to obtain integrated peak intensities. A reference sample for calibration consisting of an iodine monolayer on a gold surface[22] was prepared by immersing a gold-coated (Au - 1000 Å, Cr – 100 Å) Si wafer (1 cm x 3 cm) in a 0.1 M aqueous KI solution for 1 h. The intensities of XPS signals from this sample were compared to those from *n*-octadecanethiolate monolayers on gold[23] and demonstrated that the above procedure consistently generated reference samples with a reproducible level of iodine.

Ellipsometry. The optical constants from samples before and after silane modification were measured using a Gaertner L116A automatic ellipsometer equipped with a He-Ne laser (λ = 632.8 nm) at an incident angle of 70°. The thickness of the silane films were estimated by employing the optical constants and a refractive index of 1.45 for the organic film in a three-phase model.
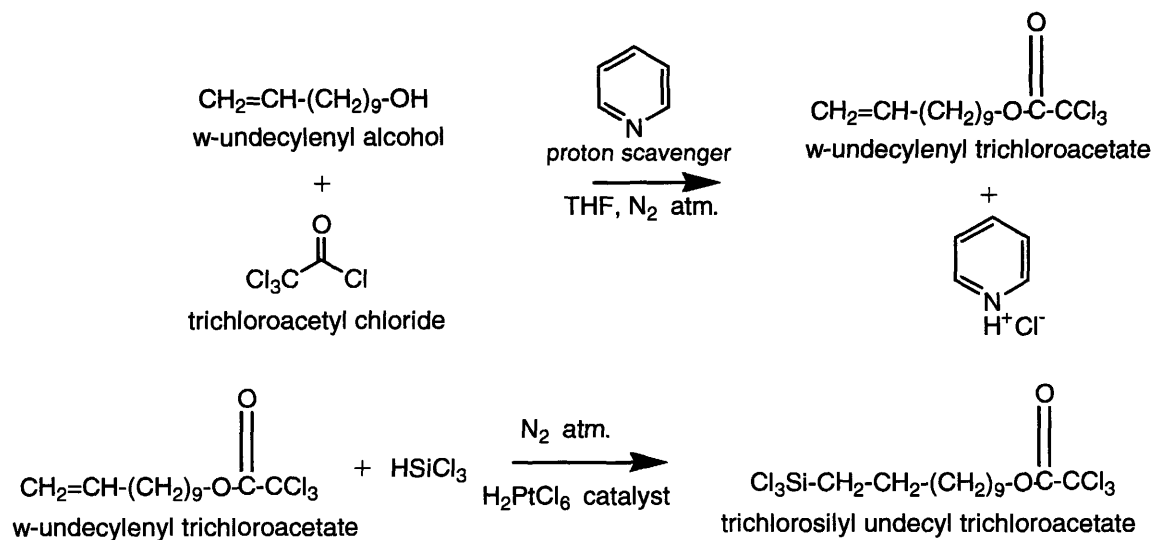
Figure 3-1 Two-step reaction scheme for the synthesis of the trichloroacetate (TCA)-protected C_{11} silane (TCA silane).

3.3 Results and Discussion

3.3.1 Surfaces with controllable probe densities

To generate surfaces with controlled differences in probe density, I modified glass surfaces with mixed monolayer films (Figure 3-2). I employed two-component films that I formed by dipping glass slides in anhydrous toluene solutions containing mixtures of a trichloroacete (TCA)-terminated silane and n-octyltrichlorosilane (C_8) silane at millimolar concentrations. The function of the TCA silane was to provide reactive hydroxyl sites for oligonucleotide attachment while that of the C_8 silane was to fill the remaining surface with an inert component. By varying the composition of the two silanes in the silanizing solution, a range of hydroxyl densities could be obtained. Ellipsometric readings showed that the silanes produced monolayer films on the surfaces with thicknesses ranging from 15-20 Å. The TCA protecting group was removed before using the surfaces for DNA synthesis by treatment with a basic solution to cleave the TCA ester and expose the hydroxyl groups.[20] A concern was that this basic solution might also cleave the Si-O bonds that link the silane film to the surface. To optimize the protocol for the removal of the TCA group, I attempted deprotection of the silane film using various basic solutions. I used X-ray photoelectron spectroscopy (XPS) to follow the effects of this treatment by monitoring the C, Si, and Cl signals on these deprotected surfaces. An effective deprotection scheme should give zero Cl signal indicating the complete removal of the TCA protecting group (each TCA group contains three chlorine atoms) and at the same time yield a high C/Si signal indicating minimal damage to the underlying silane film. I found that a deprotection process using 5 mM K_2CO_3 solution in 1:1 methanol: water for 15 min was the most effective scheme for removing the TCA groups and generating hydroxyl-terminated surfaces (see **Table 3-1**). I synthesized oligonucleotides on these hydroxyl-terminated surfaces

using commercially available reagents and a custom-built flow cell (Figure 3-3) placed within a DNA synthesizer. For our investigation, I selected a hybridizing length of 12 bases in order to avoid any effects of secondary structure on the hybridization performance. Additionally, I prepared a 4-T spacer on the surface prior to synthesis of the 12-mer oligonucleotides in order to reduce interactions between the surface probes and the substrate.

An important challenge for this study was to accurately determine the probe densities of the immobilized oligonucleotides. To make this measurement, I labeled the 5' end of the probe oligonucleotide with an iodinated uracil phosphoramidite in the final step of its synthesis and quantified the iodine levels (and hence the probe density) using x-ray photoelectron spectroscopy (XPS). XPS is well suited for quantifying iodine levels as the $3d_{3/2}$ (618 eV) and at $3d_{5/2}$ (630 eV) transitions for iodine have large photoelectric cross-sections and provide high sensitivity for measuring iodine surface concentrations.[24] In addition, the background signals for iodine are close to zero, since it is rarely present in the ambient environment. As a standard for quantifying the iodine signal, I employed gold-coated Si slides that were immersed into 0.1 M aqueous KI solution for 1 h. Studies conducted by Weaver et al.[22,25-27] have shown that iodide anions form an iodine adlayer on gold surfaces with a defined ($\sqrt{3}$ x $\sqrt{3}$) R30° lattice structure giving a surface density of 9.1 x 10^{-10} moles/cm^2 for the adsorbed iodine atoms.[22] Using this iodine-on-gold standard, I was able to obtain probe densities for the oligonucleotides by comparison of iodine signals in XPS measurements.

Figure 3-4 shows the XPS results for attaching an iodine-containing uracil as the first nucleotide on surfaces expressing different hydroxyl densities (obtained by varying the TCA-C$_8$ silane solution composition—see above). The maximum density for this nucleotide was 1.1 x 10^{14} nucleotides/cm^2, which was smaller than the density of the underlying hydroxyl groups

because of the bigger size of the phosphoramidite molecules.[23] In Figure 3-4, the probe density for the first nucleotide exhibited a linear relationship with the composition (volume%) of the silane solution allowing us to readily control the density of the oligonucleotide probes on our surfaces. I note that the data did not exhibit a linear relationship with the mole fraction of the silane solution (not shown) suggesting that one component (in this case, the TCA silane) had a greater reactivity and higher adsorptive tendency than the other (C_8) silane.[28,29]

Figure 3-4 also shows the 16-mer probe (4-T + 12-mer) density as a function of the silane composition. The 16-mer probe densities ranged from 2.1 x 10^{12} probes/cm^2 for a silane composition of 2% TCA silane and 98% C_8 silane to 5.5 x 10^{13} probes/cm^2 for a silane composition of 100% TCA silane and 0% C_8 silane. In all cases, the 16-mer probe densities were less than the first nucleotide densities on a corresponding mixed SAM because the coupling efficiencies during phosphoramidite synthesis were slightly below 100%. By comparing the iodine signals from the 16-mer probe to those from 1-mer probe on a particular mixed SAM, I calculated that the average coupling efficiencies in our syntheses varied from ~100% at the lower densities to ~97% at the highest density. It is quite likely that the coupling efficiency may have been lowest for attaching the first bases close to the substrate because of surface interactions and steric considerations, beyond which the coupling efficiencies may have been close to 99-100% thereby yielding minimal steric hindrance around a probe by surrounding incomplete strands. Since the DNA synthesizer was customized for synthesis on flat surfaces, additional experiments were performed to establish the uniformity of its synthesis over a single glass slide. Specifically, I measured the probe densities by XPS in each of twenty regions across our slide and observed less than a 10% standard deviation (Figure 3-5).

Table 3-1 Deprotection schemes to cleave the trichloroacetyl (TCA) groups and expose the hydroxyl groups on silane films formed from 100% TCA silane and 0% C_8 silane solution.

Salt (K_2CO_3 concentration)	Solvent	Time	XPS intensities C/Si
No deprotection			0.76
0.05 M	1:1 MeOH:H_2O	10 min	0.36
0.05 M	1:1 MeOH:H_2O	15 min	0.35
0.005 M	1:1 MeOH:H_2O	15 min	**0.48**
0.005 M	1:1 MeOH:H_2O	60 min	0.42
0.005 M	4:1 MeOH:H_2O	15 min	0.43
0.005 M	4:1 MeOH:H_2O	60 min	0.42
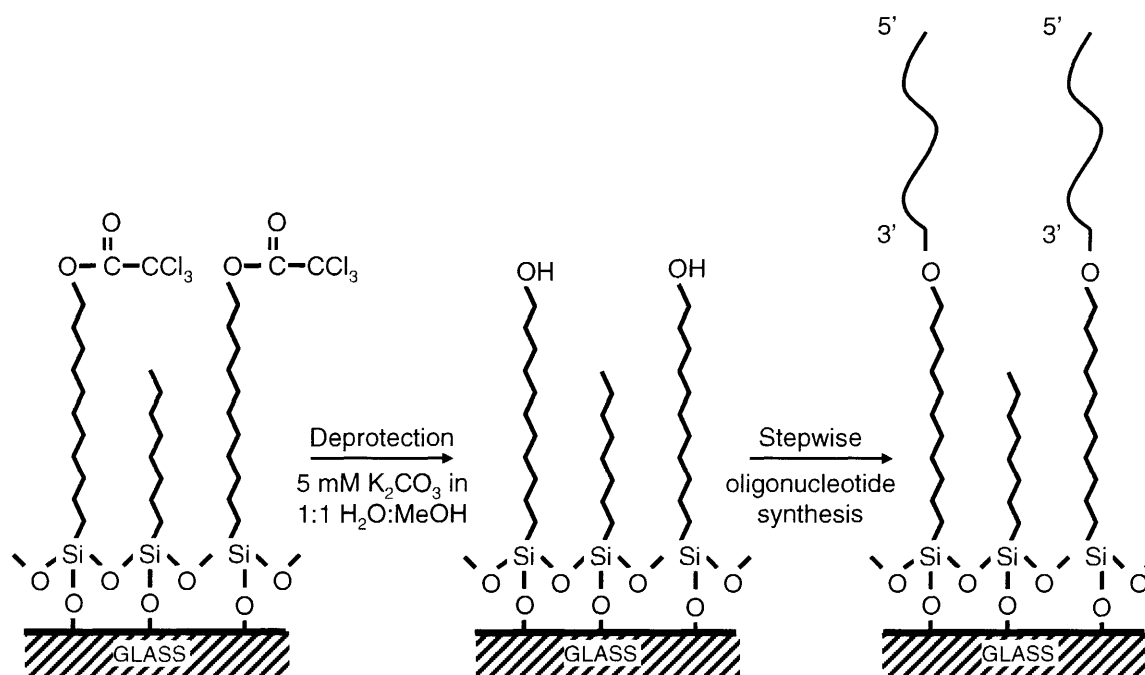
Figure 3-2 Schematic illustration of the procedure used to form end-immobilized oligonucleotides at controlled surface densities. The steps include: silanization with mixed silanes, followed by deprotection, and stepwise oligonucleotide synthesis. The concentration of the hydroxyl groups was controlled by varying the composition of the two silanes in the silanizing solution. After chemical deprotection, oligonucleotides were synthesized by a stepwise process within a custom-built flow cell that was incorporated in an ABI 392 oligonucleotide synthesizer.
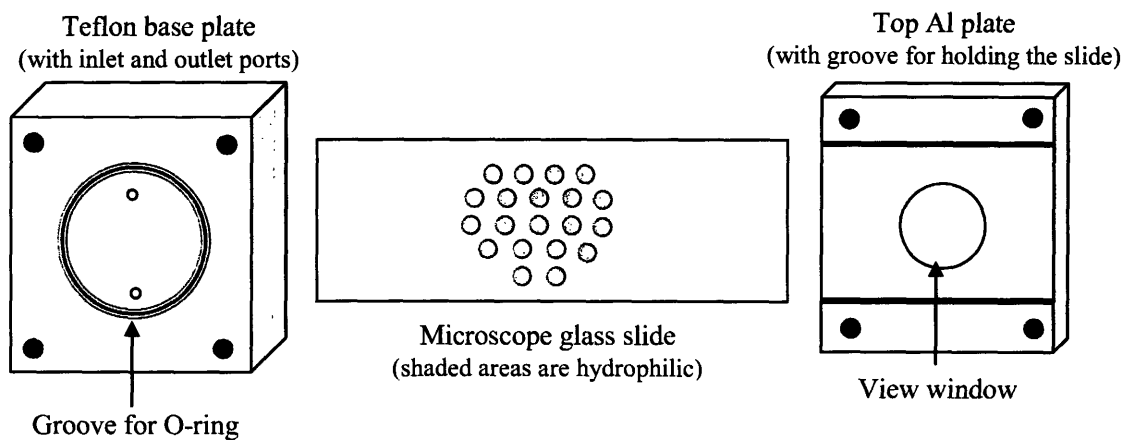
Figure 3-3 Custom-built flow cell for facilitating oligonucleotide synthesis on flat microscope glass slides within an ABI 392 DNA synthesizer.
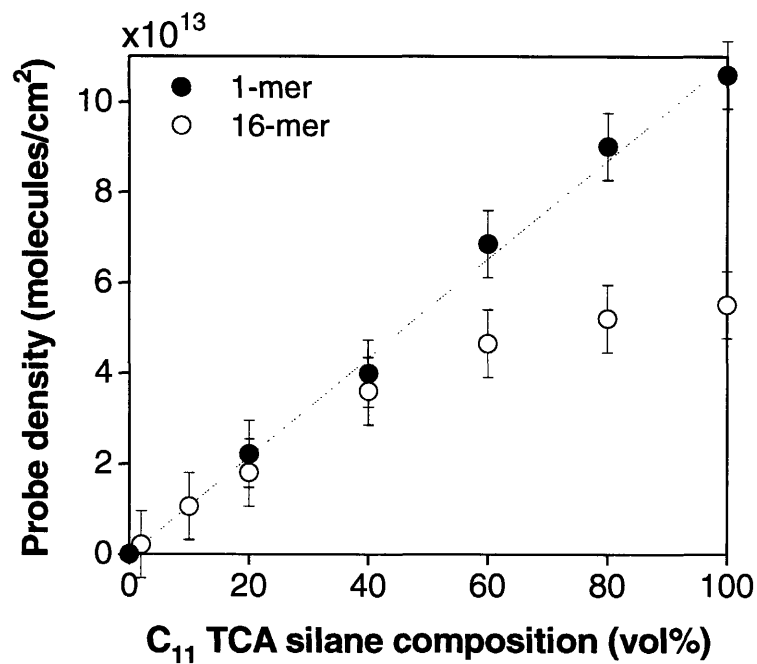
Figure 3-4 Variation in the density of the first nucleotide (O) and a 16-mer probe (●) with the composition of the silane solution. The silanizing solution contained 1 µL/mL of silanes in anhydrous toluene. The 5' nucleotide in both cases was an iodinated nucleotide. The densities were determined using iodine concentrations obtained by XPS measurements by reference to a Au-I standard (see text).
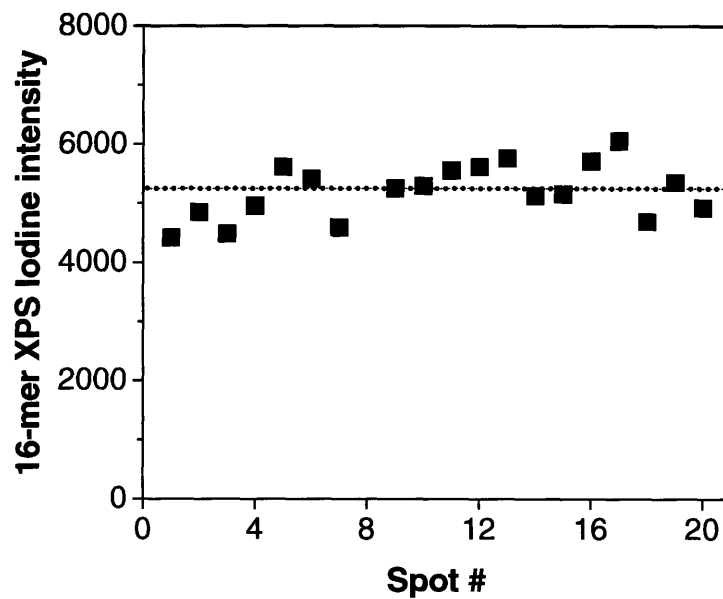
Figure 3-5 Uniformity of oligonucleotide synthesis on flat microscope glass slides. A flat microscope glass slide with twenty functional spots was used along with the flow cell in the DNA synthesizer to synthesize a 16-mer oligonucleotide on those spots. The 5' nucleotide of the 16-mer was an iodinated nucleotide. The XPS iodine signals were measured to compare the uniformity of synthesis over the various spots. The dashed line represents an average over all twenty spots.

3.3.2 Hybridization kinetics

I examined the kinetics of hybridization on surfaces expressing probe densities ranging from 0.2×10^{13} to 5.2×10^{13} probes/cm^2, representing a 25-fold difference in probe density. The hybridization solution consisted of 0.5 μM 3'-TAMRA-labeled target oligonucleotide in a 7x SSC buffer (1 M NaCl, 0.1 M Na citrate). To translate the fluorescence signals into surface coverages, I generated a calibration plot for the fluorescence intensity against known spotted surface densities of the target. For densities of target spanning the range of our surface probe levels, I observed a linear relationship between the surface density of the fluorophore-tagged oligonucleotides and its fluorescence signal intensity (Figure 3-6). Figure 3-7 shows representative fluorescence images from slides used for fluorescence calibration and hybridization kinetics experiments.

Figure 3-8 summarizes our kinetic data for the hybridization of a solution-phase target to our probe surfaces of various densities. For all probe densities, 95% of the equilibrium signal was attained in ~5 h. At the lower probe densities, ranging from 2.1×10^{12} to 3.6×10^{13} probes/cm^2 (Figure 3-8A), the fluorescence signals due to target hybridization increased with increases in probe density. For example, I observed a 10-fold increase in the equilibrium signal due to adsorbed targets by changing the probe density from 2.1×10^{12} probes/cm^2 to 3.6×10^{13} probes/cm^2. These densities correspond to average inter-strand distances of 74 Å and 18 Å, respectively. For probe densities higher than 3.6×10^{13} probes/cm^2 (Figure 3-8B), the equilibrium dsDNA density decreased with increases in the probe density in contrast to the results in Figure 3-8A. Thus, increasing the probe density beyond a certain value hampers the hybridization process and leads to reductions in signal intensities.

The equilibrium dsDNA densities on the various samples are summarized in Figure 3-9. The maximum in dsDNA density occurs for a probe density of ~3.6 x 10^{13} probes/cm^2 with ~40% efficiency, giving a surface dsDNA density of 1.4 x 10^{13} dsDNA/cm^2.[30-32] These results suggest that a control of probe density is important for attaining high signals during hybridization. The hybridization efficiency, defined as the % of probes hybridized, drops from 65% for the lowest probe density to 10% for the highest probe density (Figure 3-10). The drop in efficiency at higher probe densities can be attributed to increases in steric and electrostatic hindrances that make more probe sites inaccessible for hybridization and also reduce the stability of the DNA duplexes. The less than 100% efficiency at the lowest probe density suggests that even at that density a sizable fraction of the sites are unavailable for hybridization. The fluorescence signals obtained by hybridizing a non-complementary target to the probe molecules were close to background (data not shown). This is partly due to the stringent washing conditions and the use of the mixed silane chemistry. The C_8 silanes act as spacer groups and reduce interactions of the target oligonucleotides with the bare glass substrate.
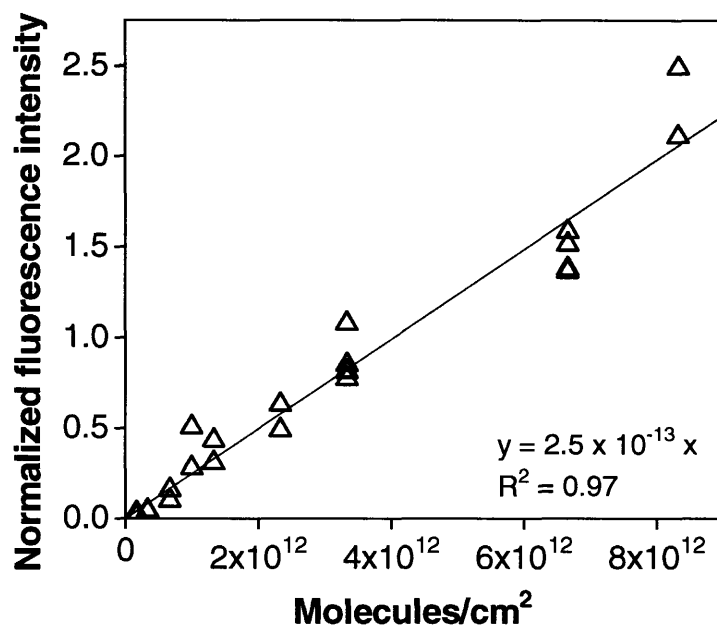
Figure 3-6 Calibration plot of normalized fluorescence intensity vs. target density on the surface. Different target densities were achieved by spotting different amounts of fluorophore-tagged target oligonucleotides and gradually evaporating the water in controlled humidity. The fluorescence signals were normalized with signals from reference spots formed by spotting 2 μL of 0.033 μM aqueous rhodamine solution followed by gradual evaporation. Linear regression of the data yields $R^2 = 0.97$. The calibration plot contains data from four different calibration slides.
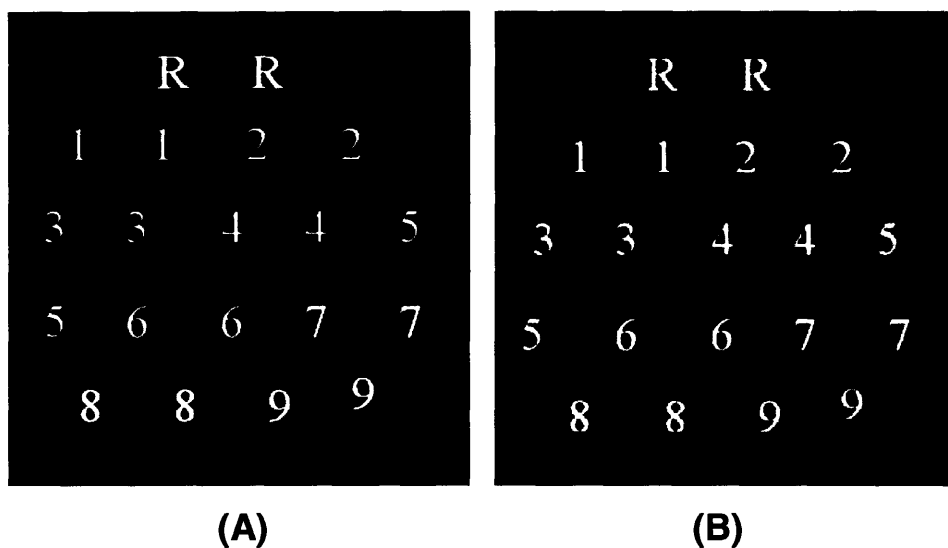
Figure 3-7 Fluorescence images obtained from a GenePix® scanner. (A) Fluorescence image of a calibration slide. To calibrate fluorescence intensities vs. target density, serial dilutions of the fluorophore-tagged target oligonucleotides were spotted on the slide and the fluorescence was measured with the fluorescence scanner. Numbers 1 to 9 indicate increasing amounts of spotted oligonucleotides. (B) Typical fluorescence image of a hybridization kinetics experiment. Numbers 1 to 9 indicate different hybridization times ranging from 15 min to 24 h. Spots labeled R were spotted with 2 µL of 0.033 µM aqueous rhodamine solution after hybridization and washing and allowed to dry slowly in high humidity. Fluorescence signals from the reference (R) spots were used to normalize the signals for all the other spots.
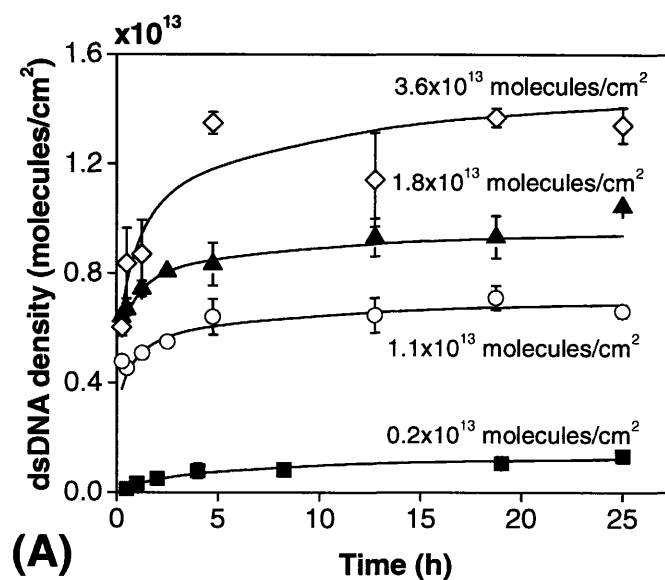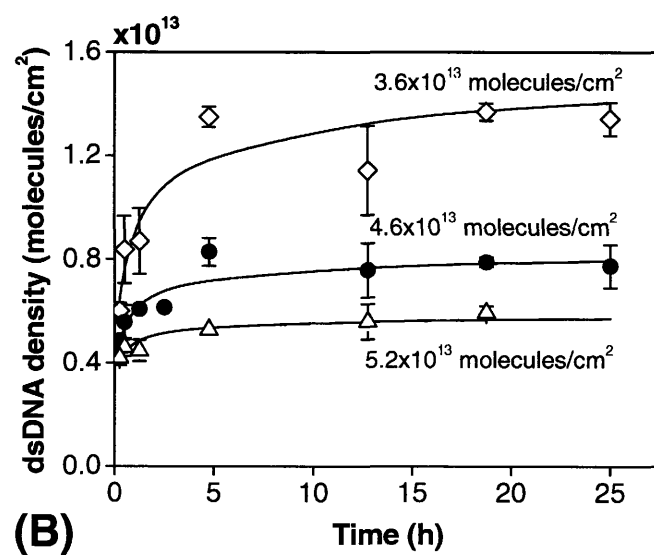
Figure 3-8 Hybridization kinetics for various probe densities: (A) 0.2 x 10^{13} probes/cm^2 (■), 1.1 x 10^{13} probes/cm^2 (○), 1.8 x 10^{13} probes/cm^2 (▲), and 3.6 x 10^{13} probes/cm^2 (◇). (B) 3.6 x 10^{13} probes/cm^2 (◇), 4.6 x 10^{13} probes/cm^2 (●), and 5.2 x 10^{13} probes/cm^2 (△). All the hybridization experiments were carried out at: 0.5 μM target oligo, 1 M NaCl, 20 °C. Post-hybridization washing was done with 1x TE buffer solution. Except for the lowest density, the lines are fits to the data points using a second-order, diffusion-limited Langmuir isotherm. A second-order Langmuir is used for the lowest density (0.2 x 10^{13} probes/cm^2).
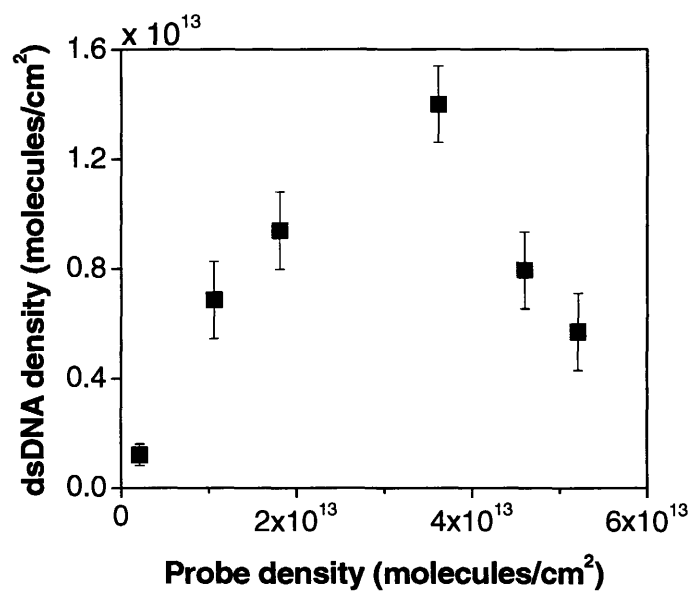
Figure 3-9 Variation of dsDNA densities with the surface probe density. The equilibrium dsDNA densities are computed from the 24 h fluorescence signals for the various probe densities. Hybridization experiments were performed at room temperature and yielded an optimal probe density of ~ 3-4 x 10^{13} probes/cm^2 for maximal dsDNA attachment.
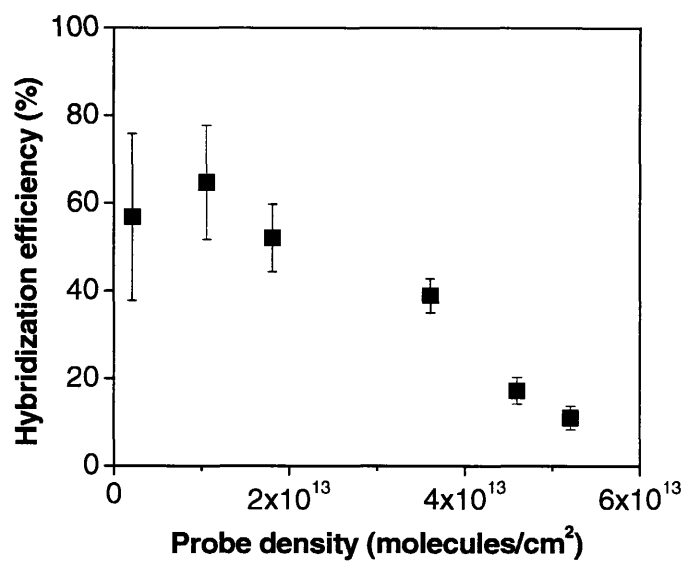
Figure 3-10 Variation in hybridization efficiency with surface probe density. Hybridization efficiency is defined as the % of probes hybridized to the target DNA. Hybridization efficiency drops with increasing probe density.

Several other groups have examined the effects of surface probe density on the hybridization performance but the probe densities used were much lower than those in this study. Southern et al.[33] also reported a decrease in dsDNA density with an increase in probe density; however, these authors did not quantify the surface probe densities employed in their experiments. Guo et al.[19] have reported an optimal probe density of ~ 2 x 10^{13} probes/cm^2 for the hybridization of a 157 base-pair long PCR product to a 15-mer on the surface. The hybridization efficiency at the optimum probe density was 20%. Tarlov et al.[8] have reported an optimal probe density of 4 x 10^{12} probes/cm^2 for the hybridization of a 25-mer probe/target system supported on a gold surface. Ferrall et al.[34] have achieved a hybridized dsDNA density of 1.1 x 10^{13} dsDNA/cm^2 with an efficiency of ~75% on a surface with a probe density of 1.4 x 10^{13} probes/cm^2 for a d(GGGG)$_5$:d(CCCC)$_5$ system. However, for other complementary sequences with lower (50%) GC content, their efficiencies were much lower (~10%). Georgiadis et al.[35] also observed a decrease in the hybridization efficiency with increases in probe density for the hybridization of a 25-mer at 1 M NaCl and 1 μM target oligonucleotide concentration. They obtained 100% efficiencies for surfaces with density of 2 x 10^{12} probes/cm^2, although their efficiency at a probe density of 1.2 x 10^{13} probes/cm^2 was around 30%, compared to ~60% achieved in this study. Using a simple electrostatic model, Krull et al.[36] have shown that above inter-strand distances of more than 50 Å, the ionic environment near the probes is unaffected by surface probe densities, as the solution ionic strength (1 M NaCl) reduces the Debye length to as low as 1 Å. Pettitt et al.[12] modeled the 25-mer DNA in solution as a ion-penetrable sphere and the probe-containing surface as an ion-impenetrable charged surface within a linearized Poisson-Boltzmann framework and showed that the onset of electrostatic repulsion and deviations from ideal Langmuir isotherm begin at inter-strand distances of ~100 Å. Their thermodynamic model

predicts a drop in hybridization efficiency with increases in the probe density due to 'coulomb blockage', with the efficiency dropping to less than 5% for a density of 1.2×10^{13} probes/cm^2. However steric effects are not incorporated in their model and to some extent the effects of electrostatic repulsion are overestimated by modeling the charge on the surface as point charges without a finite size. The wide variety of substrates and attachment chemistries employed for probe DNA immobilization and differences in experimental conditions (length of target oligonucleotide, concentration of target oligonucleotide, salt concentration etc.) make it difficult to directly compare the absolute values of optimum probe density and maximum dsDNA density observed in this study to those reported in literature. However, most experimental and modeling studies do report a drop in hybridization efficiencies with increase in probe density. A few studies also demonstrate the existence of an optimal probe density to achieve maximum hybridization signal for a given experimental setup.

3.3.3 Adsorption models

To fit the hybridization kinetics for the different probe densities, I examined various two-parameter models. These included Langmuir, second-order Langmuir, diffusion-limited Langmuir, and diffusion-limited second-order Langmuir models. I found the data were described across all the data sets by a diffusion-limited, second-order Langmuir isotherm (eq 1).[37,38] (see Appendix)

$$\Gamma = \Gamma_{max} \frac{k\sqrt{t}}{1 + k\sqrt{t}} \qquad (1)$$

The diffusion limitation is partly because of the setup of the experiments (i.e. unstirred) and the high probe densities used. The non-first/higher order dependence on the coverage is due to a decrease in the free energy of hybridization caused by the interactions between the various

probe molecules during the course of the hybridization. Specifically, hybridization at any site reduces the affinity of neighboring sites due to steric hindrance and electrostatic repulsion. These interactions are not captured by a simple Langmuir isotherm because of the inherent assumption of non-interacting sites. However, for the lowest surface probe density (2×10^{12} probes/cm^2), where the probes are widely spaced, adsorption is more limiting than diffusion, electrostatic and steric interactions, if any, are minimal, and hence a second or first-order Langmuir is sufficient to model the kinetics. The radius of gyration of a 16-mer oligonucleotide is ~15 Å [39] corresponding to a probe density of ~1×10^{13} probes/cm^2. The inter-strand steric effects are expected to be pronounced above this probe density, which is qualitatively reflected in the fitting of the kinetic plots and values of the model parameters. The fits are shown in Figure 3-8 and the values of the fitted parameters are summarized in Table 3-2. It should be noted that the values of the fitted parameters satisfy the model requirements. Specifically, the diffusion-limited, second-order Langmuir model predicts that the quantity $\Gamma_{max}k$ should be a constant. The values of this parameter were obtained within 10% of a mean value for the four highest densities. This constancy was not valid at the density of 1.1×10^{13} probes/cm^2 probably because the adsorption regime is intermediate and is not fully captured by the model. Diffusion constants (~10^{-6} cm^2/sec) calculated using the model were similar to those reported in literature.[16,40-42]

Table 3-2 Parameters obtained by fitting a second-order Langmuir model to the lowest probe density and a second-order, diffusion-limited Langmuir model to the remaining probe densities.

Probe density (probes/cm^2)	Inter-strand distance (Å)	Γ_{max} (dsDNA/cm^2)	k (hr$^{0.5}$)	Γ_{max}k (dsDNA. hr$^{0.5}$/cm^2)
2.1×10^{12}	74	1.3×10^{12}	0.6	-
1.1×10^{13}	33	7.5×10^{12}	2.0	1.5×10^{13}
1.8×10^{13}	25	1.0×10^{13}	2.6	2.6×10^{13}
3.6×10^{13}	18	1.6×10^{13}	1.3	2.1×10^{13}
4.6×10^{13}	16	8.6×10^{12}	2.5	2.1×10^{13}
5.2×10^{13}	15	6.0×10^{12}	4.1	2.5×10^{13}

Many earlier studies on DNA hybridization in solution as well on surfaces have modeled the kinetics as a pseudo first-order reaction (i.e. first-order Langmuir model).[10,43,44] Most of these studies were carried out on much lower probe densities where adsorption is limiting as compared to diffusion. Georgiadis et al.,[45] on the other hand, have modeled the hybridization kinetics for adsorption of a 25-mer onto a gold surface containing 5.2×10^{12} probes/cm^2 using a diffusion-limited, first-order Langmuir adsorption with first-order desorption model. They reckon that incorporation of dynamic equilibrium is necessary to completely explain the kinetic data. However, the constant-flux models used for comparison in their study were limited to Langmuir, second-order Langmuir, and Langmuir adsorption with first-order desorption. In a separate study,[35] they also observe a change in the kinetic regime for densities greater than 5×10^{12} probes/cm^2 consistent with the results obtained in this study.

3.3.4 Effect of probe density on thermodynamic variables

To explain the drop in hybridization efficiency with increases in probe density, I attempted to model the effect of probe density on the thermodynamics of DNA duplex formation (Figure 3-10). As probe density increases, the charge at the interface increases and free area available on the surface reduces resulting in enhanced steric and electrostatic hindrances. The binding free energy reduces with increases in probe density mostly due to the reduction in the enthalpy of hybridization. Our thermodynamic model assumes that the steric and electrostatic interactions become prominent only after the probe density exceeds a particular threshold value (P_0), relating to the increase in the steric hindrances as the probes begin to overlap. In this model, I assume that the reduction in binding free energy scales linearly with the probe density (Eqn. 2).

$$K_S = \exp\left[\frac{-\Delta G}{RT}\right] = \exp\left[\frac{-\{\Delta G_0 + a(P - P_0)\}}{RT}\right] \qquad (2)$$

ΔG_0 – binding free energy at very low probe densities

P – probe density (probes/cm^2)

P_0 – probe density above which steric and electrostatic effects become important (probes/cm^2)

$a > 0$, thus binding free energy becomes less negative when $P > P_0$

After fitting the equation to the equilibrium data (Figure 3-11), I get a surface binding free energy (ΔG_0) of -9.3 kcal/mol, close to reported solution-phase binding free energy values of -10 to -15 kcal/mol.[15,46] I chose a P_0 value of 2.1 x 10^{12} probes/cm^2, corresponding to an inter-strand distance equivalent to the length of the fully extended 16-mer ssDNA ($\sim$70 Å[40]). Although the value of ΔG_0 depends on the value of P_0 chosen, the variation with P_0 in the probe density range of interest is very small.
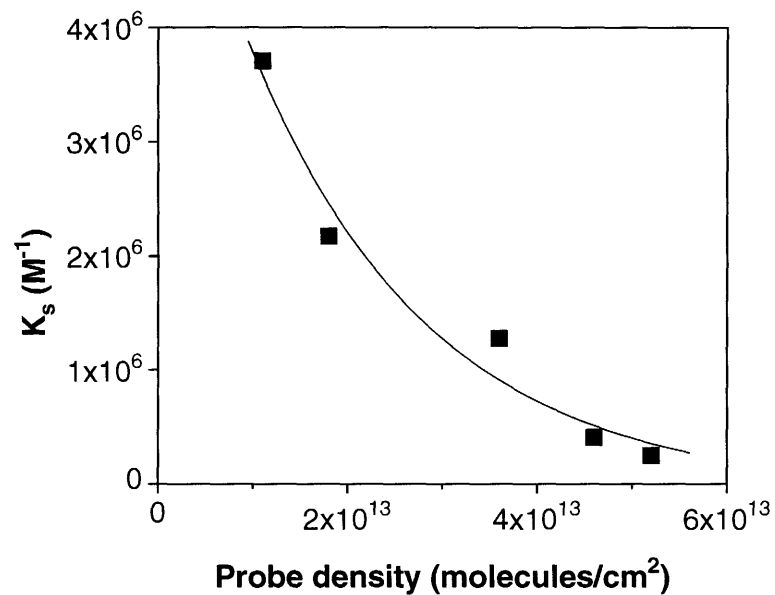
Figure 3-11 Variation of equilibrium binding constant with surface probe density. The equilibrium binding constant decreased with increases in probe density suggesting a decrease in the stability of the duplex due to an increased crowding at the interface. The line represents the fit of eq. 2 to the experimental data.

3.3.5 Duplex stability and probe density

The thermodynamic stability of a DNA duplex is strongly affected by the conditions at a surface. Based on a model including only electrostatic interactions, Pettitt et al.[12] have shown that the surface melting temperature (T_m) of a DNA duplex decreases with increases in surface probe density. A gradient of surface probe density is like a gradient of surface T_m as seen by the decreasing hybridization efficiencies (Figure 3-10). As explained before, this decrease is partly because of the inaccessibility of some probe sites and partly because of the reduced stability of the duplex. Higher probe densities progressively destabilize the duplex by reducing the free energy of adsorption and the surface T_m. Thus, if hybridization is performed at an appropriate temperature, there can be a drastic difference in the hybridization signals at low vs. high probe densities. The previous results (Figure 3-9) do show such a trend, but the differences were not as large since those experiments were conducted at temperatures far removed from the surface T_m.

To bring the surface T_m of the dsDNA duplexes close to the experimental temperature and thus amplify the effects of destabilization due to probe density, I selected a system consisting of a probe DNA on the surface containing one mismatch with the fluorophore-tagged target. The bulk T_m of the perfect complementary duplex is ~53 °C and that in the presence of the single mismatch is ~42 °C. Krull et al.[18] have shown that the melting temperatures at a surface are ~10-15 °C lower than those in the bulk. In my experiments, equilibrium dsDNA densities were measured for this probe/target system at various probe densities. For hybridization performed at 25 °C (Figure 3-12), the equilibrium dsDNA densities across various probe densities were almost similar, if not slightly lesser, than those for the perfect complementary pair (Figure 3-9). This trend suggests that even at the highest density with the greatest destabilizing influence, the duplex is well below its surface T_m at the hybridization conditions. However, for hybridizations

performed at 35 °C, there was a big drop in the dsDNA density at the highest probe density while the equilibrium dsDNA densities at the lower probe densities were almost similar to those obtained at 25 °C. The reduction in the free energy of adsorption at the highest density was such that the surface T_m of the duplex was close to 35 °C thereby resulting in less duplex formation. However, at the lower probe densities, the destabilizing influence was not large enough to cause the surface T_m to approach 35 °C causing little change in duplex formation between 25 and 35 °C. Further destabilization was examined by hybridizing the target to a probe that contained two mismatches at 25 °C; this system yielded resulted signals close to background. Here, the duplex with the two mismatches had an estimated bulk melting temperature of ~27 °C suggesting that the surface T_m, even for the lowest density, is much lower than the bulk T_m of ~27 °C. The ability to change the surface T_m by the use of different probe densities could be developed to become an effective tool in the detection of polymorphisms by amplifying mismatch discrimination through appropriate surface chemistry.
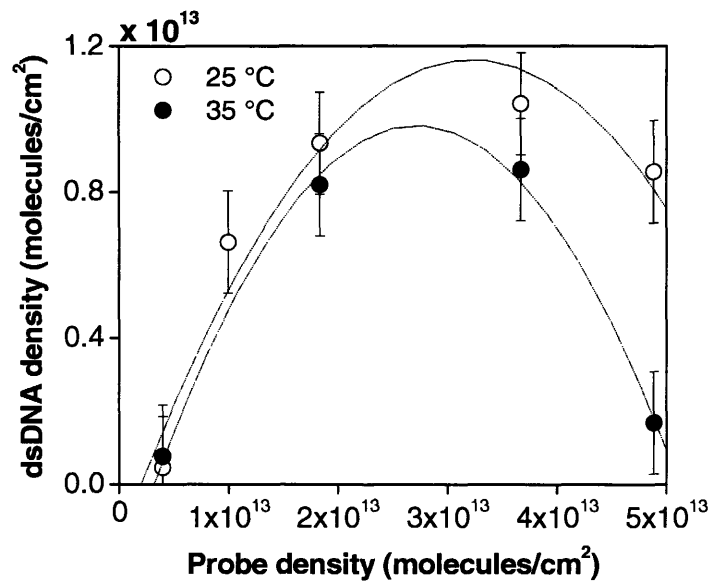
Figure 3-12 Effect of surface probe density on duplex stability. Equilibrium dsDNA densities are plotted against the probe density for hybridization of a probe/target with one mismatch at 25 °C (○) and at 35 °C (●). For the highest probe density at 35 °C, the duplex DNA stability is reduced such that the surface T_m of the duplex is close to the hybridization temperature causing a big drop in dsDNA density.

3.4 Conclusions

Surface probe density strongly affects the kinetics and thermodynamics of DNA surface hybridization. Experiments conducted on probe densities ranging from 0.2×10^{13} probes/cm^2 to 5.2×10^{13} probes/cm^2 show that increases in probe surface density lead to reduction in duplex stability. The equilibrium dsDNA densities reached a maximum for a particular surface probe density (3.6×10^{13} probes/cm^2) corresponding to an inter-strand distance of 18 Å. Further increase in the probe density reduced the equilibrium dsDNA densities. The duplex destabilization occurs due to increased steric and electrostatic hindrances caused by the high probe densities. This is the first attempt to carry out hybridization at such high probe densities and thus include steric effects. We also modeled the effects of probe density on duplex stability by assuming a linear decrease in binding free energy with increases in probe density. Additionally, the kinetic regimes were also affected due to the surface probe density. The best fits for the hybridization kinetic plots obtained at the high probe densities were achieved for a diffusion-limited, second-order Langmuir model. At the lowest probe density (2×10^{12} probes/cm^2), however, diffusion-resistance was not required to model the kinetic plots. Physically, the use of a higher-order Langmuir model is indicative of the interaction between the sites; any DNA molecule that is adsorbed on the surface inhibits the adsorption of other molecules due to steric and electrostatic repulsion. These effects of surface density can be exploited to improve mismatch discrimination and would be useful in SNP genotyping. Also, this study shows that careful selection of surface chemistry and judicious control of surface probe density is necessary for optimal DNA hybridization and thus optimal microarray performance.

3.5 Appendix: Second-order diffusion-limited Langmuir isotherm

The rate of change of surface coverage (Γ) depends on the flux of the DNA molecules

from the solution and some function of the surface sites available for adsorption Φ.

$$\frac{\partial \Gamma}{\partial t} = D \left(\frac{\partial C}{\partial x} \right)_{x=0} \Phi \tag{1}$$

where D is the diffusion constant of the adsorbing DNA molecules and t is time.

For a first-order Langmuir isotherm, Φ is equal to the fraction of sites available for adsorption

$(1-\theta)$, where θ is the fraction of sites already occupied. However, for a second-order Langmuir

model, there is a second-order dependence on the fraction of free sites.[37,38]

$$\frac{\partial \Gamma}{\partial t} = D \left(\frac{\partial C}{\partial x} \right)_{x=0} (1-\theta)^2 \tag{2}$$

Using Fick's law and assuming that the surface concentration (at x = 0) of the adsorbing DNA

molecules is close to zero, the flux at the surface is obtained as:

$$\left(\frac{\partial C}{\partial x} \right)_{x=0} = \frac{C_b}{\sqrt{\pi D t}} \tag{3}$$

where C_b is the bulk concentration of the adsorbing DNA molecules.

Substituting $\theta = \Gamma / \Gamma_{max}$ and the flux value from eq 2 in eq 3, we get

$$\frac{\partial \theta}{\partial t} = \frac{C_b}{\Gamma_{max}} \sqrt{\frac{D}{\pi t}} (1-\theta)^2 \tag{4}$$

Solving this equation with the initial boundary conditions, we get

$$\Gamma = \Gamma_{max} \frac{k\sqrt{t}}{1 + k\sqrt{t}} \tag{5}$$

where $k = \frac{2C_b}{\Gamma_{max}} \sqrt{\frac{D}{\pi}}$

3.6 References & Footnotes

(1) Gerhold, D.; Lu, M. Q.; Xu, J.; Austin, C.; Caskey, C. T.; Rushmore, T. *Physiol. Genomics* **2001**, *5*, 161-170.

(2) Der, S. D.; Zhou, A. M.; Williams, B. R. G.; Silverman, R. H. *Proc. Natl. Acad. Sci. U. S. A.* **1998**, *95*, 15623-15628.

(3) Lockhart, D. J.; Dong, H. L.; Byrne, M. C.; Follettie, M. T.; Gallo, M. V.; Chee, M. S.; Mittmann, M.; Wang, C. W.; Kobayashi, M.; Horton, H.; Brown, E. L. *Nat. Biotechnol.* **1996**, *14*, 1675-1680.

(4) Strachan, T.; Abitbol, M.; Davidson, D.; Beckmann, J. S. *Nature Genet.* **1997**, *16*, 126-132.

(5) Schena, M. *Bioessays* **1996**, *18*, 427-431.

(6) Schena, M.; Shalon, D.; Heller, R.; Chai, A.; Brown, P. O.; Davis, R. W. *Proc. Natl. Acad. Sci. U. S. A.* **1996**, *93*, 10614-10619.

(7) Caruso, F.; Rodda, E.; Furlong, D. F.; Niikura, K.; Okahata, Y. *Anal. Chem.* **1997**, *69*, 2043-2049.

(8) Steel, A. B.; Herne, T. M.; Tarlov, M. J. *Anal. Chem.* **1998**, *70*, 4670-4677.

(9) Wang, J.; Bard, A. J. *Anal. Chem.* **2001**, *73*, 2207-2212.

(10) Thiel, A. J.; Frutos, A. G.; Jordan, C. E.; Corn, R. M.; Smith, L. M. *Anal. Chem.* **1997**, *69*, 4948-4956.

(11) Vainrub, A.; Pettitt, B. M. *J. Am. Chem. Soc.* **2003**, *125*, 7798-7799.

(12) Vainrub, A.; Pettitt, B. M. *Phys. Rev. E* **2002**, *66*.

(13) Vainrub, A.; Pettitt, B. M. *Biopolymers* **2003**, *68*, 265-270.

(14) Vainrub, A.; Pettitt, B. M. *Biophys. J.* **2000**, *78*, 404A-404A.

(15) Vainrub, A.; Pettitt, B. M. *Chem. Phys. Lett.* **2000**, *323*, 160-166.

(16) Chan, V.; Graves, D. J.; McKenzie, S. E. *Biophys. J.* **1995**, *69*, 2243-2255.

(17) Herne, T. M.; Tarlov, M. J. *J. Am. Chem. Soc.* **1997**, *119*, 8916-8920.

(18) Watterson, J. H.; Piunno, P. A. E.; Wust, C. C.; Krull, U. J. *Langmuir* **2000**, *16*, 4984-4992.

(19) Guo, Z.; Guilfoyle, R. A.; Thiel, A. J.; Wang, R. F.; Smith, L. M. *Nucleic Acids Res.* **1994**, *22*, 5456-5465.

(20) Greene, T. W.; Wuts, P. G. M. *Protective Groups in Organic Synthesis*; 2nd ed.; John Wiley & Sons, Inc.: New York, 1991.

(21) Wilbur, J. L.; Kumar, A.; Kim, E.; Whitesides, G. M. *Adv. Mater.* **1994**, *6*, 600-604.

(22) Gao, X. P.; Edens, G. J.; Liu, F. C.; Hamelin, A.; Weaver, M. J. *J. Phys. Chem.* **1994**, *98*, 8086-8095.

(23) Lee, I. H. In *Chemical Engineering*; Massachusetts Institute of Technology: Cambridge, 2001.

(24) Crist, B. V. *Handbook of Monochromatic XPS Spectra - The Elements & Native Oxides*; John Wiley & Sons, Inc.: New York, 2000.

(25) Gao, P.; Weaver, M. J. *J. Phys. Chem.* **1986**, *90*, 4057-4063.

(26) McCarley, R. L.; Bard, A. J. *J. Phys. Chem.* **1991**, *95*, 9618-9620.

(27) Haiss, W.; Sass, J. K.; Gao, X.; Weaver, M. J. *Surf. Sci.* **1992**, *274*, L593-L598.

(28) Heise, A.; Stamm, M.; Rauscher, M.; Duschner, H.; Menzel, H. *Thin Solid Films* **1998**, *329*, 199-203.

(29) Bain, C. D.; Whitesides, G. M. *J. Am. Chem. Soc.* **1989**, *111*, 7164-7175.

(30) For comparison, the footprint diameter of a ssDNA is ~10 Å and that of a Watson-Crick dsDNA is ~18-20 Å corresponding to maximum packing densities for normally oriented ssDNA and dsDNA strands of ~1 x 10^{14} probes/cm^2 and ~2.5 x 10^{13} probes/cm^2, respectively.

(31) Saenger, W. *Principles of Nucleic Acid Structure*; Springer-Verlag: New York, 1984.

(32) Trohalaki, S.; Brian, A. A.; Frisch, H. L.; Lerman, L. S. *Biophys. J.* **1984**, *45*, 777-782.

(33) Shchepinov, M. S.; CaseGreen, S. C.; Southern, E. M. *Nucleic Acids Res.* **1997**, *25*, 1155-1161.

(34) Chrisey, L. A.; Lee, G. U.; Oferrall, C. E. *Nucleic Acids Res.* **1996**, *24*, 3031-3039.

(35) Peterson, A. W.; Heaton, R. J.; Georgiadis, R. M. *Nucleic Acids Res.* **2001**, *29*, 5163-5168.

(36) Piunno, P. A. E.; Watterson, J.; Wust, C. C.; Krull, U. J. *Anal. Chim. Acta* **1999**, *400*, 73-89.

(37) Rahn, J. R.; Hallock, R. B. *Langmuir* **1995**, *11*, 650-654.

(38) Hibbert, D. B.; Gooding, J. J.; Erokhin, P. *Langmuir* **2002**, *18*, 1770-1776.

(39) Steel, A. B.; Levicky, R. L.; Herne, T. M.; Tarlov, M. J. *Biophys. J.* **2000**, *79*, 975-981.

(40) Nkodo, A. E.; Garnier, J. M.; Tinland, B.; Ren, H. J.; Desruisseaux, C.; McCormick, L. C.; Drouin, G.; Slater, G. W. *Electrophoresis* **2001**, *22*, 2424-2432.

(41) Sorlie, S. S.; Pecora, R. *Macromolecules* **1990**, *23*, 487-497.

(42) According to a correlation in ref. 41, the diffusion constant for the 12-mer target oligonucleotide was calculated to be 1.3×10^{-6} cm^2/s . The value of the diffusion constant estimated from the fitted model parameters was also 1.3×10^{-6} cm^2/s.

(43) Meinkoth, J.; Wahl, G. *Anal. Biochem.* **1984**, *138*, 267-284.

(44) Keller, G. H.; Manak, M. M. *DNA Probes*; 2nd ed.; Stockton Press: New York, 1993.

(45) Georgiadis, R.; Peterlinz, K. P.; Peterson, A. W. *J. Am. Chem. Soc.* **2000**, *122*, 3166-3173.

(46) Nearest neighbor calculations performed using the software at http://www.basic.nwu.edu/biotools/oligocalc.html.

Chapter 4.   Modulating Nanoparticle Attachment by DNA

Probe Density

4.1 Introduction

There has been an increasing interest in assembling nanoparticles on surfaces to utilize their special electronic and optical properties for various chemical and biological sensing applications. Gold (Au) nanoparticles have been the most widely studied class of metal nanoparticles because of their ease of synthesis, inexpensive commercial availability, tailorable optical properties, and availability of various chemistries to functionalize their surfaces. These nanoparticles have been attached onto surfaces by covalent interactions,[1] electrostatic interactions,[2-6] avidin-biotin interactions,[7] antibody-antigen interactions,[8] and sequence-specific DNA-DNA interactions.[9-12] Sub-monolayers of Au nanoparticles have been used for SERS measurements,[13,14] enhanced SPR measurements,[15,16] enzyme-based biosensing applications,[17] and DNA detection schemes[18,19].

In the above mentioned surface applications, interparticle separation is crucial for determining the properties of the immobilized particles.[20] Various methods have been employed to modulate the surface density (and hence interparticle separation) of the adsorbed nanoparticles. In general, the adsorbed density of the nanoparticles can be changed by modulating the surface functionality and the charge on the particles, the time of deposition, the pH and the salt concentration of the depositing solution, and the density of the active groups on the capture surface. Natan et al.[21] employed kinetic control to vary the density of gold nanoparticles on surfaces exposing CN, SH, and NH_2 functional groups. For their system, the deposition was diffusion limited and proportional to $t^{1/2}$ at short times. However, eventually the

interparticle electrostatic repulsions led to a plateau in surface coverage. Liu and coworkers[3] employed pH to modulate the strength of the electrostatic interactions responsible for adsorbing negatively charged gold nanoparticles onto a surface. Miyashita et al.[22] varied the polymer composition of a copolymer film to control the adsorption of nanoparticles while Genzer and coworkers[5,6] changed the MW and grafting density of surface-anchored polymer films to create a gradient of adsorbed gold nanoparticles.

In this study, I have chosen to assemble gold nanoparticles on a silicon surface by sequence-specific DNA-DNA interactions and modulate the adsorbed nanoparticle density by tailoring the surface density of the DNA capture probes. The multiplicity and specificity of DNA-DNA interactions provide a valuable tool to self-assemble nanoparticles on surfaces in a controlled and specified manner. DNA-DNA hybridizations have been used for creating various self-assembled nanoparticulate structures.[5,6,23-32] DNA-driven assembly of nanoparticles, in particular, has been employed to provide ultra-sensitive detection methods for DNA molecules.[18,19,33] Previous reports on the DNA-driven surface assembly of nanoparticles have focused on reducing the aggregation of adsorbed nanoparticles,[11] improving the discrimination between specific and non-specific interactions,[10] and creating multilayer structures.[12] The key ingredient in these systems is the chemistry for immobilizing the DNA molecules, which should promote high specific attachment and minimize non-specific attachment of particles. In this regard, an ability to vary the surface density of the immobilized DNA probe molecules will provide a valuable handle to control the extent of DNA-driven nanoparticle adsorption.

I have employed a mixed-silane chemistry to modulate the density of the DNA probes on silicon surfaces (see Chapter 3). These surfaces with varying amounts of DNA probes were then used to immobilize 20-nm Au nanoparticles via DNA-DNA interactions. I used SEM and XPS to

visualize and quantify the nanoparticle adsorption. The main goals of this study were to control the adsorbed density of the nanoparticles via modulation of the surface DNA probe density and to increase the discrimination between the nanoparticle adsorption on surfaces bearing complementary and non-complementary DNA sequences.

4.2 Experimental Section

Chemicals. Undecylenyl alcohol, trichloroacetyl chloride, pyridine, trichlorosilane, octyl trichlorosilane, octadecyl trichlorosilane, anhydrous THF, anhydrous toluene, and chloroplatinic acid were obtained from Aldrich (Milwaukee, WI). Gold pellets were supplied by J&J Materials, Inc. (Neptune City, NJ), and chromium wires were supplied by R. D. Mathis and Company (Long Beach, CA). Acetonitrile, methanol, ethanol, acetone, sodium chloride, EDTA, tris-HCl, phosphate buffered saline tablets, and potassium carbonate were obtained from Mallinckrodt (Paris, KE). Phosphoramidites and reagents used for oligonucleotide synthesis, and empty TWIST™ columns were obtained from Glen Research (Sterling, MA). Piperidine (20%) in dimethyl formamide was obtained from Protein Technologies, Inc. (Tucson, AZ). Deionized water (Resistance = 18.2 MΩ) was provided by a MilliQ deionization system (Millipore Corp., Bedford, MA). Citrate-stabilized 20-nm gold nanoparticles were obtained from Ted Pella, Inc. (Redding, CA). Thiolated oligonucleotide 5'-TGG TCG CAC AGG TCG CAT (CH$_2$)$_3$ SH- 3' (oligo cA) was obtained from Integrated DNA Technologies, Inc. (Coralville, IA) in the disulfide form. Centri-Spin™ columns for gel filtration were obtained from Princeton Separations (Adelphia, NJ). All materials were used as received.

Surface preparation. Silicon chips (1 cm x 3 cm) were cleaned by immersing in a base bath solution (12.5 wt% NaOH in 3:4 H$_2$O: ethanol solution) for 4 h. The chips were then rinsed with deionized water and dried in a stream of nitrogen. The silanizing solution was prepared by

adding octyl trichlorosilane (C_8 silane) and trichloroacetyl (TCA) protected ω-hydroxyundecyl trichlorosilane (TCA silane) (for detailed recipe see Chapter 3) in requisite proportions to anhydrous toluene (>99.5%) to yield 1 μL/mL (~mM) solution of the silanes in toluene. The chips were immersed in this solution for 4 h at room temperature to coat them with a mixed silane layer exposing methyl and trichloroacetyl groups on the surface. After 4 h, the chips were sequentially rinsed with acetone and ethanol and dried with a N_2 gas stream. To expose the TCA-protected hydroxyl groups prior to DNA synthesis, the TCA groups were removed by immersing the slides in 5 mM K_2CO_3 solution in 1:1 H_2O: methanol for 15 min. The chips were then rinsed with copious amounts of water to remove the salt, followed by ethanol, and finally dried in a stream of N_2. The density of hydroxyl groups on the surface could be modulated by changing the relative proportions of the C_8 silane and TCA silane in the silanizing solution. Chips 1-4 with different densities of hydroxyl groups were prepared.

Oligonucleotide synthesis. Short silicon slides (0.5 cm x 0.5 cm) were cut from the bigger silicon chips. These slides were placed in TWIST™ columns on an Applied Biosystems ABI-392/394 automated DNA synthesizer to synthesize oligonucleotide A (oligo A) on these slides. UltraMild® phosphoramidites were used for synthesis in order to avoid exposing the silane films to a strong base such as ammonium hydroxide as needed for removing the base-protecting groups. The delivery and reaction times of the various reagents were manipulated to optimize the oligonucleotide synthesis on these slides. To retain the synthesized oligonucleotides on the glass surface, the ammonium hydroxide step used to normally detach the oligonucleotide from the support was disabled. Instead, the slides were washed sequentially with acetonitrile, acetone, and ethanol after synthesis and dried with N_2 gas stream. Following the automated synthesis, the slides were immersed in a 20-wt% piperidine in dimethyl formamide (DMF) solution for 4 h to

remove the cyanoethyl-protecting groups. The base-protecting groups were removed by immersing the slides in a 0.05 M K_2CO_3 solution in anhydrous methanol for 4 h. The above procedure was used to synthesize 5'- ATG CGA CCT GTG CGA CCA TTT T 3' as the probe oligonucleotide (oligo A) on the slides 1-4. Sequence 5' – TGG TCG CAC AGG TCG CAT TTT T – 3' (oligo B) was synthesized on the control slide 3nc as a sequence non-compelmentary to the target oligonucleotide on the gold nanoparticles (oligo cA).

Nanoparticle functionalization. Gold nanoparticles were functionalized with oligonucleotide cA using methods reported in literature.[34] Briefly, the thiolated oligonucleotide (oligo cA) obtained from the vendor in the disulfide form was reduced in a 0.05 M DTT solution for 30 min. Excess DTT was removed using gel filtration on Centri-Spin™ columns. The oligonucleotide solution was diluted with the citrate-stabilized nanoparticle solution to yield a 5 µM oligonucleotide concentration and a 0.6 nM nanoparticle concentration. After standing for 16 h, the solution was brought to 0.1 M NaCl, 10 mM phosphate buffer (pH 7). After ageing the solution for more than 24 h, it was centrifuged at 14000 rpm for 30 min. The precipitate was washed with 0.1 M NaCl, 10 mM phosphate buffer (pH 7) followed by centrifugation and redispersion. The final salt concentration of the nanoparticle solution was brought to 0.3 M NaCl by gradually adding drops of 1 M NaCl.

Nanoparticle adsorption via DNA hybridization. Slides 1-4 and 3nc were placed in the nanoparticle solution for 24 h, the slides were then rinsed with 0.3 M NaCl solution and briefly with H_2O followed by drying with a nitrogen stream. The nanoparticle-covered slides were visualized with a Philips XL30 FEG-ESEM in the backscatter mode. The particle density was calculated using three images (analyses areas were typically 1048 nm x 712 nm) for each probe density. The particle counting was done using Scion Image analysis software.

X-ray photoelectron spectroscopy (XPS) measurements. XPS spectra were obtained with a Surface Science Instruments Model X-100 spectrometer using a monochromatized Al Kα X-ray source (elliptical spot of 1.0 mm x 1.7 mm) and a concentric hemispherical analyzer (pass energy = 50 eV). The detector angle with respect to the surface parallel was 35°. Peak positions were referenced to Au $(4f_{7/2})$ = 84.00 eV and were fit with 80% Gaussian/20% Lorentzian profiles and a Shirley background to obtain integrated peak intensities. A reference sample for calibration consisted of a Au-coated Si surface (Au-1000 Å, Cr-100 Å) coated with oligo cA.

4.3 Results and Discussion

4.3.1 Surfaces with varying probe densities

To control the density of the adsorbed DNA-tagged gold nanoparticles, I created surfaces with varying densities of the DNA capture probes. Different densities of the DNA capture probes were achieved by modulating the DNA immobilization chemistry. Short-chain oligonucleotides were immobilized on surfaces exposing different amounts of the active hydroxyl groups. The density of the hydroxyl groups on the surface was controlled by functionalizing the Si/SiO_2 surfaces with a mixture of two silanes: a TCA-protected C_{11} hydroxy trichlorosilane and a methyl-terminated C_8 trichlorosilane. Figure 4-1 illustrates the surface chemistry. After functionalization with the silane molecules, the TCA group was deprotected using a K_2CO_3 solution in methanol and water to expose the hydroxyl groups. A commercial DNA synthesizer was then used to synthesize short-chain DNA molecules on these surfaces. Surfaces with four different DNA probe densities were prepared (slides 1-4). The DNA densities were quantified using XPS measurements (see Chapter 3). A control slide 3nc was prepared with the same probe density as slide 3 but with a DNA sequence non-complementary to the target oligonucleotide on the Au nanoparticles.

110
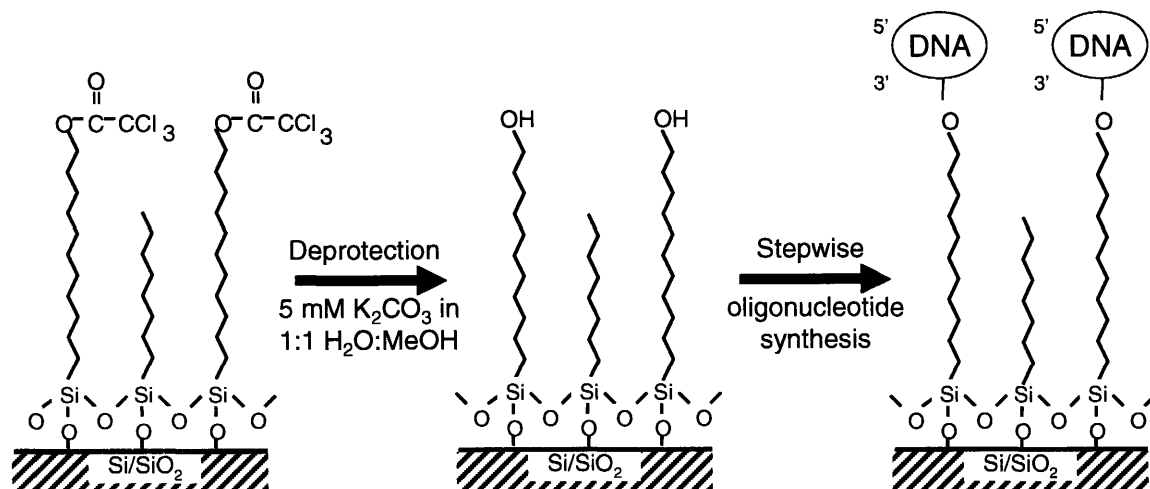
Figure 4-1 Schematic illustration of the surface preparation to form end-immobilized oligonucleotides of controlled surface densities. The steps include: silanization with mixed silanes, followed by deprotection and stepwise oligonucleotide synthesis. The concentration of the hydroxyl groups was controlled by varying the composition of the two silanes in the silanizing solution. After chemical deprotection, oligonucleotides were synthesized by a stepwise process using a ABI 392 oligonucleotide synthesizer.

4.3.2 DNA-driven nanoparticle adsorption

The 20-nm gold nanoparticles were functionalized with thiol-DNA using methods reported in literature.[34] The sequence of the DNA on the Au nanoparticles was complementary to that on slides 1-4. The DNA-tagged Au-nanoparticle solution was then brought in contact with the DNA-functionalized Si/SiO_2 surfaces and allowed to remain in contact for more than 16 h. A schematic of the process is shown in Figure 4-2. After 16 h, the slides were removed from the nanoparticle solution and washed with 0.3 M NaCl solution and dried with a stream of nitrogen gas. The slides appeared slightly reddish in color because of the nanoparticle attachment. The slides were then imaged using SEM. Figure 4-3 shows SEM images for the four densities employed in this study and for the control slide. During the drying process, increased salt concentration reduces the electrostatic repulsions between the particles and the lateral capillary forces lead to aggregation of the particles.[35-38] Figure 4-3 shows that with the increase in probe density from slide 1 to slide 3, the adsorbed nanoparticle density also increases from 480 particles/μm^2 to 1070 particles/μm^2. Notably if the probe density is increased further as in slide 4, the adsorbed nanoparticle density reduces to 590 particles/μm^2. This decrease can be attributed to the increased steric and electrostatic hindrances faced by the nanoparticles from the dense, negatively-charged DNA probe surface.

The adsorbed particle densities were also quantified by XPS measurements of the Au (4f) signals at 84 and 88 eV (Figure 4-4). **Table 4-1** lists the particle densities computed from the SEM images and the XPS measurements. The data show a general consistency, revealing a maximum in the nanoparticle surface coverages. The nanoparticle density on a control surface containing the non-complementary oligonucleotide is less than 1 particles/μm^2, demonstrating the effectiveness of the surface chemistry in blocking non-specific attachments. By comparison,

A) Nanoparticle functionalization
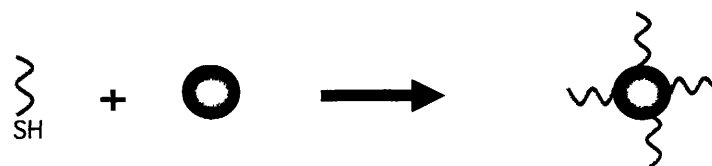
B) DNA-driven nanoparticle adsorption
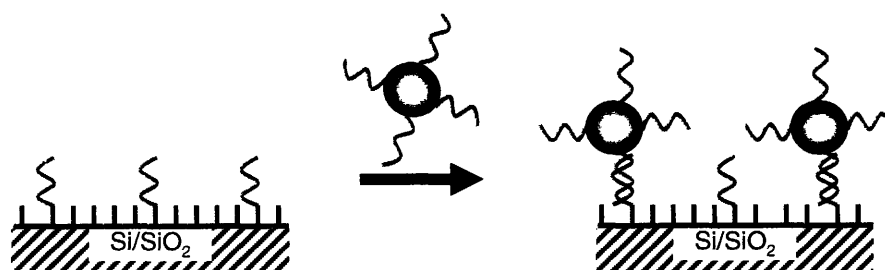
Figure 4-2 Schematic illustration of nanoparticle functionalization and subsequent adsorption via DNA-DNA hybridization. A) Citrate-stabilized gold nanoparticles are functionalized with thiol-tagged oligonucleotides. B) DNA-functionalized gold nanoparticles are assembled on Si/SiO₂ surfaces functionalized with the complementary DNA sequence.
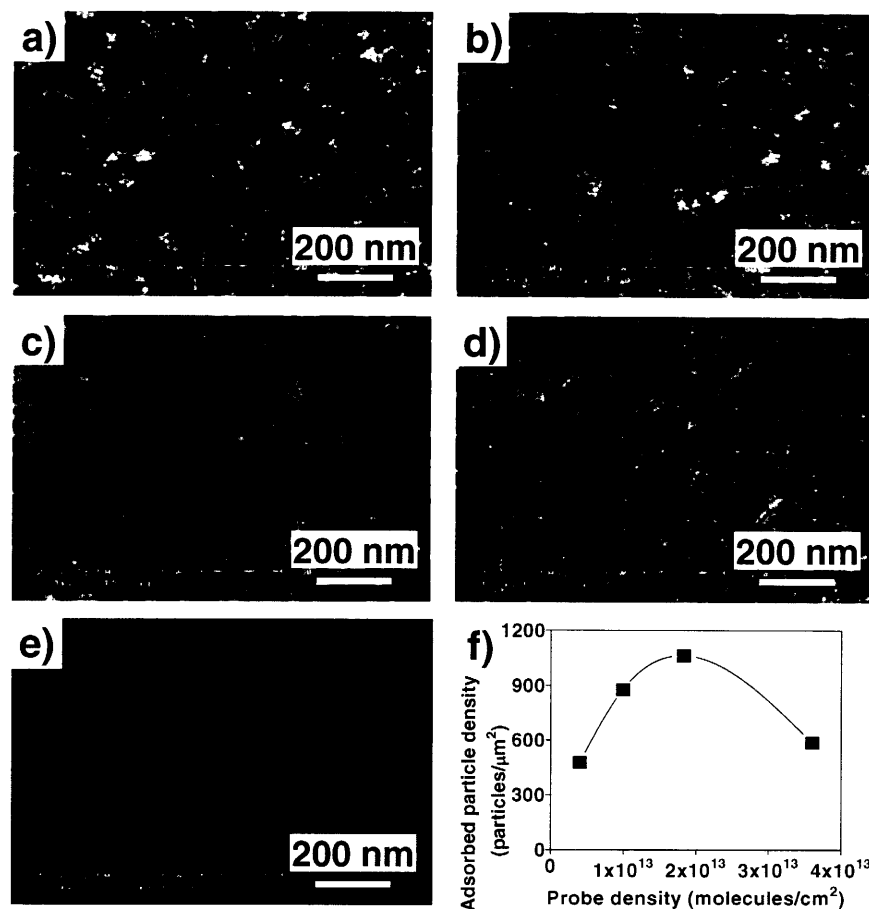
Figure 4-3 (a-d) SEM images of nanoparticle adsorption on Si/SiO$_2$ surfaces (slides 1-4) exposing complementary DNA probes (oligo A) at densities of 0.4 x 10^5 , 1.0 x 10^5, 1.8 x 10^5, and 3.6 x 10^5 probes/μm^2, respectively. (e) SEM image of non-specific nanoparticle adsorption on a control surface (slide 3nc) exposing a non-complementary DNA sequence (oligo B) at a density of 1.8 x 10^5 probes/μm^2. (f) Plot of the variation of adsorbed nanoparticle density with surface probe density.
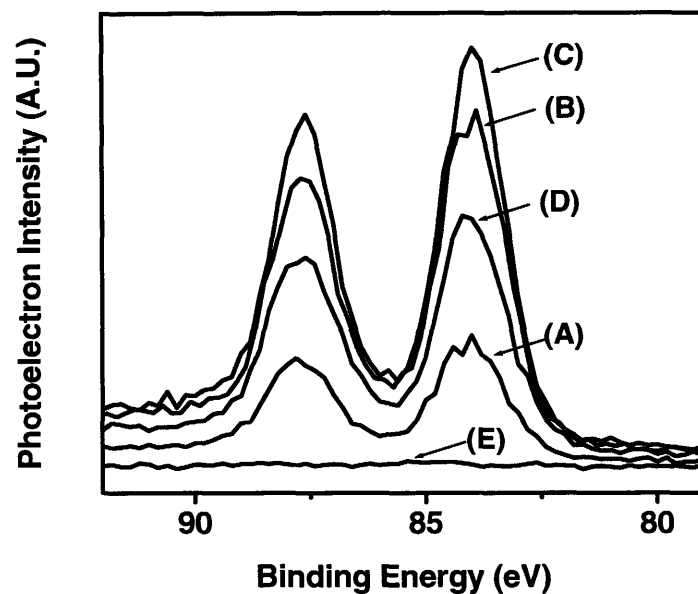
Figure 4-4 High resolution Au (4f) XPS spectra of DNA-tagged gold nanoparticles adsorbed on complementary surfaces (slides 1-4) containing (A) 0.4×10^5, (B) 1.0×10^5, (C) 1.8×10^5, and (D) 3.6×10^5 probes/μm^2. (E) Spectrum for non-specific adsorption of DNA-tagged gold nanoparticles on a non-complementary surface (slide 3nc).

Table 4-1 Nanoparticle area coverages computed from SEM images and XPS measurements.

	DNA probe density (probes/μm^2)	Nanoparticle area coverage (%)	
		SEM image analysis	XPS measurements
Complementary sequence			
1	0.4×10^5	12	10
2	1.0×10^5	22	25
3	1.8×10^5	28	28
4	3.6×10^5	15	21
Non-complementary sequence			
3nc	1.8×10^5	0.0	0.4

the highest adsorbed particle density on the complementary surface (slide 3) is three orders of magnitude greater than the adsorbed particle density on the non-complementary surface (slide 3nc). The higher discrimination between specific and non-specific event is extremely important for the formation of defect-free assembled structures.

4.3.3 Comparison with other studies

Franzen et al.[11] immobilized thiol-DNA on flat Au surfaces and used these surfaces to adsorb 5-nm and 10-nm gold nanoparticles using a salt concentration of 0.15 M NaCl. They employed FTIR, Raman spectroscopy, and STM to characterize these surfaces. The aim of their study was to obtain dense monolayers of the nanoparticles without excessive aggregation. The maximum area coverage that they could obtain with the 5-nm particles was ~3.3%, corresponding to a particle density of 1700 particles/μm^2. However, the non-specific adsorption on their surfaces was close to 500 paricles/μm^2 resulting in only a four-fold discrimination between specific and non-specific adsorption. Niemeyer et al.[10] also employed the thiol chemistry to immobilize DNA molecules on Au surfaces and were able to adsorb 35-nm Au nanoparticles with area coverage of 37%, corresponding to adsorbed particle density of 400 particle/μm^2. However, the specific adsorption of nanoparticles was only 20 times more effective than the non-specific adsorption. In contrast, our chemistry provides around three orders of magnitude discrimination between specific and non-specific adsorption. Mirkin et al.[12] immobilized thiol-DNA on ITO (Indium tin oxide) surfaces using an amino silane film on the ITO surface and SMPB (succinimidyl 4-malemidophenyl butyrate) as the crosslinker. Under hybridization conditions similar to those in our study, they could achieve an area coverage of 11% for 13-nm gold nanoparticles, corresponding to a particle density of ~800 particles/μm^2. Their surface chemistry did not provide a control over the probe density and hence the adsorbed

nanoparticle density. In summary, our surface chemistry provides nanoparticle adsorption at fairly high densities coupled with substantially higher specificities than those reported by other research groups.

4.3.4 Thermodynamic analysis

To gain a better understanding of the nanoparticle adsorption thermodynamics, the overall adsorption constant (K_s) was computed using the equilibrium values of the bound nanoparticles, unbound nanoparticles, and accessible unbound surface DNA probes. Such an estimation gave the strength of the overall attachment without making any assumptions about the number and strength of DNA interactions involved in the nanoparticle adsorption process. The K_s values for the DNA-directed nanoparticle adsorption are an order of magnitude higher than those obtained for molecular DNA adsorption under similar conditions. In this study, the nanoparticles were adsorbed onto flat surfaces by hybridization between DNA strands having an overlap length of 18 bases and at a salt concentration of 0.3 M NaCl. Georgiadis et al.[39] have reported a K_s of 3×10^7 M^{-1} for 18-mer DNA adsorption onto flat surfaces at 1 M NaCl. Corn et al.[40] have employed SPR imaging to monitor the formation of a 18-mer DNA duplex on a flat surface at 0.3 M NaCl and have estimated a K_s of 1.3×10^7 M^{-1} for this process. In contrast, the K_s values obtained for DNA-directed nanoparticle adsorption in this study range from 2.7×10^8 to 9.8×10^8 M^{-1}. These higher K_s values suggest that the nanoparticles are attached onto the surface via multiple DNA duplexes. Based on the density of DNA molecules on the surface of the nanoparticles, each nanoparticle presents ~5-10[24,41] DNA strands in the area of contact and is thus capable of forming multiple DNA-DNA interactions with the substrate surface.

Figure 4-5 illustrates the contrast between the dependence of K_s values on surface probe density for the cases of DNA-directed nanoparticle adsorption and molecular DNA adsorption.

The K_s values for nanoparticle adsorption increase with modest increases in probe density but decrease at extremely high probe densities. This trend is in contrast to that obtained in our studies of surface hybridization of 12-mer DNA molecules (see Chapter 3). The K_s values for DNA hybridization monotonically decrease with increase in probe density suggesting the continued destabilization of the duplex due to increasing steric and electrostatic hindrances. Together, these results imply that a modest increase in probe density allows more DNA strands per nanoparticle to hybridize with the surface-bound probes. This increase in the number of DNA attachments per nanoparticle offsets any loss in the stability of the individual duplexes and yields stronger nanoparticle attachment to the surface. But at extremely high densities, the increase in the number of interactions per nanoparticle is not large enough to overcome the substantial losses in individual duplex stabilities due to the steric and electrostatic repulsions resulting in lower nanoparticle adsorption. These two studies illustrate important differences between the adsorption behavior of monovalent and multivalent species onto surfaces with varying densities of receptor sites.
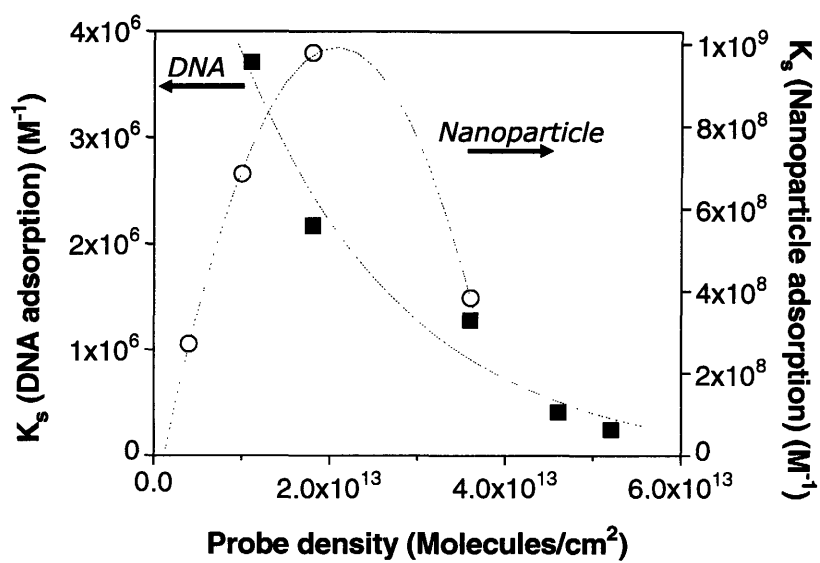
Figure 4-5 Comparison of thermodynamics of nanoparticle adsorption vs. molecular DNA adsorption. The filled squares (■) show variation of the equilibrium binding constant (Ks) with probe density for the surface hybridization of 12-mer DNA strands (Figure 3-11). The open circles (○) show variation of the equilibrium binding constant (Ks) with probe density for the DNA-directed attachment of nanoparticles involving hybridization between 18-mer DNA strands.

4.4 Conclusions

DNA-directed nanoparticle attachment on flat substrates functionalized with complementary sequences can be modulated by varying the densities of the surface probe sites. In this study, the surface probe densities were varied by using a mixed silane chemistry along with stepwise phosphoramidite synthesis. Nanoparticle adsorption at various probe densities (0.4 x 10^{13} to 3.6 x 10^{13} probes/cm^2) was examined using image analysis and XPS measurements. Maximum adsorbed particle density of 1070 particles/μm^2, corresponding to an area coverage on the surface of ~28%, was obtained on a surface with probe density of 1.8 x 10^{13} probes/cm^2. Extremely high probe densities led to decreased nanoparticle adsorption due to increased steric and electrostatic hindrances. Our chemistry was effective in shielding non-specific interactions and yielded around three orders of magnitude specificity for the DNA-directed attachment of nanoparticles on complementary surfaces vis-à-vis non-complementary surfaces. Thermodynamic analysis of the nanoparticle adsorption process showed that the multivalent nature of the DNA-directed nanoparticle attachment is aided by modest increases in probe densities resulting in higher binding free energy and higher equilibrium adsorbed amounts. This behavior is in contrast to that observed during molecular DNA adsorption (Chapter 3) where modest increases in probe density lead to higher adsorbed amounts for DNA molecules in spite of lowering of the binding free energy. The results of this study along with those of Chapter 3 show that the thermodynamics of multivalent nanoparticle attachment is different than that of the monovalent molecular DNA adsorption. A better understanding of the thermodynamics of the multivalent nanoparticle attachment process can be useful in designing strategies for the bottom-up assembly of nano-scale objects using weak interactions such as those involved in DNA-DNA hybridization. Additionally, the ability to modulate the density of nanoparticles on a surface can

be important for sensor applications based on optical, electrical, and spectroscopic methods where interparticle distance plays an important role in the detection mechanism.

4.5 References & Footnotes

(1) Grabar, K. C.; Freeman, R. G.; Hommer, M. B.; Natan, M. J. *Anal. Chem.* **1995**, *67*, 735-743.

(2) Wang, H.; Wang, C. C.; Lei, C. X.; Wu, Z. Y.; Shen, G. L.; Yu, R. Q. *Anal. Bioanal. Chem.* **2003**, *377*, 632-638.

(3) Zhu, T.; Fu, X. Y.; Mu, T.; Wang, J.; Liu, Z. F. *Langmuir* **1999**, *15*, 5197-5199.

(4) Bhat, R. R.; Fischer, D. A.; Genzer, J. *Langmuir* **2002**, *18*, 5640-5643.

(5) Bhat, R. R.; Genzer, J.; Chaney, B. N.; Sugg, H. W.; Liebmann-Vinson, A. *Nanotechnology* **2003**, *14*, 1145-1152.

(6) Bhat, R. R.; Tomlinson, M. R.; Genzer, J. *Macromol. Rapid Commun.* **2004**, *25*, 270-274.

(7) Olofsson, L.; Rindzevicius, T.; Pfeiffer, I.; Kall, M.; Hook, F. *Langmuir* **2003**, *19*, 10414-10419.

(8) Tang, D. P.; Yuan, R.; Chai, Y. Q.; Zhong, X.; Liu, Y.; Dai, J. Y.; Zhang, L. Y. *Anal. Biochem.* **2004**, *333*, 345-350.

(9) Niemeyer, C. M.; Ceyhan, B.; Gao, S.; Chi, L.; Peschel, S.; Simon, U. *Colloid Polym. Sci.* **2001**, *279*, 68-72.

(10) Peschel, S.; Ceyhan, B.; Niemeyer, C. M.; Gao, S.; Chi, L.; Simon, U. *Mater. Sci. Eng. C-Biomimetic Supramol. Syst.* **2002**, *19*, 47-50.

(11) Sauthier, M. L.; Carroll, R. L.; Gorman, C. B.; Franzen, S. *Langmuir* **2002**, *18*, 1825-1830.

(12) Taton, T. A.; Mucic, R. C.; Mirkin, C. A.; Letsinger, R. L. *J. Am. Chem. Soc.* **2000**, *122*, 6305-6306.

(13) Freeman, R. G.; Grabar, K. C.; Allison, K. J.; Bright, R. M.; Davis, J. A.; Guthrie, A. P.; Hommer, M. B.; Jackson, M. A.; Smith, P. C.; Walter, D. G.; Natan, M. J. *Science* **1995**, *267*, 1629-1632.

(14) Chumanov, G.; Sokolov, K.; Gregory, B. W.; Cotton, T. M. *J. Phys. Chem.* **1995**, *99*, 9466-9471.

(15) He, L.; Musick, M. D.; Nicewarner, S. R.; Salinas, F. G.; Benkovic, S. J.; Natan, M. J.; Keating, C. D. *J. Am. Chem. Soc.* **2000**, *122*, 9071-9077.

(16) Lyon, L. A.; Musick, M. D.; Natan, M. J. *Anal. Chem.* **1998**, *70*, 5177-5183.

(17) Zhao, J. G.; Henkens, R. W.; Stonehuerner, J.; Odaly, J. P.; Crumbliss, A. L. *J. Electroanal. Chem.* **1992**, *327*, 109-119.

(18) Park, S. J.; Taton, T. A.; Mirkin, C. A. *Science* **2002**, *295*, 1503-1506.

(19) Taton, T. A.; Mirkin, C. A.; Letsinger, R. L. *Science* **2000**, *289*, 1757-1760.

(20) Shipway, A. N.; Katz, E.; Willner, I. *ChemPhysChem* **2000**, *1*, 18-52.

(21) Grabar, K. C.; Smith, P. C.; Musick, M. D.; Davis, J. A.; Walter, D. G.; Jackson, M. A.; Guthrie, A. P.; Natan, M. J. *J. Am. Chem. Soc.* **1996**, *118*, 1148-1153.

(22) Tanaka, H.; Mitsuishi, M.; Miyashita, T. *Langmuir* **2003**, *19*, 3103-3105.

(23) Mbindyo, J. K. N.; Reiss, B. D.; Martin, B. R.; Keating, C. D.; Natan, M. J.; Mallouk, T. E. *Adv. Mater.* **2001**, *13*, 249-254.

(24) Mirkin, C. A. *Inorg. Chem.* **2000**, *39*, 2258-2272.

(25) Mirkin, C. A.; Letsinger, R. L.; Mucic, R. C.; Storhoff, J. J. *Nature* **1996**, *382*, 607-609.

(26) Mitchell, G. P.; Mirkin, C. A.; Letsinger, R. L. *J. Am. Chem. Soc.* **1999**, *121*, 8122-8123.

(27) Mucic, R. C.; Storhoff, J. J.; Mirkin, C. A.; Letsinger, R. L. *J. Am. Chem. Soc.* **1998**, *120*, 12674-12675.

(28) Nam, J. M.; Thaxton, C. S.; Mirkin, C. A. *Science* **2003**, *301*, 1884-1886.

(29) Niemeyer, C. M. *Appl. Phys. A-Mater. Sci. Process.* **1999**, *68*, 119-124.

(30) Niemeyer, C. M.; Boldt, L.; Ceyhan, B.; Blohm, D. *Anal. Biochem.* **1999**, *268*, 54-63.

(31) Alivisatos, A. P.; Johnsson, K. P.; Peng, X. G.; Wilson, T. E.; Loweth, C. J.; Bruchez, M. P.; Schultz, P. G. *Nature* **1996**, *382*, 609-611.

(32) Hartmann, D. M.; Heller, M.; Esener, S. C.; Schwartz, D.; Tu, G. *J. Mater. Res.* **2002**, *17*, 473-478.

(33) Kohler, J. M.; Csaki, A.; Reichert, J.; Moller, R.; Straube, W.; Fritzsche, W. *Sens. Actuator B-Chem.* **2001**, *76*, 166-172.

(34) Storhoff, J. J.; Elghanian, R.; Mucic, R. C.; Mirkin, C. A.; Letsinger, R. L. *J. Am. Chem. Soc.* **1998**, *120*, 1959-1964.

(35) Thill, A.; Spalla, O. *Colloid Surf. A-Physicochem. Eng. Asp.* **2003**, *217*, 143-151.

(36) Rabani, E.; Reichman, D. R.; Geissler, P. L.; Brus, L. E. *Nature* **2003**, *426*, 271-274.

(37) Demers, L. M.; Park, S. J.; Taton, T. A.; Li, Z.; Mirkin, C. A. *Angew. Chem.-Int. Edit.* **2001**, *40*, 3071-3073.

(38) The clustering of the particles in these images is an artifact of the washing and drying protocols and can be reduced in the future by using volatile salts like ammonium acetate (Ref. 37).

(39) Peterson, A. W.; Wolf, L. K.; Georgiadis, R. M. *J. Am. Chem. Soc.* **2002**, *124*, 14601-14607.

(40) Nelson, B. P.; Grimsrud, T. E.; Liles, M. R.; Goodman, R. M.; Corn, R. M. *Anal. Chem.* **2001**, *73*, 1-7.

(41) Demers, L. M.; Mirkin, C. A.; Mucic, R. C.; Reynolds, R. A.; Letsinger, R. L.; Elghanian, R.; Viswanadham, G. *Anal. Chem.* **2000**, *72*, 5535-5541.

Chapter 5.   Effect of Shape on DNA-Directed Assembly –

Assembly of Microparticles

5.1 Introduction

With the top-down approaches reaching their physical limits, there has been an increasing interest in exploring novel bottom-up ways, including self assembly, to create the next generation of functional devices in microelectronics, photonics, information storage, microanalysis, ultra-sensitive detection etc.. One strategy is the modular approach, wherein nano-scale objects are self assembled onto micron-sized objects and then these multicomponent systems are assembled to create larger functional devices. A notable aspect of the modular approach is that it would allow more flexibility in the design and construction of assembled devices. For such a scheme, the ease of manufacture and availability of building blocks with functional and structural diversity at the nano- and micro- scales is crucial. Another important requirement is the ability to assemble and align these various building blocks in a pre-determined manner based on the interactions programmed onto them.[1,2]

Various methods have been used to guide the assembly of micro- and nano-scale objects,[3-5] with DNA-DNA hybridization being among them.[6-12] Recent advances made in the functionalization of various surfaces with DNA sequences,[12-19] the printing and patterning of DNA films on surfaces,[20-26] and in the chemical modification of assembled DNA structures[27-30] are providing new possibilities for generating structures that can be assembled using DNA-DNA interactions. In the construction of MEMS devices, there has been an increasing interest to fabricate some components by performing parallel assembly of micron-sized objects. In this field, self-assembly via DNA-DNA interactions can prove to be beneficial, given the range of

mutually-selective interactions that can be accessed using DNA sequences. Other techniques for assembling micron-sized components have been based either on shape recognition[31] or differences in hydrophilicity.[5] Compared with these approaches, the use of DNA-driven assembly for such applications will greatly enhance the flexibility and scope for design. Additionally, the assembly of micron-sized particles via DNA hybridization can be useful for other applications. For example, micron-sized particles can be more useful than nanoparticles in schemes for ultra sensitive detection of DNA hybridization events as the microparticles offer more surface area for signal amplification (i.e. improved sensitivity) and the possibility for visual detection.[10,32]

In order to assemble micron-sized objects using weak forces such as those involved in DNA hybridization, it is important to ensure that the linkages are strong enough to withstand the forces that will act on the assembled structures (such as capillary forces). Structures assembled via DNA hybridization can be locked in their assembled state by methods such as crosslinking[29] or metallizing the DNA strands[27]; however, these modifications would reduce the reversibility of the assembled structures. Another approach to increasing the stability of the assembled structures is to increase the number of DNA-DNA interactions and the area of contact between pairs of objects. This arrangement would ensure that the particles are attached via adhesive forces strong enough to withstand the rigors of the self-assembly protocol and would also retain the reversible nature of the process. For such an approach, particles with large aspect ratios like rods or platelets would be desirable.

5.1.1 Forces involved in the assembly process

Table 5-1 shows the effect of shape on the various forces involved in the DNA-driven assembly of micron-scale particles. Since the assembly of the structures is performed in an aqueous medium that in most cases necessitates drying to achieve the final assembled state, the lateral capillary forces become important. Table 5-1 shows the maximum capillary force operating when two similar particles are in close contact. These values were calculated according to a formulation by Kralchevsky et al.[33,34] The adhesion forces in Table 5-1 were calculated assuming a DNA density of 3.3 x 10^{13} molecules/cm^2 on the surface of the particles and a hybridization efficiency of 15%.[35] The strength of each DNA-DNA interaction was assumed to be 30 pN.[36] In comparing the two types of particles, the cylindrical particles provide more contact area and adhesion force per unit weight as compared to the spherical particles. A shift from a spherical to a cylindrical shape increases the capillary forces by roughly one order of magnitude while the increase in the contact area and the adhesive forces is three orders of magnitude. Other forces operating on these particles (for e.g. the drag force due to the relative motion of the fluid medium) are orders of magnitude smaller than the capillary forces. These force estimations clearly suggest that in the assembly of particles using weak DNA-DNA interactions, the cylindrical shape offers significant advantages over the spherical one.

The main objective of this study was to explore the effect of shape on the assembly of micron-sized particles using DNA-DNA interactions. Further there is great interest in the use of asymmetric building blocks for performing bottom-up assembly. For example, Dwyer et al.[37] in their theoretical analysis of fabricating computing circuitry using DNA-guided assembly have identified the generation and assembly of asymmetrically functionalized building blocks as key enabling technologies that are necessary for the practical implementation of guided-assembly

schemes. Simulations performed by Glotzer et al.[38] have shown the variety of aperiodic 1-D, 2-D, and 3-D structures that can be assembled from particles that contain asymmetric functionalities. Here, I have prepared particles that expose distinct regions each containing a different DNA sequence and examined the possibility for performing an orientation-specific assembly of these particles onto a substrate based on the complementarity of their DNA-DNA interactions. The engineering behind the creation and assembly of asymmetric building blocks with multiple functionalities will be a significant addition to the 'directed-assembly toolkit'.

Table 5-1 Effect of shape on the forces acting during the self-assembly process.

	Sphere	Cylinder
Dimensions – Radius	20 μm	5 μm
Length		420 μm
Gravitational force[1]	8.2×10^{-10} N	8.2×10^{-10} N
Contact area[2]	5.0×10^{-13} m^2	1.7×10^{-10} m^2
Adhesion force[3]	7.5×10^{-7} N	2.6×10^{-4} N
Capillary force[4]	3.0×10^{-7} N	2.1×10^{-6} N

1. Length of the cylindrical particle was chosen so as to equate the gravitational force for the two particle shapes.
2. Contact area was determined to be the region within 6 nm of the particle surface (length of 18-mer duplex DNA is ~ 6 nm).
3. Adhesion force was calculated assuming a DNA density of 3.3×10^{13} molecules/cm^2 on the particle surface and a hybridization efficiency of 15%. Adhesion force per duplex DNA was taken to be 30 pN.[36]
4. Capillary force values were estimated for interactions between two identical particles using equations derived by Kralchevsky et al.[33,34] Capillary force is a function of distance; the values shown in the table are the maximum capillary force values applicable for close contact between the particles.

5.2 Experimental Section

Chemicals. Gold pellets were supplied by J&J Materials, Inc. (Neptune City, NJ), and chromium wires were supplied by R. D. Mathis and Company (Long Beach, CA). Acetonitrile, methanol, ethanol, acetone, sodium chloride, EDTA, tris-HCl, phosphate buffered saline tablets, and fine fiber glass (8 μm diameter) were obtained from Mallinckrodt (Paris, KY). Mercaptohexanol (MCH) and dithiothreitol (DTT) were obtained from Sigma-Aldrich (St. Louis, MO). N–(3–triethoxysilylpropyl)–4–hydroxybutyramide (OH- silane) was obtained from Gelest, Inc. (Tullytown, PA). Silica microspheres (30-50 μm) were obtained from Polysciences, Inc. (Warrington, PA). Phosphoramidites and reagents used for oligonucleotide synthesis, and empty TWIST™ columns were obtained from Glen Research (Sterling, MA). Piperidine (20%) in dimethyl formamide was obtained from Protein Technologies, Inc. (Tucson, AZ). Deionized water (Resistance = 18.2 MΩ) was provided by a MilliQ deionization system (Millipore Corp., Bedford, MA). Thiolated oligonucleotides 5' – SH (CH₂)₆ GCC TGA TAC CAT AAC TGA– 3' (oligo B), 5' –SH (CH₂)₆ TCA GTT ATG GTA TCA GGC– 3' (oligo cB), and 5' –TGG TCG CAC AGG TCG CAT (CH₂)₃ SH– 3' (oligo cA) were obtained from MWG Biotech (High Point, NC) in the disulfide form. Oligonucleotides 5'– CAC AGG TCG CAT – TAMRA – 3' (TAMRA-cA) and 5'– Cy5 – TCA GTT ATG GTA –3' (Cy5-cB) modified with the fluorophores tetramethyl rhodamine (TAMRA) and Cy5 respectively were obtained from Integrated DNA Technologies, Inc. (Coralville, IA). Centri-Spin™ columns for gel filtration were obtained from Princeton Separations (Adelphia, NJ). All materials were used as received.

Microrod preparation. Microrods, with lengths between 100-500 μm, were formed by finely slicing glass wool fibers (diameter 8-10 μm) with a razor blade. The resulting microrods were then cleaned by immersing in a base bath solution (12.5 wt% NaOH in 3:4 H₂O:ethanol

solution) for 4 h followed by rinsing with deionized water and ethanol. The microrods were then silanized in a ~10-20 mM solution of OH-silane in 95% ethanol for more than 16 h at room temperature. Oligo A (5'– ATG CGA CCT GTG CGA CCA TTT T – 3') was synthesized on the silanized microrods using TWIST™ columns on an Applied Biosystems ABI-392/394 automated DNA synthesizer. After the automated DNA synthesis, the microrods were immersed in a 20-wt% piperidine in dimethyl formamide (DMF) solution for 4 h to remove the cyanoethyl-protecting groups. The base-protecting groups were removed in a 0.05 M K_2CO_3 solution in anhydrous methanol for 4 h. The DNA synthesis was confirmed by putting the oligo-A-functionalized microrods in a 1 μM solution of TAMRA-cA at a salt concentration of 0.5 M NaCl. The hybridization of the TAMRA-labelled oligo cA to the oligo A on the microrods was visualized on a Zeiss Axiovert 100M confocal microscope. A similar procedure was used for functionalizing the microspheres.

Microrod assembly and imaging. Gold-coated substrates for microrod and microsphere assembly were prepared by coating silicon wafers sequentially with 100 Å chromium and 1000 Å gold in a diffusion-pumped vacuum chamber. The gold-coated substrates were functionalized with SH-DNA and mercaptohexanol using literature methods.[15] The thiolated oligonucleotides (oligos cA & cB), obtained from the vendor in the disulfide form, were reduced in a 0.05 M DTT solution for 30 min. Excess DTT was removed using gel filtration on Centri-Spin™ columns. The oligonucleotide solution was diluted to yield a 5 μM oligonucleotide concentration in 1.0 M KH_2PO_4, pH 3.5. The gold-coated substrates were placed in this oligonucleotide solution for more than 16 h. Oligo cA was used to create gold surfaces with complementarity to the oligo-A-functionalized microrods whereas oligo cB was used to make the gold surface non-complementary to the microrods. After 16 h, the gold-coated substrates were washed, and then

immersed in a 7.5 mM MCH solution for 1 h to cap sites on the gold surface not coated with the SH-DNA. The microrod solution (0.3 M NaCl, 7 mM phosphate buffer) was brought in contact with the slides coated with oligo cA and cB. The slides were placed in a horizontal orientation (gold face up) and the vial was intermittently perturbed to improve contact between the microrods and the slides. After 4 h, the slides were removed from the microrod solution and gently washed with a 0.3 M NaCl, 7 mM phosphate buffer solution and imaged using a Zeiss Axioskop optical microscope in the reflectance mode. A similar procedure was followed for assembly of the microspheres.

Dual-functionalized microrods. The microrods functionalized with oligo A were spread as a monolayer on a silicon wafer. Chromium (~50 Å) and gold (~150 Å) were sequentially evaporated at 0.5 -1 Å/s onto the microrods in a diffusion-pumped vacuum chamber operating at 2×10^{-6} torr. The microrods were briefly sonicated and gently scraped with a Teflon tape coated applicator to release them from the surface. The gold-coated microrods were imaged in a Philips XL30 FEG-ESEM. The gold side was then functionalized with oligo B.

Orientation-specific assembly. The substrates for the orientation-specific assembly were prepared in a manner similar to the substrates used for the microrod and microsphere assembly. One of the substrates (oligo cA) was complementary to the silica side of the dual-functionalized microrods and the other (oligo cB) was complementary to the gold side. These substrates were then brought in contact with the solution of dual-functionalized microrods (0.7 M NaCl, 50 mM phosphate buffer). The dual-functionalized microrods were spread over the horizontally-placed substrates, and the substrates were regularly perturbed to allow the microrods to find their preferred orientation. After 5 h, the substrates containing the assembled dual-functionalized microrods were transferred to a solution containing 1 μM TAMRA-cA and 1 μM Cy5-cB to tag

the exposed regions of the assembled microrods. This fluorophore tagging was used to detect the orientation of the assembled dual-functionalized microrods using fluorescence microscopy where the depth of focus restricted the imaging to the top half. The fluorescence images were acquired using a Nikon Eclipse E800 upright microscope.

5.3 Results & Discussion

5.3.1 Functionalization of the microparticles with DNA

To explore the effect of shape on the assembly of micron-sized particles onto flat substrates using DNA-DNA interactions, I employed commercially available silica microspheres (30-50 µm diameter) and microrods created by finely slicing commercially available glass fibers (8-10 µm diameter). The lengths of the microrods ranged from 100-500 µm with the majority being between 150-250 µm.

Figure 5-1 shows a schematic for the assembly of microrods onto a flat surface. First the microrods and microspheres were functionalized with an OH-terminated trialkoxysilane. They were later derivatized with an appropriate DNA sequence (here, oligo A) using step-wise phosphoramidite synthesis. I confirmed the DNA synthesis on the particles by testing their hybridization abilities. In these experiments, the microrods were contacted with a solution of the fluorophore (TAMRA) labeled complementary sequence of oligo A (TAMRA-cA) and imaged under a confocal microscope. Figure 5-2 shows the confocal microscopy images of a microrod after hybridization with the fluorophore-tagged complementary DNA. These images are representative of the results obtained for tens of microrods and suggest that the DNA synthesis on the surface of the microrods is fairly uniform. Similar results were obtained for the microspheres.

133

A) Microrod functionalization

Stepwise phosphoramidite synthesis
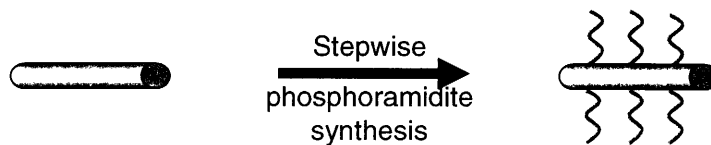
B) DNA-driven microrod adsorption
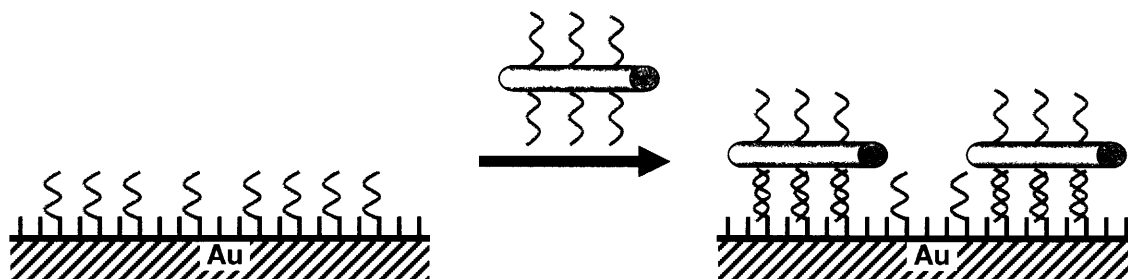
Figure 5-1 Schematic illustrating the functionalization and DNA-directed assembly of microparticles onto a flat surface. (A) First, the microparticles are derivatized with a hydroxyl-terminated trialkoxysilane followed by stepwise phosphoramidite synthesis of the desired DNA sequence. (B) For DNA-directed assembly, the DNA-functionalized microparticles are brought in contact with surfaces containing DNA sequences complementary to those on the microparticles.
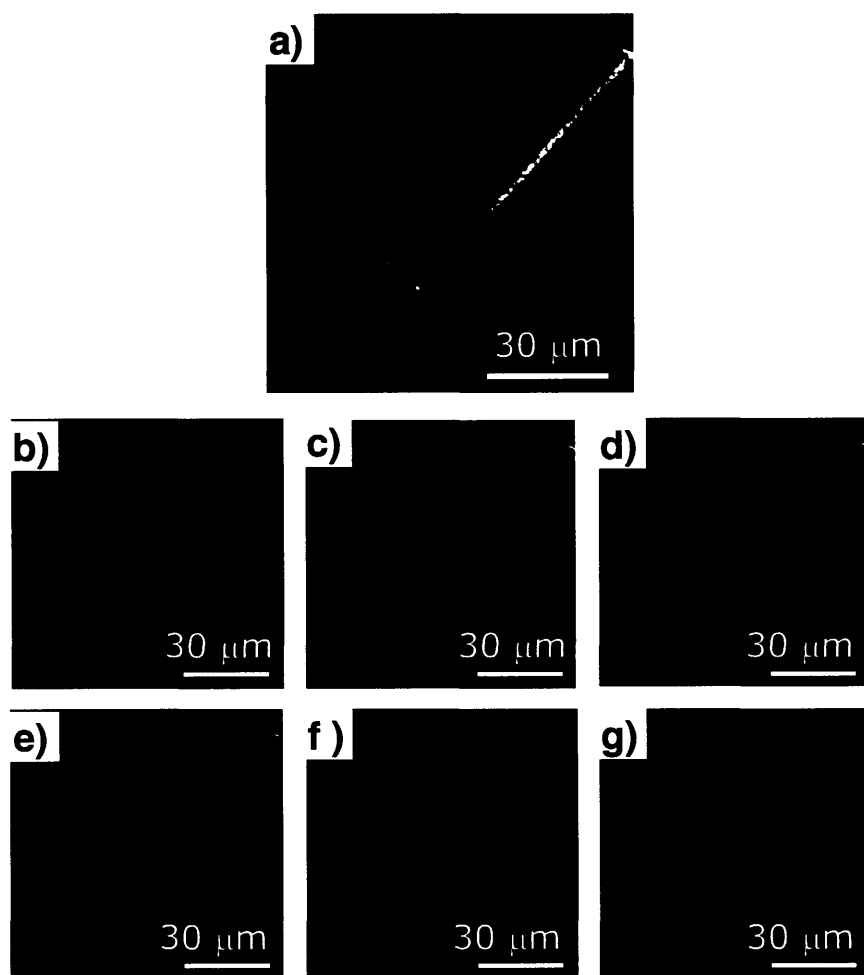
Figure 5-2 Confocal microscopy images of DNA-functionalized cylindrical microparticles after hybridization. The quality of the DNA synthesis on the microparticles was confirmed by hybridizing the DNA strands (oligo A) on the particle surface with a fluorophore-labeled complementary DNA strand (TAMRA-cA). (b)-(g) The fluorescence images obtained at different cross-sections of a microparticle moving from bottom to top. (a) 2-D projection image of the various cross-sectional images.

135

5.3.2 DNA-driven assembly of microparticles on flat surfaces

Next, the DNA-functionalized microparticles were brought in contact with flat Au-coated surfaces containing DNA sequences that were either complementary (oligo cA) or non-complementary (oligo cB) to the DNA sequence on the particles. After a suitable contact time (4 h), the surfaces were briefly rinsed with the hybridizing buffer and imaged under an optical microscope. Figure 5-3 shows the assembly of DNA-functionalized microrods and microspheres on complementary and non-complementary surfaces. The microrods assemble on the complementary surface at an area coverage of ~20% (Figure 5-3a), whereas there is negligible non-specific adsorption of these particles onto the non-complementary surface (Figure 5-3b). In contrast, the microspheres did not assemble on either the complementary or non-complementary surfaces (Figure 5-3c & d) possibly due to the low contact area and low adhesion force for the microspheres. These results are in agreement with the force calculations presented in Table 5-1; specifically, the cylindrical shape provides more contact area as compared to the spherical shape and thus helps assembly via the weak DNA hybridization forces. The DNA-driven microrod assembly on the flat complementary surface was fairly robust as the microrods did not come off even after repeated rinsing with the hybridizing buffer. However, the microspheres could not be assembled on the complementary surfaces even when higher salt concentration and longer contact times were employed. In some cases, I observed that the microspheres did attach to the surface at fairly high densities during the contacting step however most of the particles came off during the rinsing step. These results may appear counter to the results of Hammer et al.[39] who successfully obtained DNA-driven attachment of 10-μm polystyrene beads on polystyrene surfaces. An important difference likely is that in our experiments the microsphere and substrate were formed from rigid materials while the experiments employing polystyrene used a more

flexible material that might deform in its shape and cause the actual contact area between particle and substrate to be much greater than in our case.[40] Consistent with our observations of microspheres getting detached during rinsing, Hammer et al. also observed that hydrodynamic shear rate greater than a particular critical value can lead to complete particle detachment.

5.3.3 Formation of dual-functional microrods

The use of DNA interactions and the microrod geometry provided a robust method for assembling these particles when their sequences were complementary to that on the substrate. In contrast, since their adsorption was greatly diminished when the microrods presented a non-complementary sequence, I envisioned that a dual-functional building block functionalized to expose one surface with a complementary sequence and an adjoining surface with a non-complementary sequence would assemble in an orientation-specific manner onto the substrate. To maximize interactions between the microrods and the substrate the regions with the different DNA sequences were designed to extend along the length of the microrod. The dual functionality was obtained by shadow coating gold onto one half of the microrod surface. Subsequently, the gold side was functionalized with a SH-DNA (oligo B) having a sequence that was different from that on the SiO_2 surface. The combination of the silica and gold surfaces ensures that the chemistries used for functionalizing the surfaces would introduce minimal cross contamination to the other DNA sequence. Further, it is unlikely that the SH-DNA would affect the DNA on the silica side under the attachment conditions. Figure 5-4a shows the schematic of the gold deposition on the microrods. Prior to the gold deposition, it was important to spread the microrods as a monolayer on a flat substrate to ensure defect-free gold coatings. The gold deposition was done under vacuum conditions using line-of-sight vapor deposition process that coated only the exposed top faces of the microrods. Figure 5-4b shows a SEM image of the

Microrod assembly

Microsphere assembly
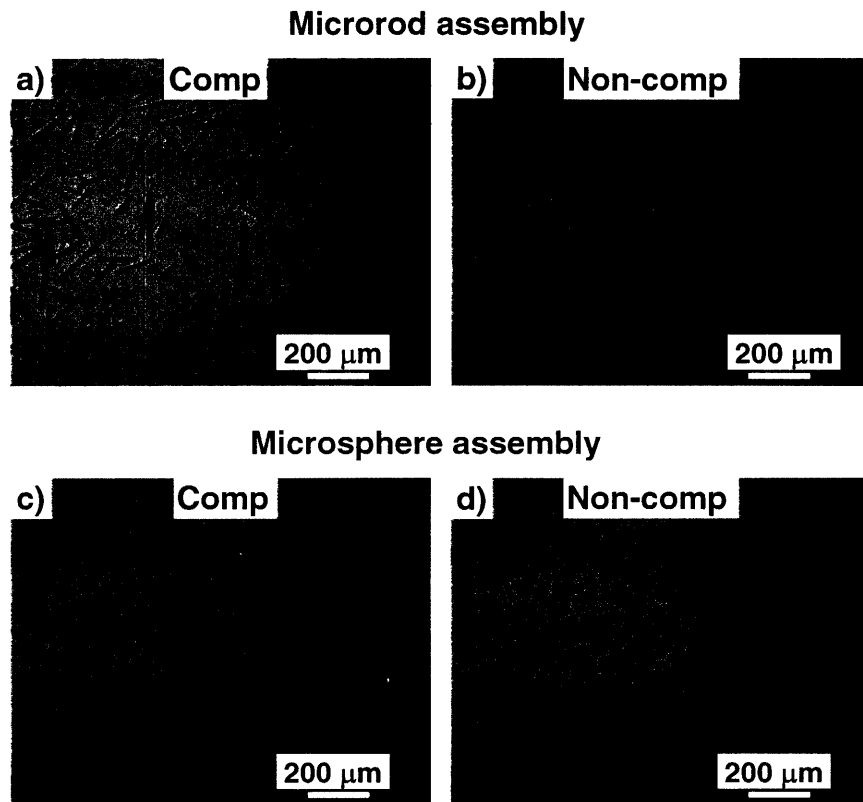
Figure 5-3 Effect of shape on the directed assembly of DNA-functionalized (oligo A) microrods and microspheres onto surfaces containing complementary (oligo cA) and non-complementary (oligo cB) sequences. (a) & (b) Optical images of DNA-directed assembly of microrods. The microrods are attached onto the complementary surface at an area coverage of ~20% while the non-specific attachment on the non-complementary surface is negligible. (c) & (d) Optical images of DNA-directed assembly of microspheres. On both complementary and non-complementary surfaces, the attachment of microspheres was low.
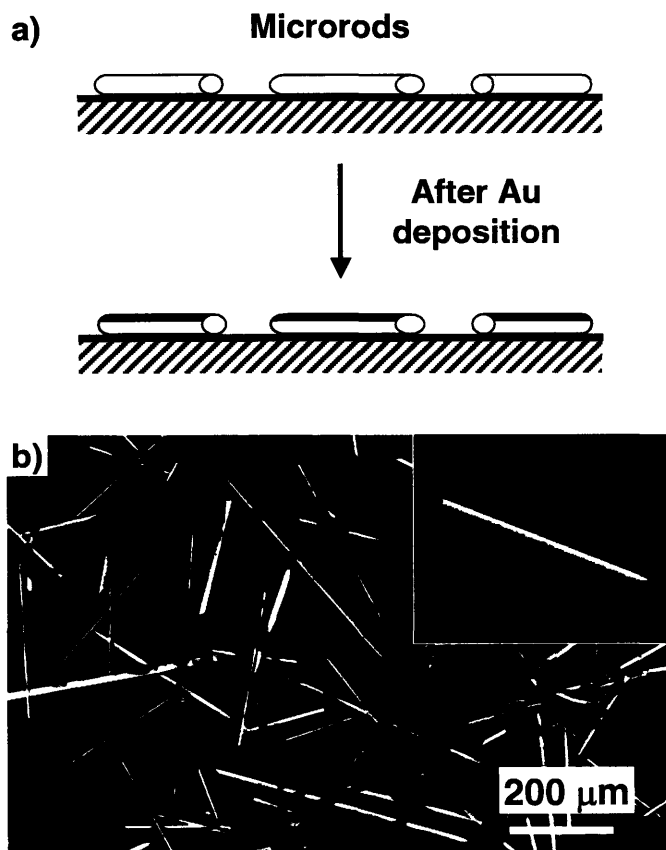
Figure 5-4 Dual-functional microrods. (a) Schematic illustration of coating the silica microrods (diameter: 8-10 μm, length: 100-500 μm) with gold using shadow deposition. (b) SEM image of the dual-functionalized microrods.

resulting dual-functional microrods. In the image, the gold-coated regions appear brighter than the non-coated regions because of greater back-scattering of electrons by gold.

5.3.4 Orientation-specific assembly of dual-functional microrods

To demonstrate the orientation-specific assembly of the dual-functional microrods, the dual-functional microrods were contacted with surfaces expressing DNA sequences that were complementary to either the SiO_2 or the Au sides of the dual-functional microrods. Figure 5-5 shows a schematic illustration of the experiments that examined the orientation-specific assembly of the dual-functional microrods onto DNA-functionalized surfaces. In one set of experiments (Figure 5-5a), gold surfaces functionalized with oligo cB provided a surface that was complementary to the Au surface of the microrods. In another set (Figure 5-5b), gold surfaces functionalized with oligo cA provided a surface complementary to the SiO_2 surface of the microrods. The dual-functional microrod solution containing 0.7 M NaCl was brought in contact with these gold surfaces. After the assembly of the dual-functionalized microrods, their orientation was probed by exposing the assembly to a solution containing two fluorophore-tagged complementary DNA sequences (TAMRA-cA and Cy5-cB). Based on their sequence complementarity, TAMRA-cA would hybridize with the DNA strands on the SiO_2 surface while Cy5-cB would hybridize with the DNA strands on the AU surface. Fluorescence signals from these specific attachments of the fluorophore-tagged target oligonucleotides were used to identify SiO_2 and Au regions of the microrods, respectively.

Figure 5-6 shows fluorescence images obtained from the dual-functional microrods assembled onto oligo cA and oligo cB surfaces. The fluorescence images were taken in the aqueous phase to avoid drying artifacts. These fluorescence images reveal the orientation of the microrods. Figure 5-5a shows that the microrods on the oligo-cB surface should be attached via

the gold side of the microrods and have their SiO_2 side facing up. In contrast, the microrods on the oligo-cA surface should be attached via the SiO_2 side and must have the Au side facing up. The fluorescence images in Figure 5-6a & b obtained from the microrods assembled onto the oligo cB surface show a strong signal from TAMRA and minimal signal from Cy5. This collection of fluorescence signals establishes that most of the microrods assembled on the oligo cB surface are oriented as shown in Figure 5-5a i.e. with their SiO_2 sides facing up and the downward-facing Au sides forming DNA-DNA interactions with the complementary oligo cB surface. In contrast, the fluorescence signals from oligo cA surface show strong Cy5 signals and minimal TAMRA signals. These fluorescence images show that microrods on the oligo-cA surface are mostly attached via the SiO_2 side and expose the fluorophore of the DNA target complementary (Cy5-cB) to the upward-facing Au side (Figure 5-6d and e). These images show that the microrods on the oligo cA surface orient themselves to have their Au sides facing up (Figure 5-5b).

In Figure 5-6c and f, the fluorescence images have been superimposed on the reflectance images of the assembled microrods. These images show the location of the fluorescence signals acquired from the microrod surfaces and better illustrate the orientation of the assembled particles. These images demonstrate that I have been successful in directing the assembly of the dual-functional microrods based on the 'instructions' programmed onto them via the different DNA sequences. However, the density of the microrod attachment for the dual-functionalized microrods is much lower than that for the mono-functionalized microrods. One possible explanation is that some of the DNA layer could have been damaged during the gold deposition and subsequent processing. These initial attempts at orientation-specific assembly of dual-

functional microrods show that with DNA-DNA interactions combined with asymmetric building blocks can be used to perform self-organization of complicated structures.

5.4 Conclusions

I have evaluated the effect of shape on the DNA-directed assembly of micron-sized particles onto flat surfaces. Force calculations as well as experimental observations demonstrate that shapes with larger aspect ratios like rods etc. are more suitable for assembly by the weak DNA-DNA interactions. The microrods in our experiments could be attached with an area coverage of ~20% onto complementary surfaces with minimal adsorption on non-complementary surfaces. On the other hand, the microspheres, because of lesser contact area could not be attached even onto complementary surfaces. Additionally, I programmed two functionalities onto the microrods by shadow coating them with a gold film. Using specific DNA-DNA interactions on the two sides of the dual-functionalized microrods I have demonstrated the orientation-specific assembly of these anisotropic particles. These attempts at building complexity into the building blocks used for directed assembly as well as employing versatile linking strategies to assemble them into novel configurations will be crucial as directed-assembly techniques mature from the proof-of-concept stage to actually creating functional devices.
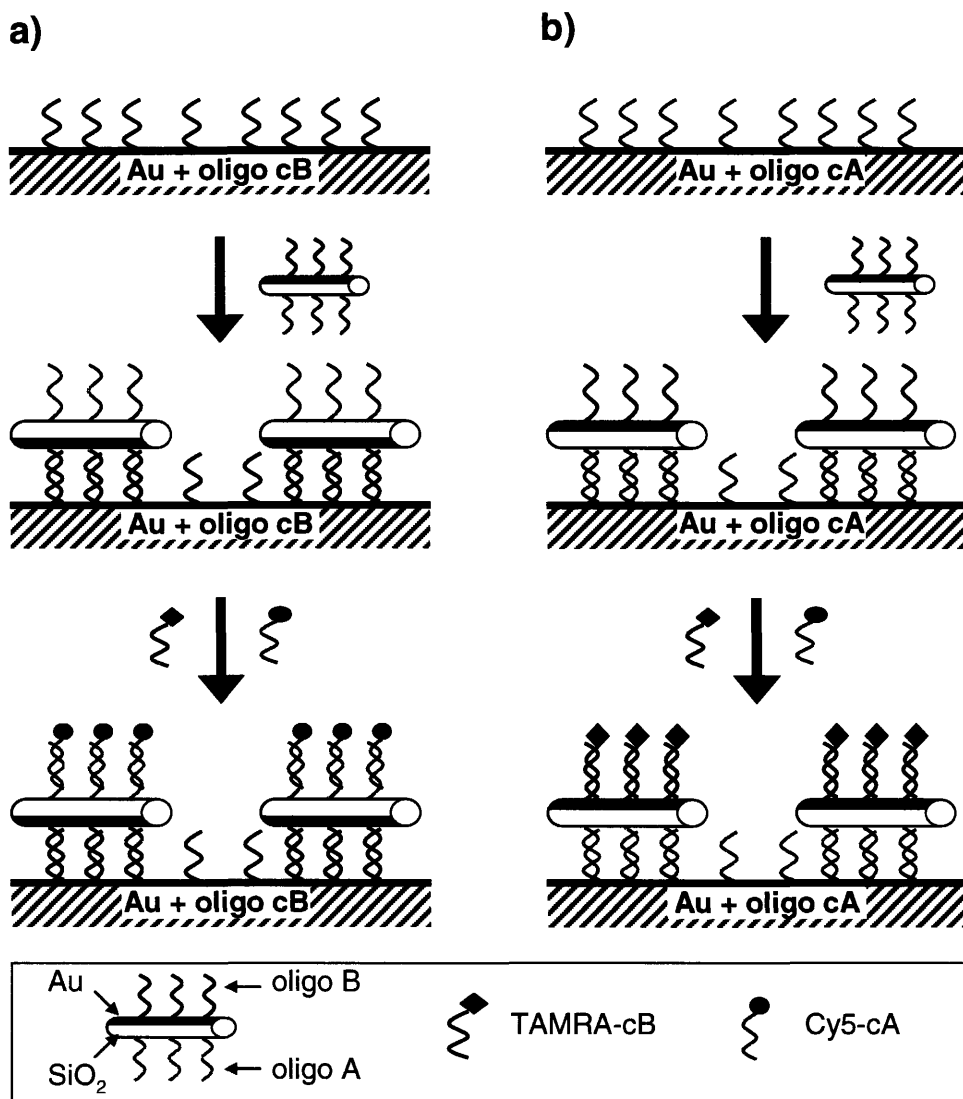
Figure 5-5 Schematic illustrating the orientation-specific assembly of dual-functionalized microrods and the use of fluorescent tags to characterize their orientation. The SiO_2 and Au sides of the microrods are functionalized with two different DNA sequences (oligo A and oligo B respectively). The microrods are then brought in contact with two DNA-functionalized surfaces, (a) one complementary to the Au side and (b) the other to the SiO_2 side. To enable the detection of the orientation of the assembled microrods, a solution containing two fluorophore-tagged oligonucleotides, TAMRA-cA and Cy5-cB is brought in contact with the assembled microrods.
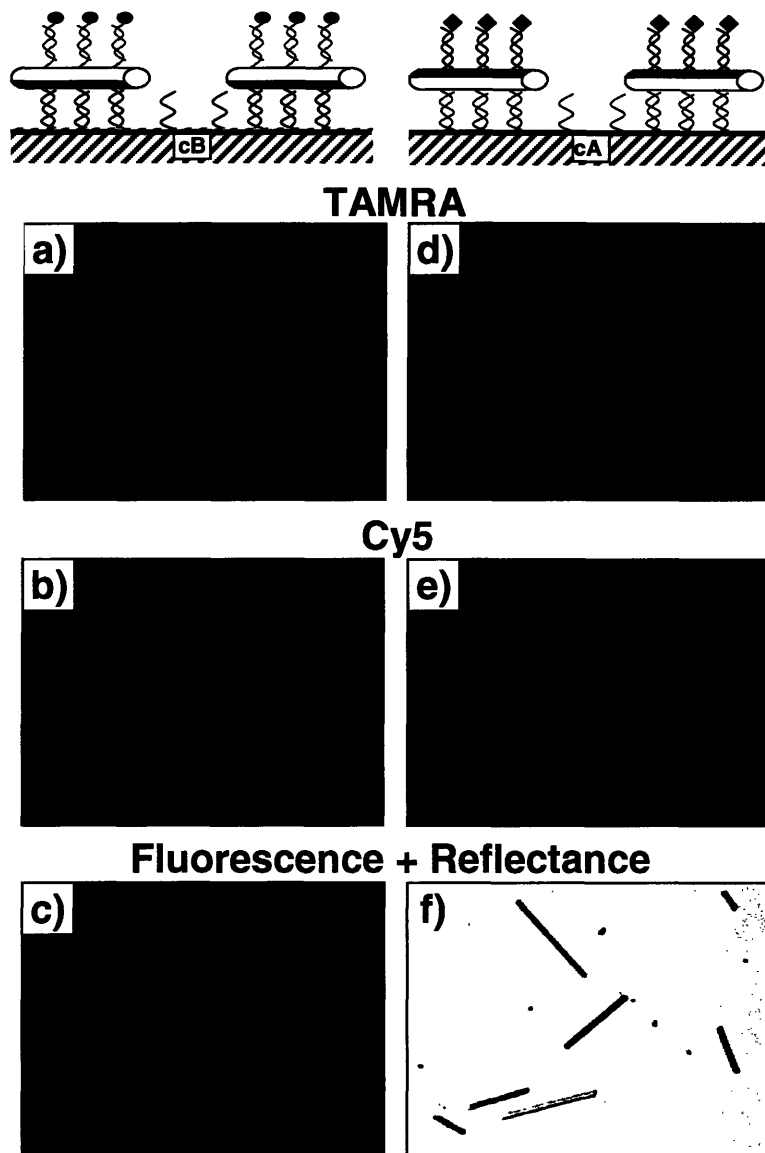
Figure 5-6 Orientation-specific assembly of dual-functionalized microrods. (a) & (d) TAMRA signals, (b) & (e) Cy5 signals from the assembled microrod layer. (c)-(f) Fluorescence signals superimposed onto the reflectance images of the assembled microrod layer. The orientation of the microrods is detected by the fluorophore-tagged DNA targets complementary to the SiO_2 (TAMRA-cA) and Au (Cy5-cB) sides. The microrods on the oligo-cB surface are mostly attached via the Au (oligo B) side as seen from the strong TAMRA signals corresponding to the upward-facing SiO_2 side and weak Cy5 intensities. Similarly, the microrods on the oligo-cA surface are mostly attached via the SiO_2 (oligo A) side as seen from the strong Cy5 signals and weak TAMRA intensities.

5.5 References & Footnotes

(1) Whitesides, G. M.; Boncheva, M. *Proc. Natl. Acad. Sci. U. S. A.* **2002**, *99*, 4769-4774.

(2) Glotzer, S. C.; Solomon, M. J.; Kotov, N. A. *Aiche J.* **2004**, *50*, 2978-2985.

(3) Bowden, N.; Choi, I. S.; Grzybowski, B. A.; Whitesides, G. M. *J. Am. Chem. Soc.* **1999**, *121*, 5373-5391.

(4) O'Riordan, A.; Delaney, P.; Redmond, G. *Nano Lett.* **2004**, *4*, 761-765.

(5) Srinivasan, U.; Liepmann, D.; Howe, R. T. *J. Microelectromech. Syst.* **2001**, *10*, 17-24.

(6) Mirkin, C. A.; Letsinger, R. L.; Mucic, R. C.; Storhoff, J. J. *Nature* **1996**, *382*, 607-609.

(7) Alivisatos, A. P.; Johnsson, K. P.; Peng, X. G.; Wilson, T. E.; Loweth, C. J.; Bruchez, M. P.; Schultz, P. G. *Nature* **1996**, *382*, 609-611.

(8) Niemeyer, C. M.; Adler, M. *Angew. Chem.-Int. Edit.* **2002**, *41*, 3779-3783.

(9) Niemeyer, C. M.; Burger, W.; Peplies, J. *Angew. Chem.-Int. Edit.* **1998**, *37*, 2265-2268.

(10) Nicewarner-Pena, S. R.; Freeman, R. G.; Reiss, B. D.; He, L.; Pena, D. J.; Walton, I. D.; Cromer, R.; Keating, C. D.; Natan, M. J. *Science* **2001**, *294*, 137-141.

(11) Mucic, R. C.; Storhoff, J. J.; Mirkin, C. A.; Letsinger, R. L. *J. Am. Chem. Soc.* **1998**, *120*, 12674-12675.

(12) Mitchell, G. P.; Mirkin, C. A.; Letsinger, R. L. *J. Am. Chem. Soc.* **1999**, *121*, 8122-8123.

(13) Henke, L.; Piunno, P. A. E.; McClure, A. C.; Krull, U. J. *Analytica Chimica Acta* **1997**, *344*, 201-213.

(14) Henke, L.; Krull, U. J. *Canadian Journal of Analytical Sciences and Spectroscopy* **1999**, *44*, 61-70.

(15) Herne, T. M.; Tarlov, M. J. *J. Am. Chem. Soc.* **1997**, *119*, 8916-8920.

(16) Strother, T.; Hamers, R. J.; Smith, L. M. *Nucleic Acids Res.* **2000**, *28*, 3535-3541.

(17) Strother, T.; Cai, W.; Zhao, X. S.; Hamers, R. J.; Smith, L. M. *J. Am. Chem. Soc.* **2000**, *122*, 1205-1209.

(18) Xu, X. H.; Bard, A. J. *J. Am. Chem. Soc.* **1995**, *117*, 2627-2631.

(19) Zeng, J.; Krull, U. J. *Chimica Oggi-Chemistry Today* **2003**, *21*, 48-52.

(20) Zhang, H.; Li, Z.; Mirkin, C. A. *Adv. Mater.* **2002**, *14*, 1472-+.

(21) Hong, S. H.; Zhu, J.; Mirkin, C. A. *Science* **1999**, *286*, 523-525.

(22) Bruckbauer, A.; Ying, L. M.; Rothery, A. M.; Zhou, D. J.; Shevchuk, A. I.; Abell, C.; Korchev, Y. E.; Klenerman, D. *J. Am. Chem. Soc.* **2002**, *124*, 8810-8811.

(23) Okamoto, T.; Suzuki, T.; Yamamoto, N. *Nat. Biotechnol.* **2000**, *18*, 438-441.

(24) Pathak, S.; Dentinger, P. M. *Langmuir* **2003**, *19*, 1948-1950.

(25) Demers, L. M.; Ginger, D. S.; Park, S. J.; Li, Z.; Chung, S. W.; Mirkin, C. A. *Science* **2002**, *296*, 1836-1838.

(26) Zhang, G. J.; Tanii, T.; Funatsu, T.; Ohdomari, I. *Chem. Commun.* **2004**, 786-787.

(27) Braun, E.; Eichen, Y.; Sivan, U.; Ben-Yoseph, G. *Nature* **1998**, *391*, 775-778.

(28) Cimino, G. D.; Gamper, H. B.; Isaacs, S. T.; Hearst, J. E. *Annu. Rev. Biochem.* **1985**, *54*, 1151-1193.

(29) Elsner, H. I.; Mouritsen, S. *Bioconjugate Chem.* **1994**, *5*, 463-467.

(30) Zhang, Y. W.; Seeman, N. C. *J. Am. Chem. Soc.* **1992**, *114*, 2656-2663.

(31) Zheng, W.; Buhlmann, P.; Jacobs, H. O. *Proc. Natl. Acad. Sci. U. S. A.* **2004**, *101*, 12814-12817.

(32) Wang, J.; Liu, G. D.; Zhu, Q. Y. *Anal. Chem.* **2003**, *75*, 6218-6222.

(33) Kralchevsky, P. A.; Paunov, V. N.; Denkov, N. D.; Ivanov, I. B.; Nagayama, K. *J. Colloid Interface Sci.* **1993**, *155*, 420-437.

(34) Kralchevsky, P. A.; Nagayama, K. *Langmuir* **1994**, *10*, 23-36.

(35) Lee, I. H. In *Chemical Engineering*; Massachusetts Institute of Technology: Cambridge, 2001.

(36) Strunz, T.; Oroszlan, K.; Schafer, R.; Guntherodt, H. J. *Proc. Natl. Acad. Sci. U. S. A.* **1999**, *96*, 11277-11282.

(37) Dwyer, C.; Vicci, L.; Poulton, J.; Erie, D.; Superfine, R.; Washburn, S.; Taylor, R. M. *IEEE Trans. Very Large Scale Integr. (VLSI) Syst.* **2004**, *12*, 1214-1220.

(38) Zhang, Z. L.; Glotzer, S. C. *Nano Lett.* **2004**, *4*, 1407-1413.

(39) Zhang, Y.; Eniola, A. O.; Graves, D. J.; Hammer, D. A. *Langmuir* **2003**, *19*, 6905-6911.

(40) Das, S. K.; Schechter, R. S.; Sharma, M. M. *J. Colloid Interface Sci.* **1994**, *164*, 63-77.

Chapter 6. DNA-Directed Assembly on Dual- and Tri-Functional Particles

6.1 Introduction

DNA as a recognition element for directed assembly has received considerable attention in the last few years. The sequence-specific base pairing of complementary DNA strands provides a unique strategy for programming the assembly of objects at the nanometer scale. Since the hybridization between two DNA strands is due to hydrogen bonding, the assembly strategy is easily reversible and achieves minimum energy states. The availability of commercial DNA synthesizers and a wide variety of synthetic precursors provide routine access to thousands of different selectable DNA sequences and thus offer easy scaling to high-throughput schemes. Most of the work in this field began after seminal contributions from Mirkin et al.[1] and Alivisatos et al.[2] DNA as a linker molecule has been used to achieve a variety of self-assembled structures. Mirkin et al.[1] showed that Au nanoparticles change their optical properties as they are linked together into aggregates by DNA hybridization. They also showed the controlled binary assembly of nanoparticles of two different sizes into regular structures.[3] Niemeyer et al.[4-6] have used DNA hybridization to assemble other biomolecules such as proteins. Keating et al.[7] demonstrated that assembling nanoparticles using DNA hybridization helps to enhance the detection of hybridization events using SPR. Smith et al.[8] have shown that DNA hybridization and subsequent modification of the DNA material using enzymes can be used for DNA-based computation. Since DNA molecules by themselves do not have high electrical conductivity, Ben-Yoseph et al.[9] have chemically metallized DNA strands to achieve small wires with almost Ohmic-type electrical behavior. Recently, Mirkin et al.[10] and Niemeyer et al.[11] have

demonstrated an ultra-sensitive detection scheme for proteins using DNA-derivatized nanoparticles.

As a rule in self-assembly processes, the more complex the building block, the higher the level of organization possible in the self-assembled structures.[12] To achieve higher-order structures by DNA-based assembly, there have been few attempts to use asymmetric building blocks. Mann et al.[13] have used gold nanorods to demonstrate DNA-driven assembly into anisotropic 3D-aggregates. Natan et al.[14] have used multifunctional nanorods as their starting material and achieved assembly using DNA hybridization. With a goal toward producing greater hierarchical complexity in such structures assembled using DNA hybridization, I targeted the generation of dual-functional and tri-functional spheres as our asymmetric building blocks. I used a simple shadow deposition technique to achieve a hemi-spherical coating of gold onto silica microspheres to create the dual-functional particles and a coating of gold and aluminum to create the tri-functional particles. These metal coatings were subsequently derivatized with organic films to provide functionality.

A technique for producing hemispherical gold coatings on polystyrene particles by evaporation was first used by Takei et al,[15] who subsequently modified these particles to create an optical sensor for avidin-biotin binding.[16] Many other methods have also been detailed in the literature to achieve a selective coating of a material on one side of a sphere. Kawaguchi et al.[17,18] have used various techniques including Langmuir-Blodgett to selectively functionalize one-half of spherical particles. Fitzmaurice et al.[19] have used a filtration-based technique that relies on shadow deposition in the liquid phase. Delville et al.[20] have achieved dual functionality on particles using laser photochemical deposition. Muller et al.[21] have used tri-block copolymers to create bifunctional 'Janus' particles. Applications of such bifunctional structures include

construction of ultra-hydrophobic surfaces[22] and systems for gene delivery[23]. Bifunctional particles with hydrophobic and hydrophilic faces are noted to show surfactant-like behavior and can stabilize emulsions.[24]

The main objectives of this study were twofold: one to create asymmetric dual-functional and tri-functional silica particles using the shadow deposition of metals (Au and Al) and secondly to achieve a selective orthogonal assembly of DNA molecules onto the different faces of these particles via DNA hybridization. I accomplished the goal of producing dual-functional particles by derivatizing the silica side with a DNA sequence followed by shadow deposition of gold and derivatization of the gold side with a different DNA sequence. A tri-functional particle was produced with an additional Al surface, where the Al surface was passivated with stearic cid to provide an inert surface. These particles were then challenged with various fluorophore-tagged target DNA molecules to demonstrate the orthogonal assembly. The selective assembly of DNA molecules onto these surfaces is the first step in the process of employing DNA-directed assembly for generating more complex structures.

6.2 Experimental Section

Materials. Silica microparticles (30-50 μm) were obtained from Polysciences, Inc. (Warrington, PA). Octyl trichlorosilane (C_8 silane), dithiothreitol (DTT), and 6-mercapto-1-hexanol (MCH) were obtained from Aldrich (Milwaukee, WI). Trichloroacetyl (TCA) protected ω-hydroxyundecyl trichlorosilane (TCA silane) was custom synthesized in our laboratory (see Chapter 3). Gold pellets were supplied by J&J Materials, Inc. (Neptune City, NJ), and chromium-coated tungsten filaments were supplied by R. D. Mathis and Company (Long Beach, CA). Acetonitrile, methanol, ethanol, acetone, sodium chloride, sodium citrate, EDTA, tris-HCl, and potassium carbonate (K_2CO_3) were obtained from Mallinckrodt (Paris, KE).

149

Phosphoramidites and reagents used for oligonucleotide synthesis, and empty TWIST™ columns were obtained from Glen Research (Sterling, MA). Piperidine (20%) in dimethyl formamide was obtained from Protein Technologies, Inc (Tucson, AZ). Deionized water (resistivity = 18.2 MΩ) was provided by a MilliQ deionization system (Millipore Corp., Bedford, MA). Target oligonucleotides 5'–CAC AGG TCG CAT-TAMRA –3' (TAMRA-cA), 5'–Cy5- TCA GTT ATG GTA –3' (Cy5-cB), and 5'–FAM- TCA GTT ATG GTA TCA –3' (FAM-cB1) modified with the fluorophores tetramethyl rhodamine (TAMRA), Cy5, and fluorescein (FAM) respectively were obtained from MWG Biotech (High Point, NC). Thiolated oligonucleotide 5'-SH $(CH_2)_6$ GCC TGA TAC CAT AAC TGA- 3' (oligo B) and 5'-SH $(CH_2)_6$ TCA GTT ATG GTA TCA GGC– 3' (oligo B1) ware obtained from Integrated DNA Technologies, Inc. (Coralville, IA). Centri-SpinTM columns for gel filtration were obtained from Princeton Separations (Adelphia, NJ).

Functionalizing silica surface. The microparticles were cleaned in a 12.5 wt-% NaOH solution in a 3:4 H_2O:EtOH for 2 h. Subsequently, they were washed 3-4 times with deionized water and dried. The silanizing solution was prepared by adding octyl trichlorosilane (C_8 silane) and trichloroacetyl (TCA) protected ω-hydroxyundecyl trichlorosilane (TCA silane) in a 20:80 volume proportion to anhydrous toluene (>99.5%) to yield 1 μL/mL (~mM) solution of the silanes in toluene. The particles were immersed in the silanizing solution for 4 h. After 4 h, the particles were washed once with toluene and twice with acetone and dried.

To expose hydroxyl groups on the particle surfaces prior to DNA synthesis, the TCA protecting groups were removed by immersing the particles in a 5 mM K_2CO_3 solution in 1:1 H_2O: methanol for 15 min. Stepwise synthesis of oligonucleotide 5'–ATG CGA CCT GTG CGA CCA TTT T–3' (oligo A) was performed on the particles using a Applied Biosystems ABI-

392/394 automated DNA synthesizer. Cyanoethyl groups present on the phosphorus linkages were removed by immersing the slides in a 20-wt% piperidine in dimethyl formamide (DMF) solution for 4 h. Protecting groups on the nucleic bases were removed by immersing the particles in a 0.05 M K_2CO_3 solution in anhydrous methanol for 4 h. To functionalize the particles with sequence non-complementary to the TAMRA-labeled target, 5'–AGC CAA TTG GCC TTT T–3' (oligo A1) was synthesized on the particles.

Gold coating. The silica particles functionalized with oligo A or A1 were spread as a monolayer on a Petri dish. Chromium (~50 Å) and gold (~300 Å) were sequentially evaporated at 0.5-1 Å/s onto the particles in a diffusion-pumped vacuum chamber operating at 2 x 10^{-6} torr. The slow deposition rate was chosen to avoid heating of the particles which could damage the DNA layer on the silica surface. For the same reason, the silicon wafer holding the particles was placed on a surface cooled to less than 4 °C. The particles were briefly sonicated to release them from the surface. The gold-coated particles were imaged in a Philips XL30 FEG-ESEM. Optical microscopy experiments were performed on a Zeiss Axioskop in the reflectance mode.

Functionalizing gold surface. The thiolated oligonucleotides (oligos B & B1) were obtained from the vendor in the disulfide form. The disulfide group was reduced in a 0.05 M DTT solution for 30 min. Excess DTT was removed using gel filtration on Centri-Spin™ columns. The oligonucleotide solution was diluted to yield a 5 μM oligonucleotide concentration in 1.0 M KH_2PO_4, pH 3.5. The particles were added to this oligonucleotide solution and stirred for more than 16 h. Oligo B was used to create gold surfaces with complementarity to the Cy5-labeled target (Cy5-cB) while oligo B1 was used to make the gold surface non-complementary to the Cy5-labeled target. After 16 h, the particles were washed, and then immersed in a 7.5 mM MCH solution for 1 h to cap sites on the gold surface not coated with the SH-DNA.

Hybridization and confocal microscopy. Three kinds of particles were formed: complementary - complementary (C-C), non-complementary - complementary (NC-C), and complementary - non-complementary (C-NC). For C-C particles, both the silica and gold sides have sequences complementary to the respective target DNA molecules. For NC-C particles, the silica side bears a sequence non-complementary (oligo A1) to the TAMRA-labeled target (TAMRA-cA) while the gold-side has a sequence (oligo B) complementary to the Cy5-labeled target (Cy5-cB). For the C-NC particles, the silica side bears a sequence complementary (oligo A) to the TAMRA-labeled target (TAMRA-cA) while the gold-side has a sequence (oligo B1) non-complementary to the Cy5-labeled target (Cy5-cB). The particles functionalized with DNA on both the silica and gold sides were contacted with a solution containing the complementary target oligonucleotides (TAMRA-cA and Cy5-cB) at 0.5 μM concentration in 3x SSC (0.5 M NaCl, 0.05 M sodium citrate) for more than 16 h. The particles were then washed successively with 0.3 M NaCl in 1x TE buffer, 0.1 M NaCl in 1x TE buffer, and 0.3 M NaCl in 1x TE buffer. Confocal microscopy of the particles was conducted on a Zeiss Axiovert 100M using two He-Ne lasers (544 nm and 633 nm) and 63x oil objective.

Formation of particles coated with gold and aluminum. The silica microparticles were spread as a monolayer on a silicon wafer. Chromium (~50 Å) and gold (~200 Å) were sequentially evaporated at 0.5-1 Å/s onto the particles in a diffusion-pumped vacuum chamber operating at 2×10^{-6} torr. After the gold deposition, the silicon wafer containing the particles was tilted by an angle of 90° and aluminum (200 Å) was deposited onto the particles at 0.5-1.0 Å/s. Brief sonication (15-20 s) was used to release the particles from the surface of the silicon wafer after the deposition process.

Functionalization of the Al and Au surface. First, the Al surface was passivated by immersing the coated particles in a 5 mM solution of stearic acid in isooctane for ~40 h.[25] Independent experiments on flat Al surfaces showed that the stearic acid layer resists non-specific DNA adsorption. The particles were then successively washed in isooctane, acetone, and H_2O. The gold surface of the tri-functional particles was then functionalized with oligo B in a manner similar to that used for the dual-functional particles. Since the Al layer could be damaged by the phosphate ions, the oligonucleotide functionalization was done in a 10 mM phosphate buffer, 0.5 M NaCl, pH 7 solution instead of the 1.0 M KH_2PO_4, pH 3.5 solution

Assembly of DNA molecules onto tri-functional particles. The tri-functional particles were immersed in a 1.0 μM solution of TAMRA-cA and FAM-cB1 for 4 h at a salt concentration of 0.5 M NaCl. After hybridization, the particles were cleaned once in the hybridizing buffer solution. The fluorescence and reflectance images of the particles were acquired using a Nikon Eclipse E800 upright microscope.

6.3 Results and Discussion

6.3.1 Formation of dual-functional microparticles

The silica particles were first silanized to make the surfaces reactive towards phosphoramidite synthesis. I used a system of mixed monolayers, consisting of C8 silane and TCA silane. Our previous studies have shown that these two silanes can be used to achieve DNA immobilization at high surface densities with minimal non-specific adsorption (see Chapter 3). Based on our previous results, I selected a silane composition of 20 vol% TCA and 80 vol% C_8 silane to achieve a high density of surface DNA molecules. After the silanization, the TCA protecting groups were removed using a deprotection protocol that has been optimized to minimize damage to the silane surface (see Table 3-1). The particles were then placed in a DNA

synthesizer to conduct the stepwise synthesis of DNA on their surface using phosphoramidite chemistry. The use of an automated oligonucleotide synthesizer gives flexibility for changing the sequence synthesized on the surface with great ease.

After DNA synthesis on the silica particles, the particles were spread as a monolayer on a Petri dish and were coated with gold in a thermal evaporation system. Care was taken to avoid the formation of particle multilayers on the surface as they would reduce the efficiency of creating dual-functional spheres with perfect hemispherical coatings. Even after the gold deposition, the DNA synthesized on the uncoated half of the particles did not lose much of their activity as will be seen by the confocal microscopy results.

Figure 6-1 shows a scheme for the shadow deposition of gold onto the silica particles and an SEM image of these coated particles in the backscatter mode. The regions coated with gold appear brighter because of the greater backscattering properties of the gold atoms. The image also shows that some particles do not have a hemispherical coating. This effect is due to formation of some particle multilayers that could not be avoided when spreading the particles on the flat surface before gold deposition. The protocol for this procedure could likely be optimized to reduce these defects in the future.

a) Silica µparticles 30-50 µm

After Au evaporation

b) 20 µm

c) 200 µm
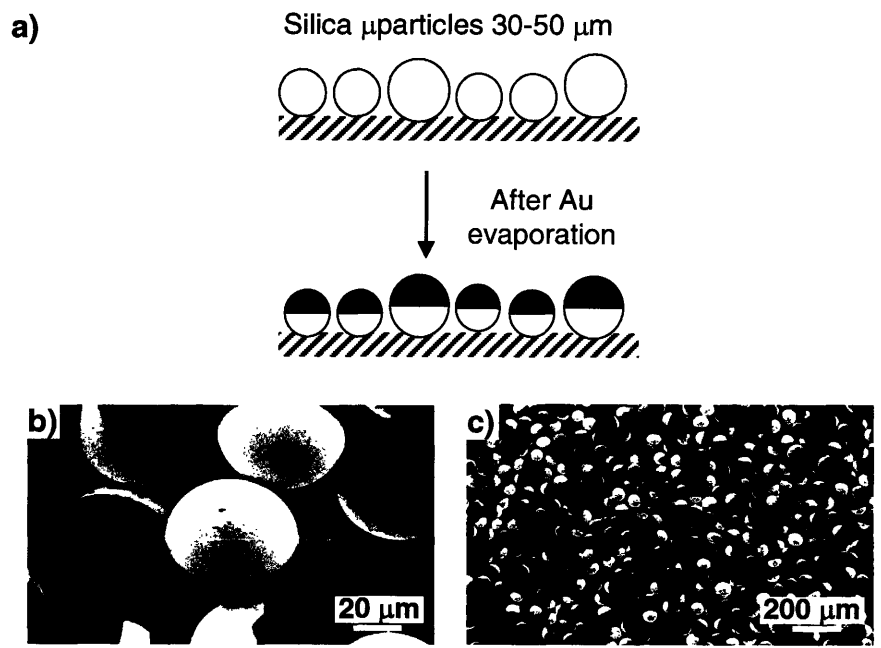
Figure 6-1 (a) Schematic illustration of coating the silica particles (30-50 µm) with gold using shadow deposition. (b) & (c) SEM images of the dual-functional particles.

6.3.2 Separation of the dual-functional particles

Because of the differing wetting properties of the gold and silica surfaces, the dual-coated particles could be easily separated from the uncoated particles using a simple surface-pinning approach. Specifically, when the particles are placed on an air-water interface (Figure 6-2a), before the particles are completely wet, most of the particles stay at the interface, as the interfacial tension is able to counteract gravitational forces. However, when the particles are stirred, the uncoated particles become completely wetted and settle to the bottom of the container (Figure 6-2c) while most of the dual-functional particles remain at the interface (see Figure 6-2b). The particles that stay at the interface also show an increased amount of clustering that occurs as a means to minimize their interfacial energy. This physical picture is further illustrated in Figure 6-2d, where the dual-functional particles become pinned at the air-water interface at the boundary of the gold coating. This behavior can be explained by the differing wetting properties of the two surfaces. The silica side is coated with negatively charged DNA molecules and thus is hydrophilic. The gold surface though inherently hydrophilic, readily picks up a layer of contamination because of its high surface energy and becomes hydrophobic. Wetting studies done on dual-functional particles by Veyssie et al.[26-28] also confirm the observed results. An important consequence is that I could quickly and easily separate the coated particles from the uncoated ones using this change in wettability.
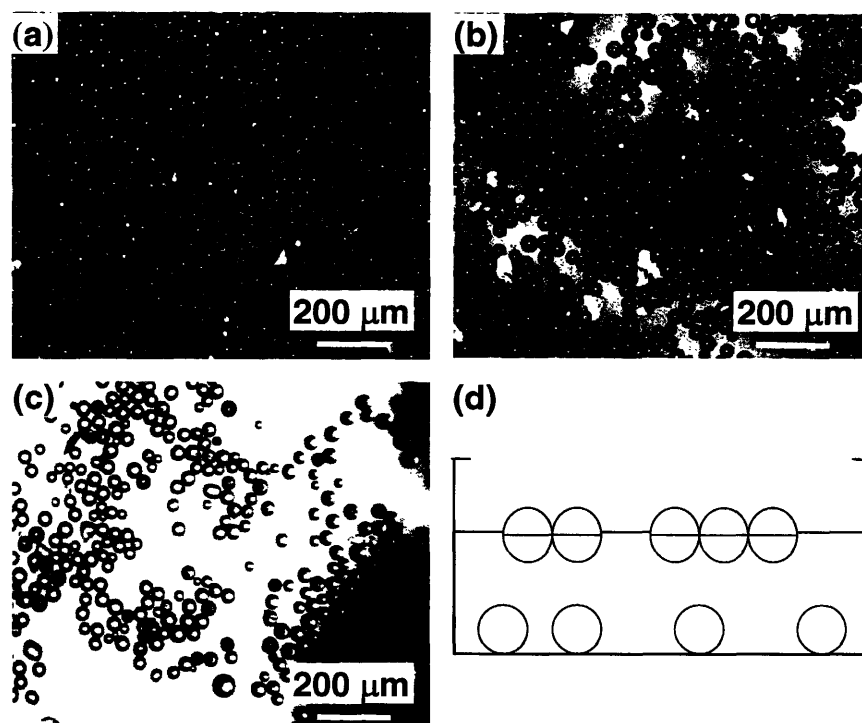
Figure 6-2 Images of the dual-functional particles taken under an optical microscope. (a) Image of the particles at the air-water interface after they are slowly sprinkled onto the water surface. Only the darker particles have a hemispherical gold coating. (b) Image of the particles at the air-water interface after gentle stirring. The particles remaining at the interface are mostly those with the hemispherical gold coating. (c) Image of flask bottom after gentle stirring. The uncoated particles settle to the bottom of the container under gravity. (d) Schematic illustration showing the pinning of the dual-functional particles at the air-water interface.

6.3.3 Orthogonal assembly of DNA molecules on dual-functional particles

The gold-coated particles were then treated with SH-DNA to functionalize the gold side selectively. The combination of the silica and gold surfaces ensures that the chemistries used for functionalizing the surfaces would introduce minimal cross contamination to the other DNA sequence. Further, it is unlikely that the SH-DNA would affect the DNA on the silica side under the attachment conditions. Subsequently, the remaining sites on the gold side were capped with MCH[29] to reduce non-specific adsorption. Figure 6-3 shows the overall scheme for making the dual-functional particles.

These particles were then immersed in a solution containing their fluorophore-tagged complementary target molecules. The target complementary to the silica side (TAMRA-cA) was labeled with TAMRA and that to the gold side (Cy5-cB) was labeled with Cy5. The two fluorophores were selected to have minimal spectral overlap enabling the simultaneous detection of each fluorophore and allowing measurement of their respective spatial locations. To ensure the robustness of the assembly, I prepared three different kinds of particles: C-C, NC-C, and C-NC. The C-C particles have sequences complementary (C) to the respective target DNA on both the silica and gold sides. The silica side for the NC-C particles and the gold side for the C-NC particles have sequences non-complementary (NC) to either of the target DNA molecules (TAMRA-cA & Cy5-cB).

Figure 6-4 shows representative fluorescence images of the three different kinds of particles as obtained by confocal microscopy after their contact with the fluorescently-tagged target DNA molecules. These images are 2-D projections of the fluorescence images obtained at various cross sections of the particles. In these images the particles are oriented such that the top half represents the uncoated silica surface while the bottom half represents the gold-coated

surface. For C-C particles (Figure 6-4a), I observe only TAMRA signals on the SiO_2 surface and only Cy5 signals on the gold surface. For the C-NC particles (Figure 6-4b), I observe no Cy5 fluorescence from either hemisphere, suggesting the efficiency of the DNA immobilization procedure for reducing non-specific adsorption; however, TAMRA signal is seen on the silica side indicating successful hybridization of the complementary sequences. For the NC-C particles (Figure 6-4c), no Cy5 signal was obtained on the silica side but a very faint TAMRA signal was observed on the gold side, suggesting a small amount of non-specific adsorption on the gold side. These observations were corroborated for tens of particles of the three different types. Together, these confocal images show that I could achieve orthogonal assembly of two DNA molecules onto two specific regions determined by the base-pair complementarity of the DNA sequences. This study can be readily extended to achieve orthogonal assembly of nanoparticles by attaching the target oligonucleotides with nanoparticles. The experiments in this chapter formed the basis of the work described in Chapter 7.
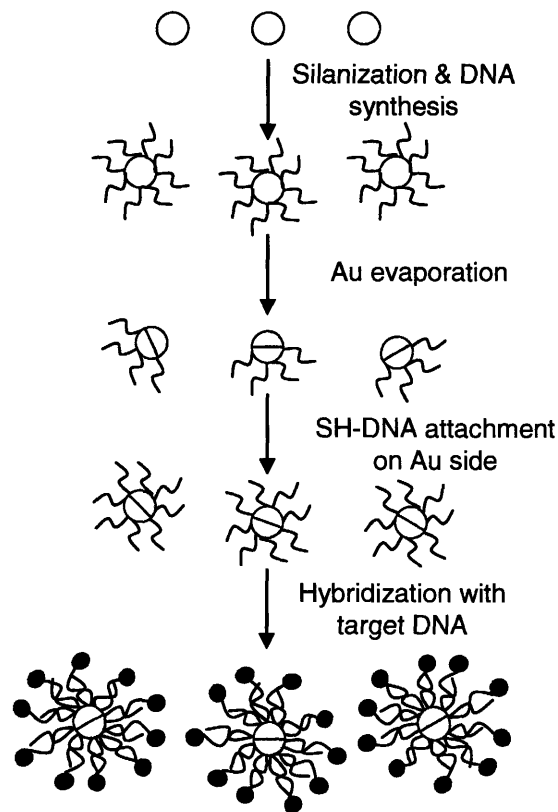
Figure 6-3 Schematic illustration of the overall process of making the dual-functional particles and demonstrating the orthogonal assembly of fluorophore-tagged target DNA molecules onto C-C particles. Briefly, the process begins with DNA immobilization on the silica particles, followed by Au deposition on one hemisphere, and SH-DNA attachment to the gold side. These dual-functional particles are then used for hybridizing with target molecules tagged with two different fluorophores (TAMRA & Cy5). The TAMRA-tagged target DNA is complementary to the DNA attached to the silica side and the Cy5-tagged target DNA is complementary to the DNA attached to the gold side.
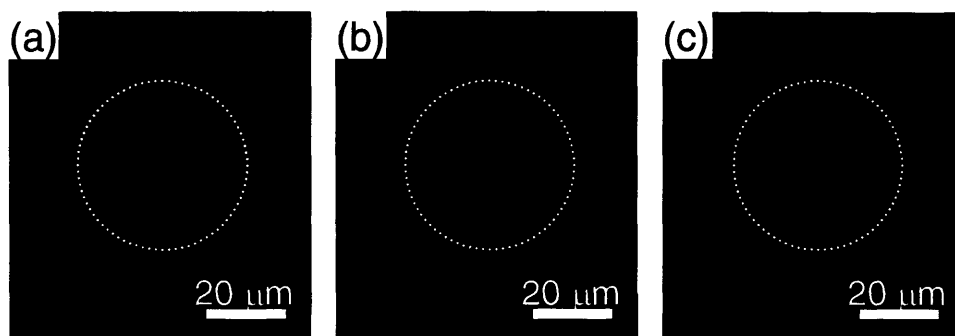
Figure 6-4 2-D projection of the confocal microscopy images collected at various cross-sections of the dual-functional particles. In these images, the particles are oriented such that the top half represents the silica side and the bottom half represents the gold side. TAMRA (red) and Cy5 (blue) signals from (a) a C-C particle with complementary sequences to the fluorophore-tagged target DNA molecules on both the silica side and the gold side. (b) a C-NC particle with complementary sequence on the silica side and non-complementary sequence on the gold side. (c) a C-NC particle with non-complementary sequence on the silica side and complementary sequence on the gold side.

161

6.3.4 Formation and functionalization of tri-functional particles

After the assembly of DNA molecules on the dual-functional microspheres, I decided to increase the level of complexity by adding one more functionality to the microspheres. I again employed the shadow deposition technique to coat the microspheres with a second metal surface. Al was chosen as a second metal since the surface chemistries for derivatizing the Al and Au surfaces are sufficiently different to allow selective functionalization.

Figure 6-5 shows the schematic for coating different regions of the microspheres with the two different metals. Gold was deposited onto silica particles that were functionalized with DNA and spread as a monolayer on a flat surface. In a second step, the orientation of the particles was shifted by 90° and Al was deposited onto the particles. Given the order of the deposition of the metals and the geometry of the shadow deposition technique, I expected one hemisphere of the particles to be coated with Al, whereas the gold-coated and uncoated SiO_2 surfaces to occupy approximately one quadrant each. The composition of the particle surface was confirmed by energy dispersive X-ray analysis (EDX) (Figure 6-6). The EDX images confirmed that the particle surface composition was as expected according to the geometry of the deposition scheme.

In orthogonal assembly of complex structures, it is also important to have templates that include inactive surfaces, in order to place constraints on the structures formed during the assembly process. Thus, instead of functionalizing the Al surface to contain an additional recognition element I chose to passivate it with a layer of stearic acid to provide a surface that would be inactive toward any adsorption event. One requirement for generating this inactive surface is that the chemistry used for passivating the surface should be stable under the conditions employed for the further stages of the assembly process. The functionalization of the
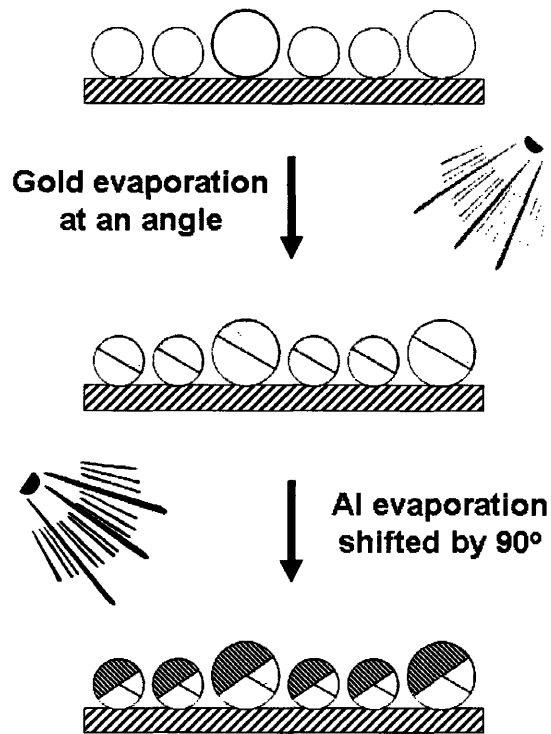
Figure 6-5 Schematic illustration of the process used to generate particles with three different surfaces. First, gold is evaporated onto silica microspheres spread as a monolayer on a flat surface. Next, the deposition angle is changed by 90°, and Al is deposited onto the particles.
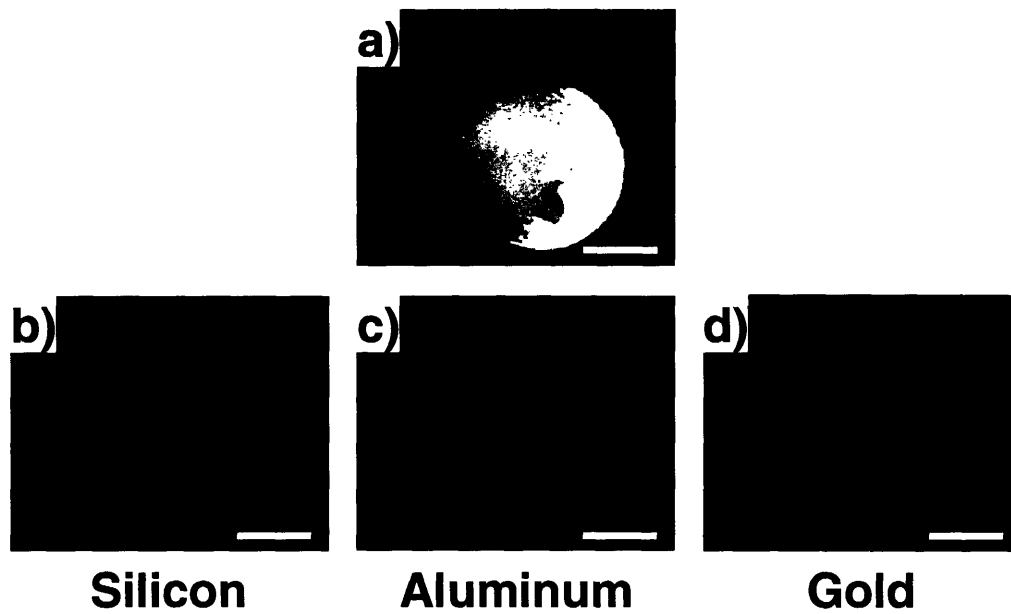
Figure 6-6 Energy dispersive X-ray analysis (EDX) images of a silica microsphere after shadow deposition of Au and Al. (a) SEM image of the particle. (b), (c) & (d) show the locations of the SiO_2, Au, and Al regions on the particle, respectively.

Au surface as well the hybridization steps are performed under fairly high salt concentrations, conditions that might compromise the performance of the stearic acid layer on the Al surfaces. This issue was addressed by monitoring the wetting properties of stearic acid layers on flat Al surfaces after exposing them to salt concentrations encountered in the subsequent steps (0.5 M NaCl). I observed the water and hexadecane contact angles on the passivated Al surfaces were largely unaffected by exposure to the salt solution. However, the hysteresis in the wetting properties for these liquids showed a slight increase indicating some damage to the stearic acid/Al layer.

6.3.5 Orthogonal assembly on the tri-functional particles

The complete functionalization and assembly process is shown in Figure 6-7. After the passivation of the Al layer, I functionalized the gold surface with oligo B. Next, I placed these tri-functional particles– oligo A on SiO2, oligo B on Au, inert on Al –in a solution containing both TAMRA-cA and FAM-cB1, fluorophore-tagged DNA sequences complementary to those on the SiO2 and Au surfaces. Figure 6-8 shows the fluorescence images of the particles after the hybridization step. These images show that the fluorescence signals are limited to only one half of the particles; the other half corresponding to the Al layer does not exhibit any fluorescence. Since Al was coated last, it is expected to cover one half of the particle surface; the uncoated-SiO2 and Au-coated surfaces would constitute the other hemisphere. The fluorescence images show TAMRA (Figure 6-8a) and fluorescein (FAM) (Figure 6-8b) signals corresponding to the SiO2 and Au regions, respectively. The absence of any fluorescence signal on the Al side shows that the stearic acid layer was successful in preventing non-specific adsorption of either target DNA sequence onto its surface. Additionally, the minimal overlap in the regions providing fluorescein and TAMRA signals suggests that the surface chemistries used for functionalizing
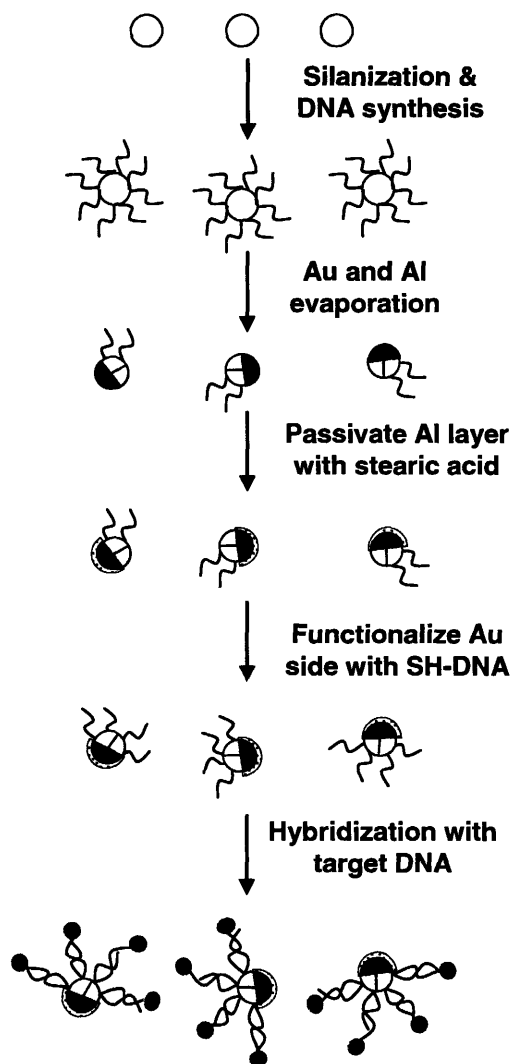
Figure 6-7 Schematic illustration of the overall process for making the tri-functional particles and demonstrating the orthogonal assembly of fluorophore-tagged target DNA molecules onto them. Briefly, the process begins with DNA immobilization on the silica particles, followed by Au and Al deposition, passivation of the Al side with stearic acid, and SH-DNA attachment to the gold side. These tri-functional particles are then contacted with target molecules tagged with two different fluorophores (TAMRA & FAM).
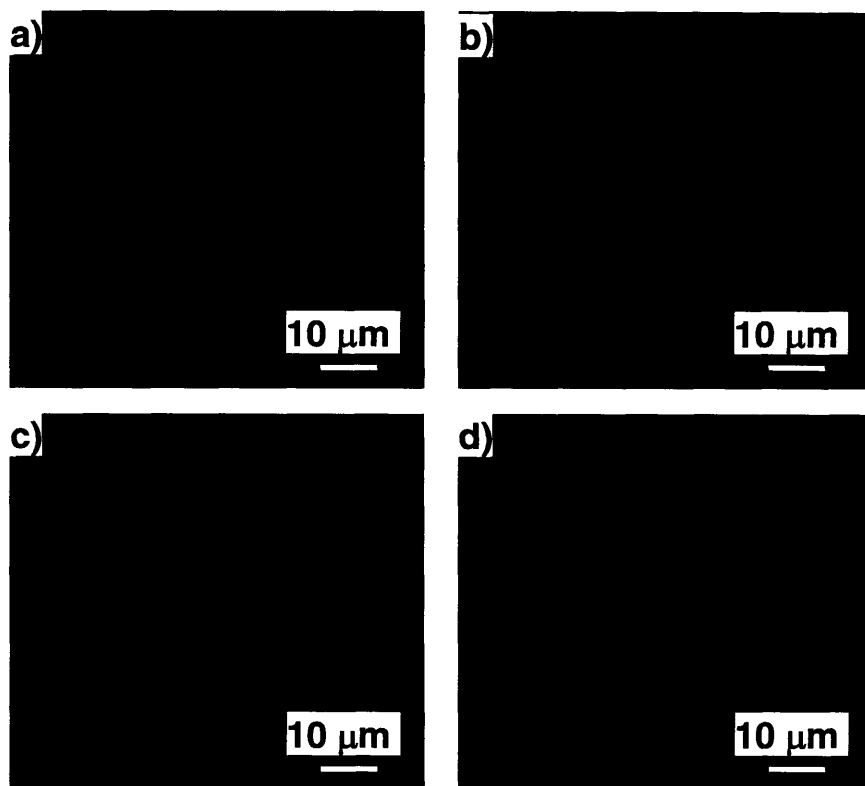
Figure 6-8 DNA-directed assembly onto a tri-functional particle. (a) TAMRA & (b) Fluorescein (FAM) signals obtained from the particle. (c) Combined fluorescence image of the particle. (d) Combined fluorescence and reflectance image of the particle showing the exact locations of the fluorophores on the particle.

the SiO_2 and Au surfaces have been successful in providing specific adsorption of the target probe and in avoiding any non-specific adsorption of the other target probe. Together these results show the ability to direct two targets to two regions specifically while providing an additional region that is inert to the assembly process.

6.4 Conclusions

A combination of shadow deposition, surface functionalization, and specific DNA-DNA interactions have been used to demonstrate the orthogonal assembly of two target DNA molecules specifically onto dual-functional and tri-functional particles. For the dual-functional particles, I employed two non-interfering chemistries to first achieve the orthogonal attachment of two different DNA receptor molecules onto specific surfaces. For the tri-functional particles, I modified three different surfaces (SiO_2, Au, and Al) with non-interfering chemistries to create a microstructure exposing three different functionalities. In this case, two of the functionalities were active with DNA molecules, while the third one was inactive. Upon exposure of these particles to a solution containing two fluorescently-tagged DNA molecules, the target DNA molecules were assembled selectively onto the specific regions of the particles based on DNA sequence complementarity. By assembling DNA molecules selectively onto the active surfaces of these asymmetric building blocks, I have demonstrated the applicability of surface chemistry along with DNA-based recognition in guiding a novel micron-scale assembly. These initial experiments on the orthogonal assembly of DNA molecules can be developed to achieve the self-assembly of complex hierarchical structures using DNA as the linker molecule between selectable particle-based building blocks (see Chapter 7). Such attempts at building asymmetric micro- and nano- structures along with advancements in directed-assembly techniques and

surface chemistry schemes will be crucial in developing bottom-up assembled devices for use in electronic, optical, magnetic, and other applications.

6.5 References & Footnotes

(1) Mirkin, C. A.; Letsinger, R. L.; Mucic, R. C.; Storhoff, J. J. *Nature* **1996**, *382*, 607-609.

(2) Alivisatos, A. P.; Johnsson, K. P.; Peng, X. G.; Wilson, T. E.; Loweth, C. J.; Bruchez, M. P.; Schultz, P. G. *Nature* **1996**, *382*, 609-611.

(3) Mucic, R. C.; Storhoff, J. J.; Mirkin, C. A.; Letsinger, R. L. *J. Am. Chem. Soc.* **1998**, *120*, 12674-12675.

(4) Niemeyer, C. M.; Ceyhan, B.; Blohm, D. *Bioconjugate Chem.* **1999**, *10*, 708-719.

(5) Niemeyer, C. M.; Boldt, L.; Ceyhan, B.; Blohm, D. *Anal. Biochem.* **1999**, *268*, 54-63.

(6) Niemeyer, C. M. *Appl. Phys. A-Mater. Sci. Process.* **1999**, *68*, 119-124.

(7) He, L.; Musick, M. D.; Nicewarner, S. R.; Salinas, F. G.; Benkovic, S. J.; Natan, M. J.; Keating, C. D. *J. Am. Chem. Soc.* **2000**, *122*, 9071-9077.

(8) Liu, Q. H.; Wang, L. M.; Frutos, A. G.; Condon, A. E.; Corn, R. M.; Smith, L. M. *Nature* **2000**, *403*, 175-179.

(9) Braun, E.; Eichen, Y.; Sivan, U.; Ben-Yoseph, G. *Nature* **1998**, *391*, 775-778.

(10) Nam, J. M.; Thaxton, C. S.; Mirkin, C. A. *Science* **2003**, *301*, 1884-1886.

(11) Niemeyer, C. M.; Wacker, R.; Adler, M. *Nucleic Acids Res.* **2003**, *31*.

(12) Whitesides, G. M.; Boncheva, M. *Proc. Natl. Acad. Sci. USA* **2002**, *99*, 4769-4774.

(13) Dujardin, E.; Hsin, L. B.; Wang, C. R. C.; Mann, S. *Chem. Commun.* **2001**, 1264-1265.

(14) Martin, B. R.; Dermody, D. J.; Reiss, B. D.; Fang, M. M.; Lyon, L. A.; Natan, M. J.; Mallouk, T. E. *Adv. Mater.* **1999**, *11*, 1021-1025.

(15) Takei, H.; Shimizu, N. *Langmuir* **1997**, *13*, 1865-1868.

(16) Himmelhaus, M.; Takei, H. *Sens. Actuator B-Chem.* **2000**, *63*, 24-30.

(17) Nakahama, K.; Kawaguchi, H.; Fujimoto, K. *Langmuir* **2000**, *16*, 7882-7886.

(18) Fujimoto, K.; Nakahama, K.; Shidara, M.; Kawaguchi, H. *Langmuir* **1999**, *15*, 4630-4635.

(19) Nagle, L.; Ryan, D.; Cobbe, S.; Fitzmaurice, D. *Nano Lett.* **2003**, *3*, 51-53.

(20) Hugonnot, E.; Carles, A.; Delville, M. H.; Panizza, P.; Delville, J. P. *Langmuir* **2003**, *19*, 226-229.

(21) Erhardt, R.; Zhang, M. F.; Boker, A.; Zettl, H.; Abetz, C.; Frederik, P.; Krausch, G.; Abetz, V.; Muller, A. H. E. *J. Am. Chem. Soc.* **2003**, *125*, 3260-3267.

(22) Love, J. C.; Gates, B. D.; Wolfe, D. B.; Paul, K. E.; Whitesides, G. M. *Nano Lett.* **2002**, *2*, 891-894.

(23) Salem, A. K.; Searson, P. C.; Leong, K. W. *Nat. Mater.* **2003**, *2*, 668-671.

(24) Binsk, B. P.; Fletcher, P. D. I. *Langmuir* **2001**, *17*, 4708-4710.

(25) Allara, D. L.; Nuzzo, R. G. *Langmuir* **1985**, *1*, 45-52.

(26) Casagrande, C.; Fabre, P.; Raphael, E.; Veyssie, M. *Europhys. Lett.* **1989**, *9*, 251-255.

(27) Casagrande, C.; Veyssie, M. *Comptes Rendus De L Academie Des Sciences Serie Ii* **1988**, *306*, 1423-1425.

(28) Ondarcuhu, T.; Fabre, P.; Raphael, E.; Veyssie, M. *J. Phys. Paris* **1990**, *51*, 1527-1536.

(29) Herne, T. M.; Tarlov, M. J. *J. Am. Chem. Soc.* **1997**, *119*, 8916-8920.

Chapter 7.   Orthogonal Assembly of Nanoparticles on

Dual-Functional Microspheres

7.1 Introduction

Orthogonal assembly is one of the key methodologies that would facilitate the generation of functional self-assembled devices from smaller units (so called 'bottom-up' synthesis). The key requirements for orthogonal assembly are the availability of multiple mutually-selective recognition motifs and ways to attach and pattern them on different surfaces. In this regard, research in developing newer templates, recognition motifs, and attachment chemistries would broaden the range of structures that can be created by self-assembly methods. Various techniques[1] for patterning receptor sites on surfaces include microcontact printing,[2,3] DPN,[4,5] lithography,[6,7] etc. These techniques are used for designing templates needed for assembling the functional components. The number of steps required to perform the assembly of the individual components onto the templates will be lesser if the number of selectively-reactive surfaces present in a system are large. For instance, an orthogonal assembly of ten different components can be performed in a single step if the functionalities directing the different components to their corresponding location on the template are mutually-selective. A system where the number of mutually-selective reactive functionalities are smaller then the number of components to be assembled, in contrast, would require multiple sequential steps to assemble the components onto their respective locations on the template. Thus, techniques for orthogonal assembly of components by incorporation of selectively-reactive surfaces would lead to simplification of assembly protocols and would allow large-scale parallel assembly of components.

The orthogonal assembly of nanoscopic structures has been achieved using either electrostatic interactions[8] or specific macromolecular interactions.[9] Assembly by electrostatic interactions exploits the charges on the surface of an object and their attraction to complementarily charged surfaces. Recent work by Ivanisevic et al.[10] has shown that various redox-active inks can used to create templates for nanoparticle assembly and then each ink can be specifically "switched on" by tuning the applied voltage to promote particle deposition by electrostatic interactions. DNA-DNA interactions based on sequence complementarity, in contrast, give tremendous freedom for programming a multitude of specific recognition events. Mirkin et al.[9] have shown that nanoparticles can be assembled onto DNA features as generated by dip-pen nanolithography. Their experiments show the ability to adsorb two types of particles selectively onto specific sites of a surface. Their technique illustrates the usefulness of DNA-DNA interactions in creating multiple unique molecular recognition events.

Several research groups[11-14] have demonstrated the orthogonal assembly of molecular components based on the reactivity of specific functional groups with different surfaces (thiols with Au, carboxylic acids with Al, isonitriles with Pt, etc.). Here, using these differences in surface reactivity in combination with shadow metal deposition, I created a template, a micron-scale asymmetric building block, with DNA-based recognition motifs. The asymmetric particles were formed by the shadow deposition of gold onto silica microspheres; their formation did not necessitate use of sophisticated techniques like lithography or DPN. Because of the two different surfaces employed (SiO$_2$ and Au), I was able to selectively functionalize them with different DNA sequences to form the dual-functional particles. This study is an extension of the experiments described in Chapter 6 wherein DNA molecules were orthogonally assembled onto dual- and tri-functional particles. Here, instead of assembling DNA molecules, two different

nanoparticles were regio-specifically assembled onto the dual-functional particles via DNA-DNA interactions to form a spatially-defined multiparticle assembly.

7.2 Experimental Section

Materials. Silica microspheres (30-50 μm) were obtained from Polysciences, Inc. (Warrington, PA). Octyl trichlorosilane (C_8 silane), dithiothreitol (DTT), and 6-mercapto-1-hexanol (MCH) were obtained from Aldrich (Milwaukee, WI). Trichloroacetyl (TCA) protected ω-hydroxyundecyl trichlorosilane (TCA silane) was custom synthesized in our laboratory. Gold pellets were supplied by J&J Materials, Inc. (Neptune City, NJ), and chromium-coated tungsten filaments were supplied by R. D. Mathis and Company (Long Beach, CA). Acetonitrile, methanol, ethanol, acetone, sodium chloride, sodium citrate, EDTA, tris-HCl, and potassium carbonate (K_2CO_3) were obtained from Mallinckrodt (Paris, KE). Phosphoramidites and reagents used for oligonucleotide synthesis, and empty TWIST™ columns were obtained from Glen Research (Sterling, MA). Piperidine (20%) in dimethyl formamide was obtained from Protein Technologies, Inc (Tucson, AZ). Deionized (resistivity = 18.2 MΩ) water was provided by a MilliQ deionization system (Millipore Corp., Bedford, MA). Thiolated oligonucleotides 5'– SH – $(CH_2)_6$ – GCC TGA TAC CAT AAC TGA – 3' (oligo B), 5' – SH – $(CH_2)_6$ – TCA GTT ATG GTA TCA GGC – 3' (oligo cB), and 5'– TGG TCG CAC AGG TCG CAT – SH – $(CH_2)_3$ – 3' (oligo cA) were obtained from MWG Biotech (High Point, NC) in the disulfide form. Centri-Spin™ columns for gel filtration were obtained from Princeton Separations (Adelphia, NJ). Citrate-stabilized 20-nm and 40-nm gold nanoparticles were obtained from Ted Pella, Inc. (Redding, CA). All materials were used as received.

Functionalizing silica microspheres. The microparticles were cleaned in a 12.5 wt-% NaOH solution in a 3:4 H_2O:EtOH for 2 h. Subsequently they were washed 3-4 times with

deionized water and dried. The silanizing solution was prepared by adding octyl trichlorosilane

(C$_8$ silane) and trichloroacetyl (TCA) protected ω-hydroxyundecyl trichlorosilane (TCA silane)

in a 20:80 volume proportion to anhydrous toluene (>99.5%) to yield 1 μL/mL (~mM) solution

of the silanes in toluene. The particles were immersed in the silanizing solution for 4 h. After 4 h,

the particles were washed once with toluene and twice with acetone and dried.

To expose hydroxyl groups on the particle surfaces prior to DNA synthesis, the TCA

protecting groups were removed by immersing the particles in a 5 mM K$_2$CO$_3$ solution in 1:1

H$_2$O: methanol for 15 min. Stepwise synthesis of oligonucleotide 5'–ATG CGA CCT GTG CGA

CCA TTT T–3' (oligo A) was performed on the particles using a Applied Biosystems ABI-

392/394 automated DNA synthesizer. Cyanoethyl groups present on the phosphorus linkages

were removed by immersing the slides in a 20-wt% piperidine in dimethyl formamide (DMF)

solution for 4 h. Protecting groups on the nucleic bases were removed by immersing the particles

in a 0.05 M K$_2$CO$_3$ solution in anhydrous methanol for 4 h. To functionalize the particles with

sequence non-complementary to the TAMRA-labeled target, 5'–AGC CAA TTG GCC TTT T–

3' (oligo A1) was synthesized on the particles.

Functionalizing gold surfaces. The thiolated oligonucleotide (oligo B) was obtained from

the vendor in the disulfide form. The disulfide group was reduced in a 0.05 M DTT solution for

30 min. Excess DTT was removed using gel filtration on Centri-SpinTM columns. The

oligonucleotide solution was diluted to yield a 5 μM oligonucleotide concentration in 1.0 M

KH$_2$PO$_4$, pH 3.5. Au substrates were added to this oligonucleotide solution and kept in contact

for more than 16 h. After 16 h, the slides were washed, and then immersed in a 7.5 mM MCH

solution for 1 h to cap sites on the gold surface not coated with the SH-DNA.[15] A similar

procedure was used to functionalize the Au side of the dual-functional microspheres.

Nanoparticle functionalization. Gold nanoparticles were functionalized with oligonucleotides using methods reported in literature.[16] Briefly, the thiolated oligonucleotide obtained from the vendor in the disulfide form was reduced in a 0.05 M DTT solution for 30 min. Excess DTT was removed using gel filtration on Centri-Spin™ columns. The oligonucleotide solution was diluted with the citrate-stabilized nanoparticle solution to yield a 5 μM oligonucleotide concentration and a 0.6 nM nanoparticle concentration. After standing for 16 h, the solution was brought to 0.1 M NaCl, 10 mM phosphate buffer (pH 7). After ageing the solution for more than 24 h, it was centrifuged at 14000 rpm for 30 min. The precipitate was washed with 0.1 M NaCl, 10 mM phosphate buffer (pH 7) followed by centrifugation and redispersion. The final salt concentration of the nanoparticle solution was brought to 0.3 M NaCl by gradually adding drops of 1 M NaCl.

Nanoparticle adsorption onto SiO₂ microspheres and flat Au substrates. Silica microspheres functionalized with oligos A and A1 were placed in the nanoparticle solution for 16 h. After 16 h, the microspheres were rinsed with 0.3 M NaCl, 10 mM phosphate buffer solution. A similar procedure was used for Au surfaces functionalized with oligo B and oligo cA.

Gold coating on microspheres. The silica particles functionalized with oligo A were spread as a monolayer on a Petri dish. Chromium (~50 Å) and gold (~200 Å) were sequentially evaporated at 0.5-1 Å/s onto the particles in a diffusion-pumped vacuum chamber operating at 2 x 10^{-6} torr. The particles were briefly sonicated to release them from the surface.

Orthogonal assembly of nanoparticle onto dual-functional microspheres. The gold on the gold-coated microspheres was functionalized with oligo B according to the above mentioned procedure. The dual-functional microspheres were placed in a solution of oligo-cA-functionalized 20-nm Au particles for more than 16 h. The microspheres were then washed in a

175

0.3 M NaCl, 10 mM phosphate buffer solution. To coat the gold side of these microspheres, they were placed in a solution of oligo-cB functionalized 40-nm Au particles, and subsequently washed in the above buffer solution.

SEM imaging. Special care was required to avoid drying artifacts (like salt crystallization) in the SEM images. First, a few drops of the nanoparticle-coated microsphere solution were placed on a filter paper to soak out the liquid. The liquid-free microspheres were then transferred onto a strip of carbon tape for SEM imaging. The nanoparticle-covered microspheres and gold substrates were visualized using a Philips XL30 FEG-ESEM. The nanoparticle area coverage was estimated using the Scion Image analysis software.

7.3 Results & Discussion

7.3.1 Nanoparticle adsorption onto silica microspheres

Before attempting the orthogonal DNA-directed assembly of two different nanoparticles onto dual-functional microspheres, I first optimized the protocols for attaching nanoparticles onto the individual SiO_2 and Au surfaces. Figure 7-1a shows the schematic for the DNA-driven attachment of 20-nm Au nanoparticles onto the surface of DNA-functionalized silica microspheres (30-50 μm). The nanoparticles were functionalized with oligo cA using protocols mentioned in literature.[16] The silica microspheres were functionalized by step-wise phosphoramidite synthesis on a commercial DNA synthesizer. The nanoparticle solution was brought in contact with the microspheres.

Figure 7-1b shows the two vials containing the microspheres functionalized with oligo A (C – complementary to the DNA sequence on the nanoparticles) and oligo A1 (NC – non-complementary to the DNA sequence on the nanoparticles) in contact with the nanoparticle

solution. As can be seen from this figure, the oligo-A-functionalized microspheres (C) turn reddish and the contacting solution becomes almost colorless due to the adsorption of the nanoparticles from solution onto the microspheres. In contrast, the oligo-A1-functionalized microspheres (NC) remain colorless and the solution in contact with them remains reddish suggesting that nanoparticle adsorption on these microspheres is minimal. This visual change in the color of the nanoparticle solution due to nanoparticle adsorption onto microspheres functionalized with complementary DNA sequences can be used to develop inexpensive colorimetric DNA detection schemes. Figure 7-1c & d show SEM images of the two different microspheres after their contact with the nanoparticle solution. The adsorbed nanoparticle density on the oligo-A-functionalized microspheres corresponds to an area coverage of ~15-20% area coverage while that on the oligo-A1-functionalized surface corresponds to less than 1%. These results indicate that the attachment chemistry is successful in selectively assembling nanoparticles onto surfaces with complementary DNA sequences with negligible adsorption on those with non-complementary sequences. The nanoparticle adsorption was fairly uniform across the surface of the microspheres except for some clustering that likely occurred while preparing the sample for SEM imaging. The observed nanoparticle distribution suggests that the DNA synthesis on the microspheres using the DNA synthesizer was fairly uniform.
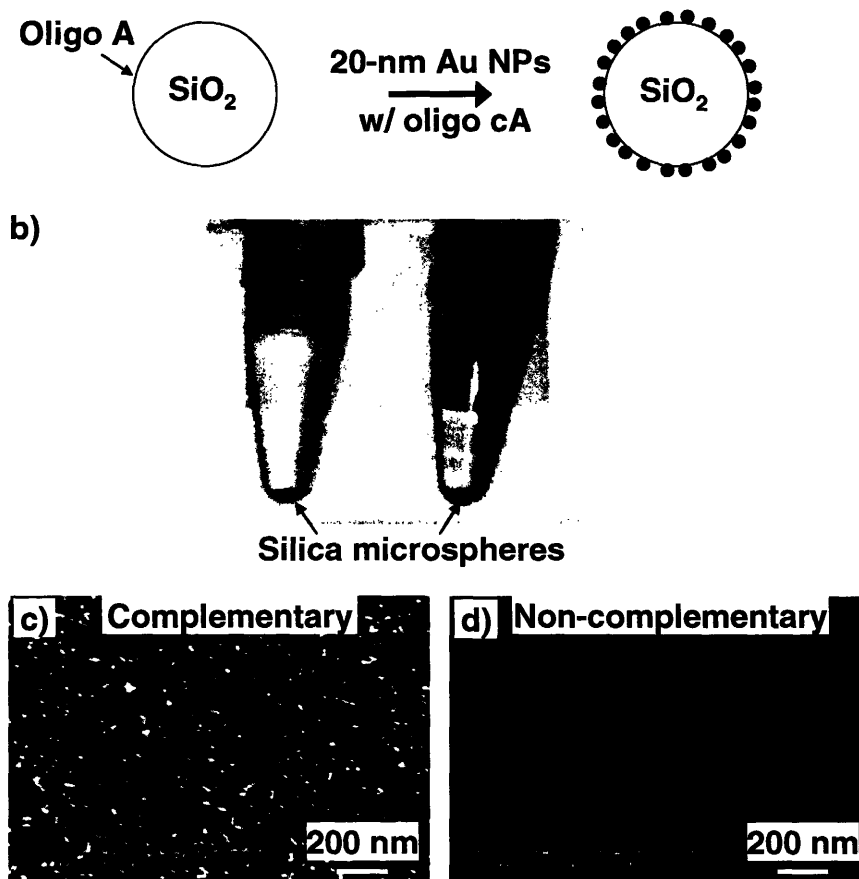
Figure 7-1 DNA-driven nanoparticle adsorption onto silica microspheres. (a) Schematic illustration of the assembly of DNA-functionalized Au nanoparticles (NP) onto oligonucleotide-functionalized silica microspheres. (b) Photograph of vials containing solutions of oligo A (C) and oligo A1 (NC) functionalized microspheres in contact with the Au nanoparticles that shows the visual changes due to DNA-driven nanoparticle adsorption onto the microspheres. Two batches of silica microspheres coated with oligo A (C) and oligo A1 (NC) were placed in oligo-cA-functionalized 20-nm Au nanoparticle solution. (c) & (d) SEM images of the surfaces of microspheres functionalized with oligo A and oligo A1, respectively, after contacting the nanoparticle (NP) solution.

7.3.2 Nanoparticle adsorption onto Au surfaces

Key requirements for the assembly of nanoparticles of two different sizes selectively onto specific regions of dual-functional microspheres were effective attachment chemistries for functionalizing the two surfaces (SiO_2 and Au). After optimizing the protocol for nanoparticle attachment onto silica microspheres, I established a protocol for attaching nanoparticles onto Au surfaces. Figure 7-2a shows a schematic illustration of the nanoparticle attachment onto flat DNA-functionalized Au surfaces. In these experiments, Au slides were functionalized with thiolated oligonucleotides. To reduce non-specific adsorption of nanoparticles the uncoated sites on the Au surface were capped with mercaptohexanol (MCH).[15] The MCH capping is especially important given that the gold surfaces have high affinity for each other which could lead to significant non-specific adsorption of the Au nanoparticles onto the Au surface, especially on the bare regions. During the functionalization of the Au slides, I observed that the salt concentration was important in ensuring that the Au surfaces are densely coated with the SH-DNA. For example, nanoparticle adsorption by DNA hybridization onto Au slides that had been functionalized in SH-DNA solutions that contained no salt was extremely low. In contrast, the use of 1.0 M KH_2PO_4 during the SH-DNA attachment led to a high specific adsorption of nanoparticles onto the Au slides.[15] Figure 7-2b shows SEM images of the Au slides functionalized with complementary (oligo B) and non-complementary (oligo cA) DNA sequences after contact with oligo-cB-functionalized 20-nm Au nanoparticles. The area coverage of the nanoparticles due to specific adsorption onto the Au surfaces was ~20% while that due to non-specific adsorption was less than 1%. The high levels of specific adsorption combined with the low levels of non-specific adsorption show the quality of the surface chemistry employed.

a)

Oligo B

20-nm Au NPs
⟶
w/ oligo cB

b) Complementary

200 nm

c) Non-complementary

200 nm
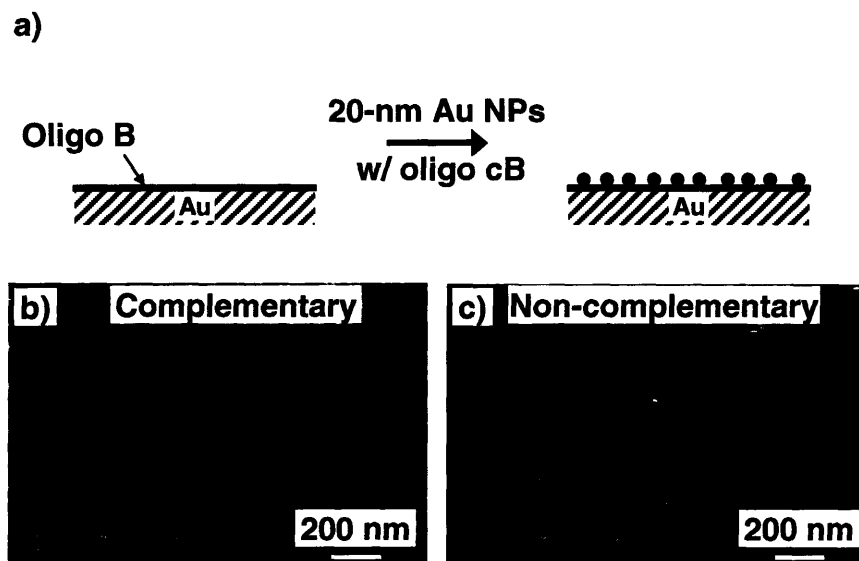
Figure 7-2 DNA-driven nanoparticle adsorption onto flat gold-coated substrates. (a) Schematic illustration of the DNA-directed assembly of DNA-functionalized Au nanoparticles (NP) onto flat oligonucleotide-functionalized Au surfaces. (b) & (c) SEM images of Au-coated surfaces functionalized with complementary and non-complementary sequences, respectively, after their contact with the 20-nm Au nanoparticle solution.

7.3.3 Orthogonal nanoparticle assembly onto dual-functional microspheres

Having established effective protocols for guiding DNA-driven adsorption of Au nanoparticles onto SiO_2 and Au surfaces individually, the SiO_2 procedure was used to adsorb 20-nm particles selectively onto the SiO_2 side of the dual-functional microspheres. In these experiments, dual-functional microspheres with oligo A and oligo B on the SiO_2 and Au sides, respectively, were brought in contact with 20-nm Au nanoparticles functionalized with oligo cA. After more than 16 h of contact, the microspheres were washed with the hybridizing buffer and imaged using SEM. Figure 7-3 shows the SEM images of the SiO_2 and Au sides after contact with the nanoparticle solution. The SiO_2 surface adsorbed a high density of nanoparticles corresponding to an area coverage of ~20% while adsorption onto the Au side was minimal. These images demonstrate the ability of this approach for selectively directing the adsorption of nanoparticles to a chosen region of the dual-functional microspheres using recognition events based on DNA sequence complementarity.

These microspheres with 20-nm Au particles adsorbed onto the SiO_2 surface were then immersed in a solution of 40-nm Au nanoparticles functionalized with oligo cB. Based on the DNA-DNA complementarity, the 40-nm Au particles are expected to adsorb selectively onto the Au side of the dual-functional microspheres. Figure 7-4 shows the SEM images of the SiO_2 and Au sides of the microspheres after more than 16 h of contact with a 40-nm Au nanoparticle solution followed by a wash in the hybridizing buffer. These images show that the deposition of the 40-nm particles on the Au surface was highly specific while the non-specific adsorption of these nanoparticles on the SiO_2 side was minimal. The extent of non-specific nanoparticle adsorption onto the nanoparticle-coated SiO_2 surface is slightly higher than that observed on SiO_2 surfaces without any previously adsorbed nanoparticles (Figure 7-1d). We hypothesize that

some of the non-specific adsorption of the 40-nm particles onto the SiO$_2$ surface is due to the presence of the 20-nm particles on the surface as evidenced by our observation of particle aggregation and precipitation following contact between the 40-nm and 20-nm particle solutions. The coverage of the 40-nm particles on the Au surface is ~10-15%. In summary, 20-nm particles were attached with an area coverage of ~20% onto the SiO$_2$ surface and 40-nm particles were attached with an area coverage of ~10-15% onto the Au surface of the dual-functional microspheres. These high specific adsorption values combined with minimal non-specific adsorption of 20-nm and 40-nm particles onto the Au and SiO$_2$ surfaces, respectively, demonstrate the orthogonal assembly of the two nanoparticles onto the dual-functional microspheres.

7.4 Conclusions

In this study, I have demonstrated the ability of orthogonal assembly to selectively functionalize an asymmetric building block regio-specifically with nanoparticles of two different sizes. Selective orthogonal adsorption was a result of the selective DNA-DNA interactions between the nanoparticles and the surfaces of an asymmetric building block consisting of a dual-functional microsphere that expressed two different DNA sequences. Our results also show that the amount of non-specific adsorption—a crucial parameter to generate defect-free self-assembled devices[17]—on the two surfaces is low indicating the effectiveness of the surface functionalization techniques in providing selectivity. Our multiparticle assembly illustrates the potential of constructing various self-assembled structures by suitably programming the 'assembly instructions' using DNA sequences. The use of asymmetric building blocks accompanied by schemes for orthogonal assembly of nanoscopic structures will greatly enhance the ability to create fairly complex hierarchical structures.

a)

Oligo A

SiO₂

Au

Oligo B

20-nm Au NPs
w/ oligo cA

SiO₂

Au

b) SiO₂

200 nm

c) Au

200 nm
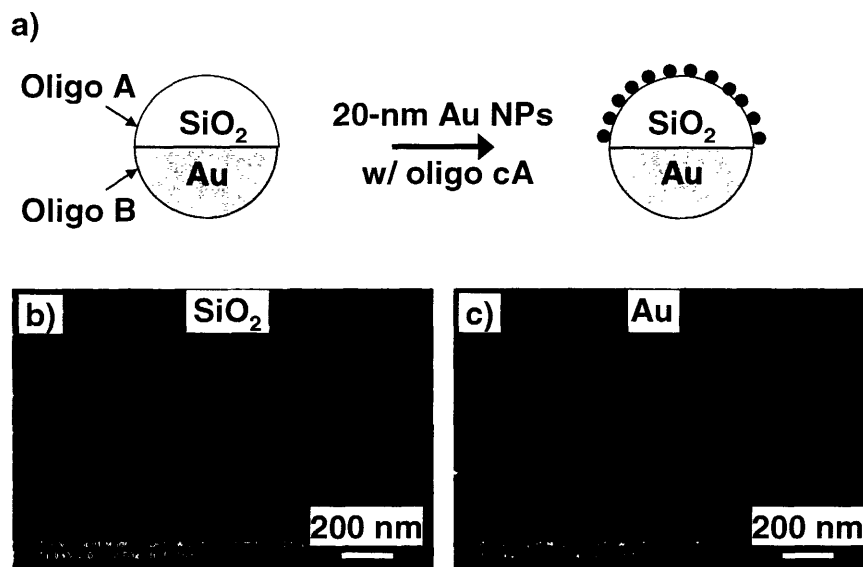
Figure 7-3 Selective DNA-driven nanoparticle adsorption onto the SiO₂ side of dual-functional microspheres. (a) Schematic illustration of selective (b) & (c) SEM images of the SiO₂ and Au-coated surfaces of a dual-functional silica microsphere after contact with a 20-nm Au nanoparticle (NP) solution. The 20-nm particles were functionalized with DNA sequences complementary to those on the SiO₂ side.
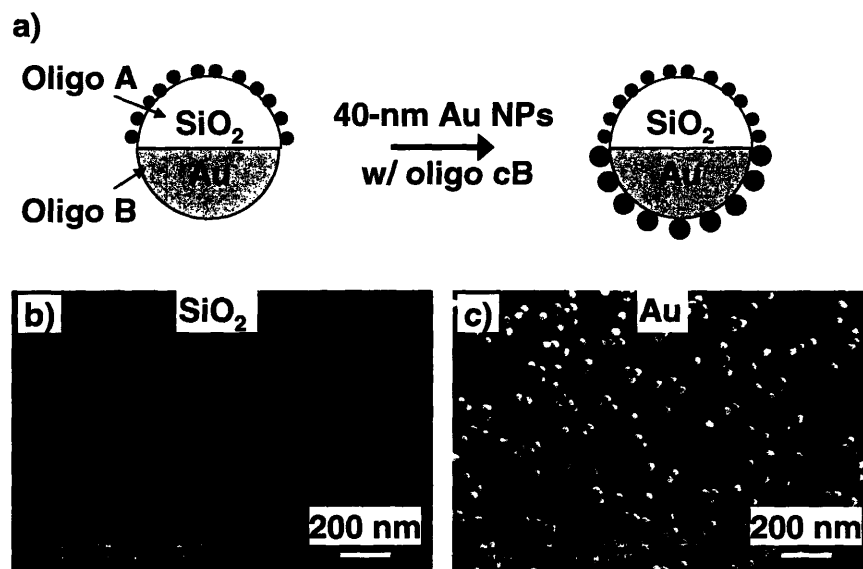
Figure 7-4 Orthogonal DNA-driven nanoparticle assembly onto dual-functional silica microspheres. (a) Schematic illustration showing the orthogonal assembly of 20-nm and 40-nm Au nanoparticles onto the two sides of a dual-functional microsphere. (b) & (c) SEM images of the SiO_2 and Au-coated surfaces after contacting with the 20-nm and 40-nm nanoparticle (NP) solutions. The 20-nm and 40-nm particles were functionalized with DNA sequences complementary to those on the SiO_2 and Au-coated sides, respectively.

7.5 References & Footnotes

(1) Geissler, M.; Xia, Y. N. *Adv. Mater.* **2004**, *16*, 1249-1269.

(2) Xia, Y. N.; Whitesides, G. M. *Ann. Rev. Mater. Sci.* **1998**, *28*, 153-184.

(3) Santhanam, V.; Andres, R. P. *Nano Lett.* **2004**, *4*, 41-44.

(4) Piner, R. D.; Zhu, J.; Xu, F.; Hong, S. H.; Mirkin, C. A. *Science* **1999**, *283*, 661-663.

(5) Zhang, H.; Li, Z.; Mirkin, C. A. *Adv. Mater.* **2002**, *14*, 1472-+.

(6) Haynes, C. L.; Van Duyne, R. P. *J. Phys. Chem. B* **2001**, *105*, 5599-5611.

(7) Kosiorek, A.; Kandulski, W.; Chudzinski, P.; Kempa, K.; Giersig, M. *Nano Lett.* **2004**, *4*, 1359-1363.

(8) Kruger, C.; Jonas, U. *J. Colloid Interface Sci.* **2002**, *252*, 331-338.

(9) Demers, L. M.; Park, S. J.; Taton, T. A.; Li, Z.; Mirkin, C. A. *Angew. Chem.-Int. Edit.* **2001**, *40*, 3071-3073.

(10) Ivanisevic, A.; Im, J. H.; Lee, K. B.; Park, S. J.; Demers, L. M.; Watson, K. J.; Mirkin, C. A. *J. Am. Chem. Soc.* **2001**, *123*, 12424-12425.

(11) Laibinis, P. E.; Hickman, J. J.; Wrighton, M. S.; Whitesides, G. M. *Science* **1989**, *245*, 845-847.

(12) Gardner, T. J.; Frisbie, C. D.; Wrighton, M. S. *J. Am. Chem. Soc.* **1995**, *117*, 6927-6933.

(13) Martin, B. R.; Dermody, D. J.; Reiss, B. D.; Fang, M. M.; Lyon, L. A.; Natan, M. J.; Mallouk, T. E. *Adv. Mater.* **1999**, *11*, 1021-1025.

(14) Hickman, J. J.; Laibinis, P. E.; Auerbach, D. I.; Zou, C. F.; Gardner, T. J.; Whitesides, G. M.; Wrighton, M. S. *Langmuir* **1992**, *8*, 357-359.

(15) Herne, T. M.; Tarlov, M. J. *J. Am. Chem. Soc.* **1997**, *119*, 8916-8920.

(16) Storhoff, J. J.; Elghanian, R.; Mucic, R. C.; Mirkin, C. A.; Letsinger, R. L. *J. Am. Chem. Soc.* **1998**, *120*, 1959-1964.

(17) Dwyer, C.; Vicci, L.; Poulton, J.; Erie, D.; Superfine, R.; Washburn, S.; Taylor, R. M. *IEEE Trans. Very Large Scale Integr. (VLSI) Syst.* **2004**, *12*, 1214-1220.

Chapter 8. Summary and Future Directions

8.1 Summary

Broadly, the main objective of my thesis was to explore and analyze the DNA-driven assembly of species at the molecular, nano-, and micron scales. The key requirements for DNA-directed assembly to generate novel functional devices are the surface chemistries to attach DNA on surfaces and at high surface densities, the techniques to pattern the DNA molecules on surfaces in specified ways, and the generation of building blocks that incorporate asymmetry and specific functionalities for directing the DNA-DNA interactions. The progress in surface chemistry would be translated directly into stronger and reliable assembly on a variety of surfaces. The techniques to pattern DNA will help to create templates for the assembling components and will translate into a broader range of structures that can be made possible by DNA-directed assembly. Lastly, the availability of novel asymmetric building blocks will help to incorporate elements for 3-D hierarchies into such self-assembled systems. For example, Dwyer et al.[1] have modeled the fabrication of computing circuitry via the DNA-guided assembly of cubic unit cells made of silicon nanorods. According to their analysis, advances in the asymmetric functionalization of the building blocks as well as a reduction in non-specific binding events will be crucial for determining the success of DNA-directed assembly in generating functional electronic devices.

In this thesis, I have addressed the problem of the surface chemistry optimization and demonstrated the high-density specific attachment of DNA molecules and DNA-tagged nanoparticles onto surfaces that exhibit substantially low levels of non-specific adsorption (Chapters 3 and 4). I have created various building blocks (dual- and tri-functional particles and

187

dual-functional microrods) and employed them in the DNA-directed assembly process at both the micron and nano- scales (Chapters 5, 6, and 7). I have also created new types of supraparticulate structures from these building blocks employing DNA-DNA interactions to guide the assembly.

Chapter 3 demonstrated the role played by immobilized probe density in defining various aspects of DNA hybridization at surfaces. In my experiments, mixed self-assembled monolayers were used to systematically control the density of end-immobilized probe DNA strands. The corresponding effects on the kinetics and thermodynamics of hybridization were studied using a fluorescently labeled complementary target DNA. The immobilized 12-mer probe DNA densities ranged from 0.2 x 10^{13} to 5.2 x 10^{13} molecules/cm^2, corresponding to average inter-strand distances of 74 Å to 15 Å. The equilibrium dsDNA amount was maximum on surfaces with ss-DNA probe densities corresponding to average inter-strand distances of 18 Å, close to the Watson-Crick double helix diameter of 20 Å. At higher surface probe densities, steric hindrance resulted in reduced hybridization yields. Hybridization efficiencies ranged from 65% at the lowest density to 10% at the highest density. The hybridization kinetics were reasonably modeled using a diffusion-limited second-order Langmuir adsorption isotherm. I also found that the reduction in duplex stability with probe density can be reasonably modeled assuming that free energy change scales linearly with probe density. This study clearly showed that the density of immobilized DNA strands on a surface can significantly affect hybridization yields and that improvements in the signal-to-noise ratios obtained from hybridization experiments on microarrays is possible by optimization of surface chemistry.

Probe density also plays a key role in characterizing aspects of DNA-tagged nanoparticle adsorption onto surfaces (Chapter 4). In these experiments, I varied the probe density using a

mixed silane chemistry. I achieved a maximum adsorbed particle density of 1070 particles/μm^2 corresponding to an area coverage of ~28%. The non-specific nanoparticle adsorption was about three orders of magnitude lower than the specific attachment. As with the adsorption of DNA molecules, I observed that excessive probe density was detrimental to the nanoparticle adsorption because of electrostatic and steric hindrances. A thermodynamic analysis of the nanoparticle attachment showed that the particles are attached via multiple DNA-DNA interactions. Due to the multivalent nature of the attachment, the effect of probe density on the thermodynamics of nanoparticle adsorption is different than that on the thermodynamics of molecular DNA adsorption. Chapters 3 and 4 together show that surface probe density can have a significant impact on the DNA-directed assembly of DNA molecules and nanoparticles and if properly employed can be an effective tool for modulating characteristics of these assemblies.

Changes in the shape of assembling building blocks from a spherical to a cylindrical geometry can offer benefits in stability to structures assembled via DNA-DNA interactions. In studies exploring the effect of shape on the assembly, microrods proved to be superior to microspheres when used in a DNA-directed assembly process (Chapter 5). Based on theoretical as well as experimental observations, microrods adsorb at much higher densities (~20% area coverage) than the microspheres to a flat surface because of the larger contact areas possible with the cylindrical geometry. Additionally, I have employed shadow deposition of metals (Au and Al) onto silica microparticles to generate dual- and tri-functional particles. By using non-interfering chemistries for the silica, gold and aluminum regions I have been able to impart multiple spatially-defined functionalities to these particles. Extension to dual-functional microrods allowed the assembly of these objects in an orientation-specific manner on flat surfaces as guided by the complementarity of the DNA sequences. The orientation of the

microrods was confirmed by hybridizing the upward-facing sides with their respective fluorophore-tagged complementary sequences.

A notable achievement in this thesis was the generation of dual-functional and tri-functional silica microspheres that expressed two different DNA sequences. Such structures will be key building blocks for constructing complex hierarchical assemblies by DNA-directed assembly. The dual-functional particles functionalized with a different DNA sequence on each of the silica and gold surfaces were shown to selectively adsorb 20-nm and 40-nm Au particles, respectively, onto specific locations of the microparticles based on the specific DNA-DNA interactions. The nanoparticles were adsorbed at fairly high densities on their complementary surfaces (15-20% area coverage). The non-specific adsorption on both the surfaces was very small indicating the robustness of the surface chemistries employed.

This thesis has covered topics ranging from the fundamentals of DNA-DNA interactions at a surface to the use of these interactions for forming assembled structures from various nano- and micro objects. Key advances for this field are the generation of multifunctional particles, the clever use of surface chemistry to selectively functionalize their surfaces, and the use of these particles for the selective orthogonal assembly of DNA molecules and nanoparticles of different sizes. These efforts will be useful as the self-assembly community tries to create functional 1-D, 2-D, and 3-D assembled structures for electronic, optical, and magnetic applications.

8.2 Future Directions

Mismatch discrimination and surface probe density. My experiments in Chapter 3 showed how the probe density can significantly impact the stability of a surface-bound DNA duplex. Specifically, high probe densities caused substantial losses in duplex stability. These particular effects may allow the generation of surfaces that could discriminate strongly between

perfectly matched and mismatched sequences, thereby providing a useful strategy for designing assays for SNP (single nucleotide polymorphism) analysis where the commonest mutations in the human genome are detected and employed for treating and understanding various diseases.

Enhancing hybridization efficiencies for DNA-driven nanoparticle attachment. Results presented in Chapter 4 show that the nanoparticles are attached to the flat surfaces by multiple DNA-DNA interactions. The strength of these multivalent attachments might be possibly improved by incorporating modifications in the nanoparticle functionalization process that would improve the hybridization efficiency and facilitate the formation of additional duplexes. Specifically, the use of a longer linker between the nanoparticle surface and the hybridizing sequence could help reduce some of the surface interactions. Additionally, the bare nanoparticle surface could be capped with MCH as a way to improve the orientation of the probe molecules on the nanoparticle surface. Hamad-Schifferli[2] et al. have observed increased hybridization efficiencies in solution with this approach.

Strengthening attachment by DNA-DNA interactions. Force calculations in Chapter 5 showed that the DNA-DNA interactions in these systems are rather weak and under certain circumstances can be overcome by the capillary and other forces acting on the particles during the assembly process. The overall strength of the attachment can be increased by increasing the contact area, increasing the density of DNA molecules in the attachment area, or strengthening the DNA-DNA interactions. The contact area can be increased by moving to structures with high aspect ratios like platelets, while post-assembly crosslinking methods[3] (such as cisplatin or psoralen crosslinking) could enhance the strength of the formed linkages.

Particle-particle assembly of multifunctional particles. In my studies, I have focused on the assembly of particles onto flat surfaces or the assembly of nanoparticles onto asymmetric

micron-sized particles. The full potential of the asymmetric dual- and tri-functional particles will only be realized if they are utilized to achieve interparticle assembly between particles of equivalent sizes. Such an assembly can potentially lead to novel 2-D and 3-D structures. If the composition and size of the particles is chosen correctly, they can be useful for some novel optical applications (Manoharan et al.[4]). To broaden the possibilities further, efforts should be made to expand the formation of multifunctional particles at the nanometer level.

Microfluidics and DNA-directed assembly. Microfluidic systems can provide various tools to manipulate the DNA-directed assembly of particles. Hammer et al.[5] have recently studied the effect of shear rate on the detachment of microspheres attached to surfaces by DNA-DNA interactions. They found that at high enough flow rates the particles can be completely detached from a surface. The flow-based systems can be useful in regulating the assembly process by applying changes in salt or reagent concentration, or by introducing building blocks via different streams, etc. Other techniques such as electrophoretic transport of DNA,[6] site-selective photothermal denaturation or UV deactivation of DNA,[7] crosslinking to covalently bond and strengthen the DNA duplex,[3] and metallizing to improve the conductivity of the DNA strands[8] etc. provide additional abilities for enhancing the properties of the assembled structures and will be useful in developing real-world applications for these DNA-directed assemblies.

8.3 References & Footnotes

(1) Dwyer, C.; Vicci, L.; Poulton, J.; Erie, D.; Superfine, R.; Washburn, S.; Taylor, R. M. *IEEE Trans. Very Large Scale Integr. (VLSI) Syst.* **2004**, *12*, 1214-1220.

(2) Park, S.; Brown, K. A.; Hamad-Schifferli, K. *Nano Lett.* **2004**, *4*, 1925-1929.

(3) Lee, I. H. In *Chemical Engineering*; Massachusetts Institute of Technology: Cambridge, 2001.

(4) Manoharan, V. N.; Elsesser, M. T.; Pine, D. J. *Science* **2003**, *301*, 483-487.

(5) Zhang, Y.; Eniola, A. O.; Graves, D. J.; Hammer, D. A. *Langmuir* **2003**, *19*, 6905-6911.

(6) Edman, C. F.; Raymond, D. E.; Wu, D. J.; Tu, E. G.; Sosnowski, R. G.; Butler, W. F.; Nerenberg, M.; Heller, M. J. *Nucleic Acids Res.* **1997**, *25*, 4907-4914.

(7) Zhang, G. J.; Tanii, T.; Funatsu, T.; Ohdomari, I. *Chem. Commun.* **2004**, 786-787.

(8) Braun, E.; Eichen, Y.; Sivan, U.; Ben-Yoseph, G. *Nature* **1998**, *391*, 775-778.